9. Telescope structure and kinematics

The design, fabrication, integration operation and maintenance of the supporting structure of a 100-m class telescope is one of the major challenges of the OWL project. The structure must provide sufficient bandpass for the motion control system as well as the required tracking accuracy and dimensional stability under varying gravity, thermal and wind loads. The achievable limits of structural eigen-frequencies impose that image stabilisation be implemented downstream in the optical train.

The mechanical structure shall be seen as a "*skeleton*", which supports all the sub-systems of the telescope. The demonstration of its feasibility is therefore one of the major steps to be performed during the first phase of the project.

9.1 Design Principles

In order to have a coherent development of the telescope structure design, a set of design principles has been defined at a very early stage of the project.

Table 9-1 summarizes these design principles and it is a design tool, which helps to evaluate and control the most significant parameters involved on the project, to evaluate quickly new ideas and criticisms.

Domain	Problems	Guideline / remedy
Environment (Site)	Earthquakes. Wind. Solar radiation. Dust. Rain, Snow and Fog. Overall dimensions. Access roads.	Maximise the stiffness Minimise the wind-exposed area. Wind shield. Covers. Reduce solar absorption on exposed surfaces. Dust rejecting concept. Enclosure. Minimise the overall dimensions of the complete observatory.
Subsystems	Optical elements. Optical path. Re-centering system. Control. Passive Damping.	Integrated design, definition for each sub-system: Location. Volume. Mass.

Domain	Problems	Guideline / remedy
	Thermal Control. Drives. Auxiliary drives. Bearings. Cabling and Piping. Mirror covers. Cleaning units. Mirror handling. Instrument handling. Human access. Metrology system.	Supplies
Structural Parts Material	Dimensional instability Dynamic and static performances. Thermal expansion. Affordability.	Minimise the stresses (microyield strength) Run in. Differentiated parking positions. Specific modulus Mild Steel Composites
Large Optics Material	Suitability (polishable, etc) Dimensional stability. Homogeneity Thermal expansion. Dynamic and static performances due to the mass. Affordability.	Zerodur SiC
Control.	Friction disturbance. Wind load disturbance. Cross talk. Gravity. Thermal.	Minimise the friction Maximise the stiffness. Drives. Bearings. Wind screen. Passive damping.
Thermal Control	Solar Radiation Energy consumption. Thermal inertia.	Covers, Shields, Sliding or deployable enclosures,. Surface treatment. "Inner flow`" cooling system.
Fabrication	Affordability	Material choice Modular design. Mechanical tolerances. Commercial available parts. Maximise the number of potential Contractors. Minimise the gap between Design Phase and Fabrication Phase
Transportability	Oversized pieces. Access to the site Affordability	Modular design Max 2,4 m x 2,4m x 6 or 12m Max 20 Tons Fabrication on site
Assembly on site	Hoisting facilities Alignment. Safety.	Modular Design. Minimise the mass of each part. Self-machining structure. Self-supporting structure.
Operation	Sky coverage Change of modes. Energy consumption. Manpower resources. Safety.	± 60 degrees from zenith. Minimise the time between: Stand by mode. Operation mode Safety mode. Low mass.

Domain	Problems	Guideline / remedy
		High number of automatism.
Maintenance	Technical Down time. Manpower resources. Accessibility Large Optics handling Instrumentation. Cleaning. Safety.	Altitude rotation ± 90 degrees from zenith. Handling facilities. Cleaning facilities. Parking positions. Component standardisation.

Table 9-1: Design guidelines

9.2 Design Assumption

As per today the OWL site is not selected yet. Therefore the design has evolved based on the following design assumptions, which correspond to average environmental conditions typical of Astronomical Observatories around the world.

- Soil characteristic, value range:
  - o Paranal 50000 MPa.
  - o La Palma 5000 MPa.
- Existing infrastructures within reasonable distance.
  - o Harbor.
  - o Roads.
- Seismicity 0,2 g, intermediate value between:
  - o Paranal 0,34 g
  - o La Palma 0,06 g.
- Wind, observation mode.
  - o 10 m/s.

9.3 Design Evolution

During the evolution of OWL optomechanical concept design, which started in 1997, some key parameters have been monitored. These values give an indication of the achieved design improvements. The total rotating mass (see Figure 9-2) of the telescope supplies an indirect estimation of the telescope costs and the locked rotor frequency (see Figure 9-1) gives a direct indication of how well the telescope will perform and how complex the various sub systems of the telescope have to be.

- Low rotating mass, implying low cost;
- High locked rotor frequency, implying good dynamic and static performance, lower complexity of sub-systems and eventually low costs;

From the early design phases the optical and mechanical design evolved in a synergetic manner. And the level of details modelled in the FE also evolved considerably. Because of

these reasons, the various design concepts cannot be compared exactly one to one. Nevertheless a clear trend can be deduced throughout all the designs.

- Decrease of the M1-M2 de-space.

- Decrease of the M2 size.

- Decrease of the stability tolerance of M2.

- Decrease of the total rotating mass.

- Increase of dynamic performance.

- Increase the level of details of the subsystems.

- Increase the level of details embedded into the concepts for manufacturing, transport, integration, operation, maintenance and safety.
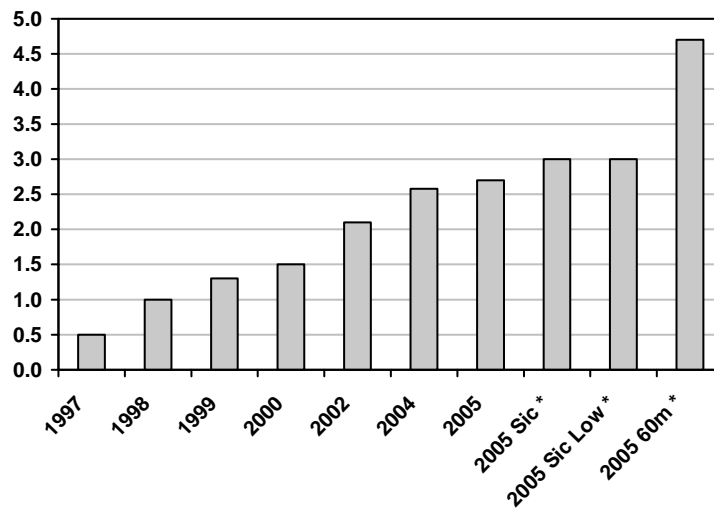
Figure 9-1: locked rotor mode evolution
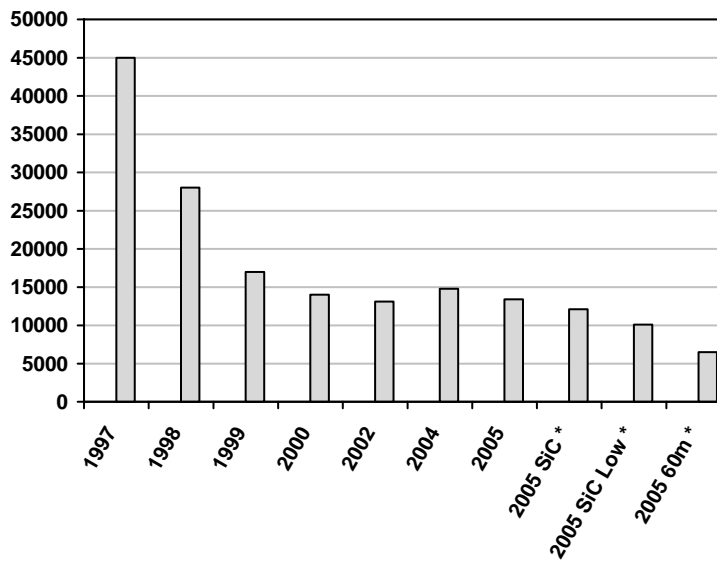
Figure 9-2: Rotating Mass evolution.

Telescope structure and kinematics

All the design concepts described in the following sections are based on:

- 6 mirrors optical design.

- Glass ceramic mirror substrate.

- Mild Steel for mechanical structural parts.

Figure 9-1 and Figure 9-2 summarize the design evolution. The 2005 designs are discussed in section 9.4.onwards.

9.3.1   1997 Design

Two optomechanical concepts (see Figure 9-3 and Figure 9-4) developed in 1997 and presented in [10].

Major Characterisitcs:

- The M1 – M2 de-space was 120 m

- The rotating mass 45000 tons.

- The Locked rotor frequency 0,5 Hz

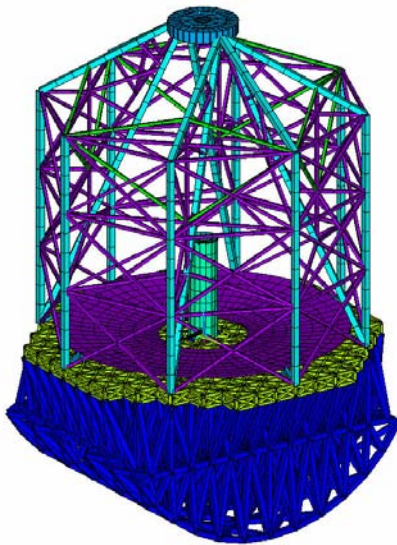- Only the altitude structure was modelled and analysed.

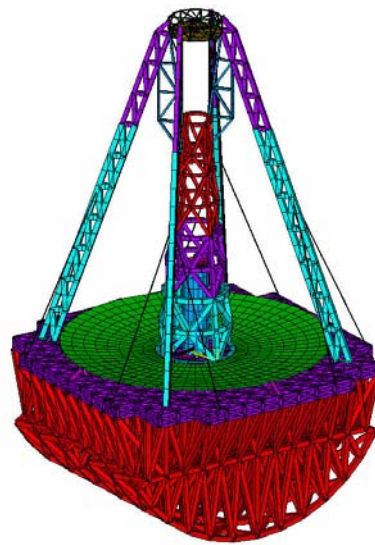Figure 9-3: 1997 design, rocking chair design I.   Figure 9-4: 1997 design, rocking chair design II.

9.3.2   1998 Design

The opto-mechanical concepts developed in 1998 (see Figure 9-5). Modular design was introduced, allowing to build up the complete telescope structure using the same basic modules. With subsequent designs this concept evolved towards a high level of standardization of parts. This was a major step forward in reducing the costs of the mechanics.

In the 1998 design, the aperture was divided in four sections, creating a larger primary mirror and leaving design volume for the mechanics around the four mirror petals.

Primary mirror cover and maintenance concepts integrated into the opto-mechanical design.

Major Characterisitcs:

- M1 – M2 de-space   150 m
- Primary mirror diameter   150 m
- Rotating mass   28000 tons.
- Locked rotor frequency   1 Hz
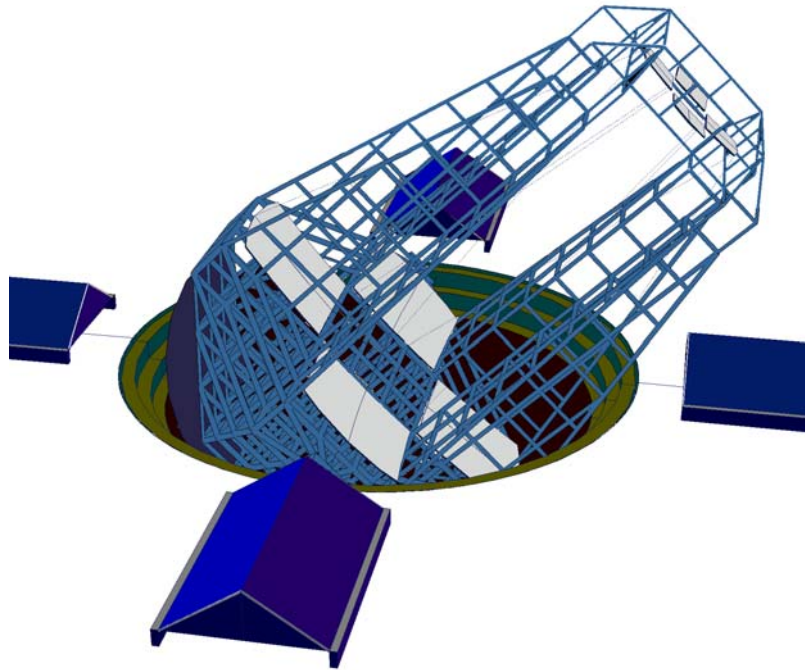- Only the altitude structure was modelled and analysed.

Figure 9-5: 1998 design. Four petals design.

9.3.3   1999 Design

Three optomechanical concepts developed in 1999 and were presented in [32]. These 3 concepts explored different configurations based on modular design principle set in 1998. A detailed Design guideline has been established in 1999, which provided a design strategy for the future evolution of the concept.

Concept 1:   Attempt to decouple the secondary mirror from the rest of the optical elements (see Figure 9-6). The poor dynamic performance of the arch structure, indicated that this structural concept cannot deliver sufficient stability for adequate tracking accuracy.

Concept 2:   Altitude structure rotating on 3 cradles (see Figure 9-7).

Concept 3:   altitude structure rotating on one cradle and two altitude bearings (see Figure 9-8). The altitude cradle supplied the housing for the altitude drive. This concept delivered the best results in terms of rotating mass and dynamic performance. It also included design provisions for manufacturing, transport, integration, operation, and maintenance. Design aspects related to safety issues present during the whole life of the telescope were evaluated and provisions implemented into the concept.

Major Characterisitcs:

- M1 – M2 de-space   120 m
- Primary mirror diameter   100 m
- Rotating mass   16800 tons.
- Locked rotor frequency   1.35 Hz.
- Telescope altitude structure has a four fold symmetry along the altitude and drive axes.
- Only the altitude structure was modelled and analysed.
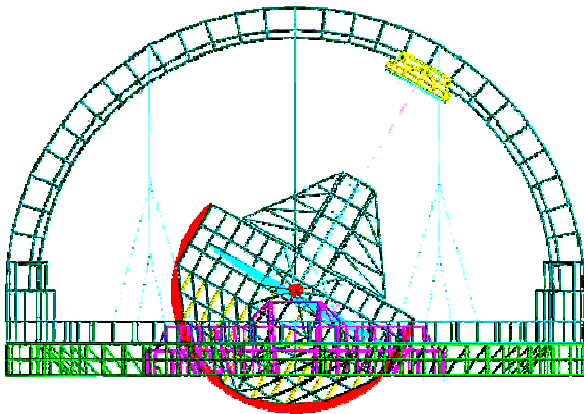
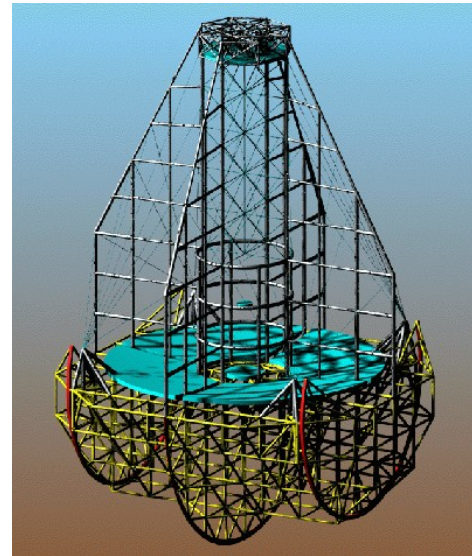Figure 9-6: 1999 design I. Decoupled M2 unit.

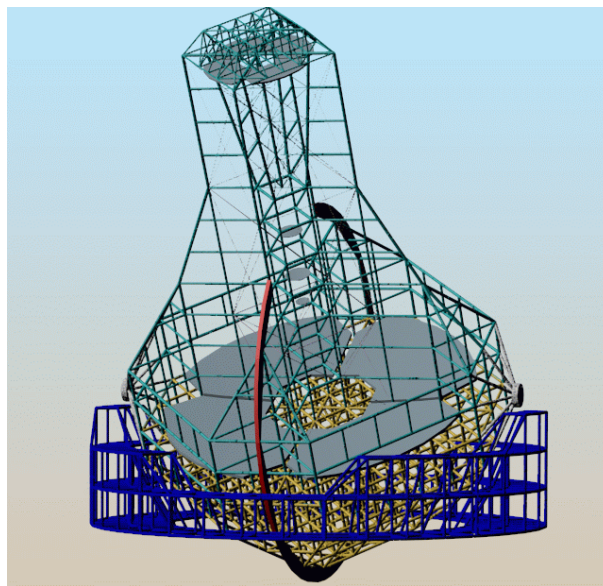Figure 9-7: 1999 design II. Light rocking chair design.

Figure 9-8: 1999 design III. Cradle and bearings design.

9.3.4 2000 Design

Optomechanical concepts developed in 2000 (see Figure 9-9) and were presented in [33]. A major optical design iteration reduced the M1-M2 de-space from 120m to 95 m. Major operation and maintenance operations have been analysed. Several design assumptions have been investigated and traded off: Iso static configuration, hyperstatic configuration, SiC substrate.

Major Characterisitcs:

- M1 – M2 de-space   95 m
- Primary mirror diameter   100 m
- The rotating mass   14500 tons.
- Locked rotor frequency   1.55 Hz
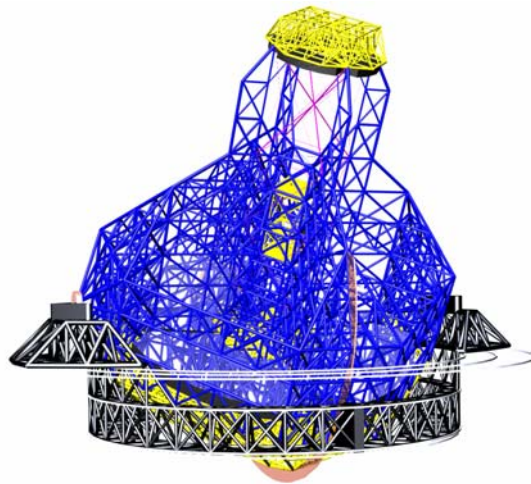- Both altitude and azimuth structure were modelled and analysed.

Figure 9-9: 2000 design. Cradle and bearings design evolution.

9.3.5 2002 Design

Optomechanical concepts developed in 2002 (see Figure 9-10) and were presented in [30], [31]. Further structure optimisation and performance improvement were achieved. Detail trade off of the main axes bearing and drive system with related cost analyses took place, as well as a first study on wind loading. Start feasibility and costs verification with industries, external engineering offices, and institutes.

Major Characterisitcs:

- M1 – M2 de-space   95 m
- Primary mirror diameter   100 m
- Rotating mass   13100 tons.
- Locked rotor frequency   2.1 Hz
- Drive and bearing systems trade-off.
- Friction drive and bogies base line.
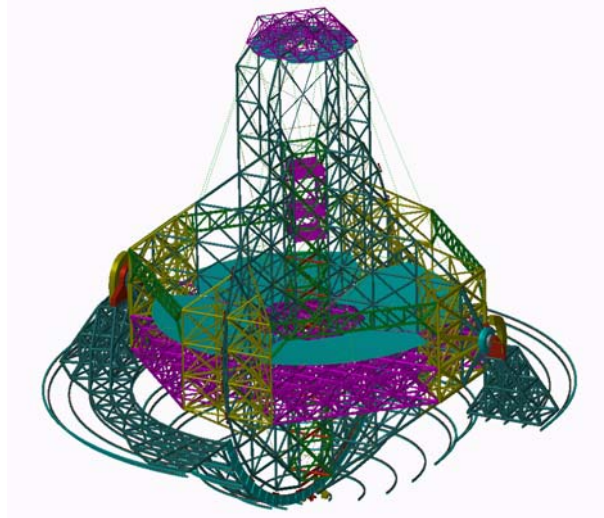- Foundation analyses

Figure 9-10: 2002 design. Cradle and bearings design evolution.

9.3.6 2004 Design

Opto-mechanical concepts developed in 2004 (see Figure 9-11) and were presented in [29]. Complete redesign of the mechanical structure based on "fractal" design derived from the mirror segment geometry.

Major Characterisitcs:

- M1 – M2 de-space   95 m

- Primary mirror diameter   100 m

- Secondary mirror diameter reduced to 25,6 m.

- Rotating mass   14800 tons.

    Increase of mass due to the higher altitude axis from the ground level and 500 tons for auxiliary equipments.

- Locked rotor frequency   2.6 Hz

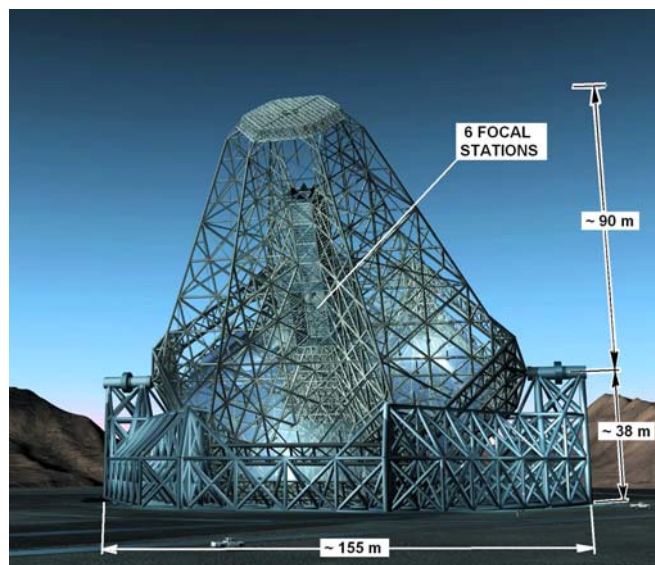- Friction drive and bogies were modelled and analysed.

Figure 9-11: 2004 design. Fractal design.

9.3.7   2005 Design (current baseline).

The 2005 design is an improved version of the 2004 design. It differs only slightly from the 2004 version (see also section 9.6.1). Most significant changes are:

- Reduction of the rotating mass. Due to further optimization.

- Increase of Static and dynamic performance. Due to improved constrains of the altitude cradles. This is particular beneficial to the eigen-mode parallel to the altitude axis.

- Axial friction drives and bearings only for the azimuth axis. Dedicated analyses demonstrate that the radial friction drives and bearings do not contribute to the dynamic performance of the telescope. This design generates a substantial reduction of complexity and costs.

9.4   Conceptual Design.

Figure 9-12 and Figure 9-13 show the current design, and the overall dimensions of OWL alt-azimuth conceptual design.
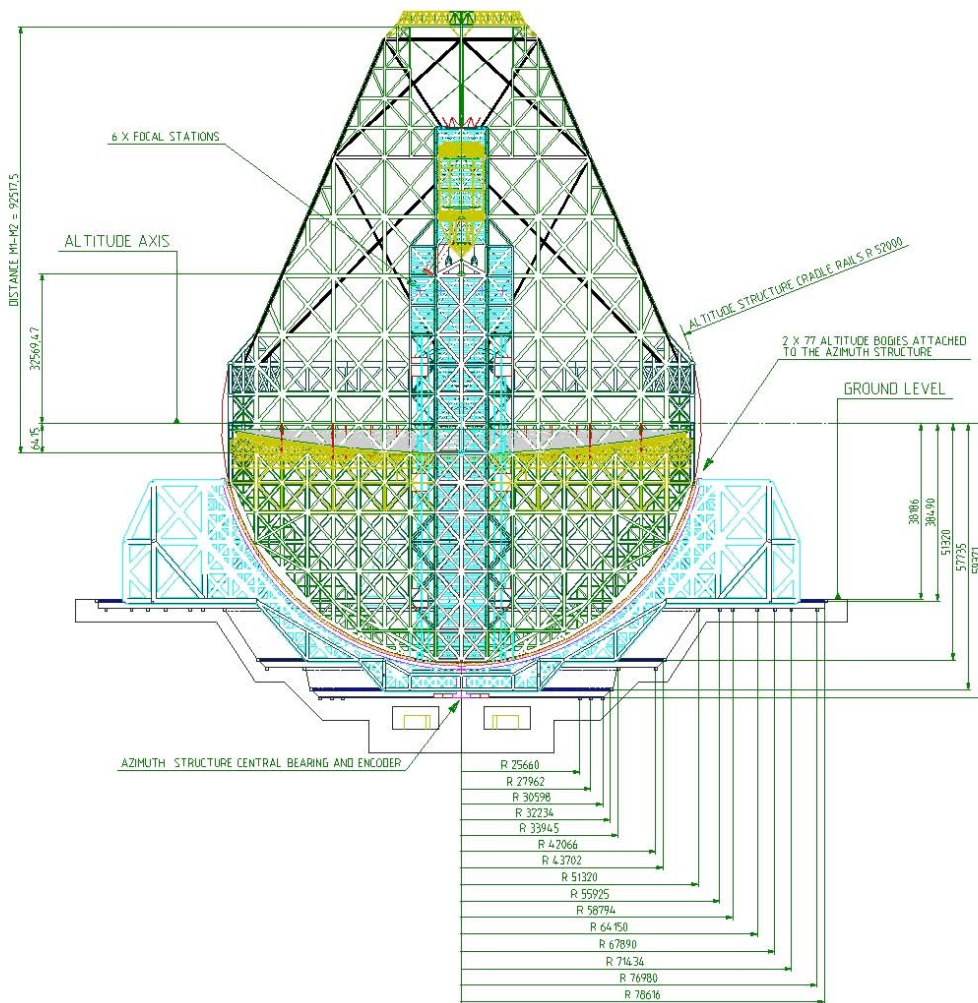

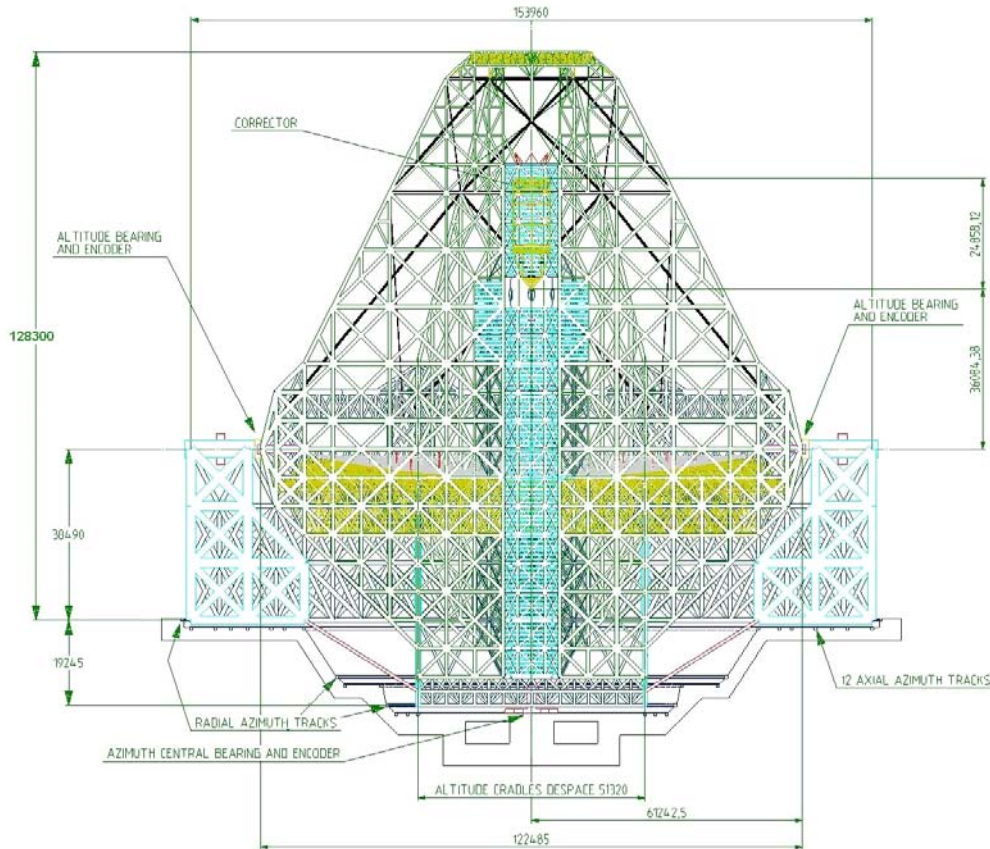*Figure 9-12: OWL telescope structure. Side view.*

Figure 9-13: OWL telescope structure. Side view.

9.4.1 Structural design

9.4.1.1 Material selection

The following materials have been chosen for the structural part of the telescope:

- St 37 for the part with low-mid stresses.

- St 52 for part with higher stress (See RD29, RD30, RD31 and RD32)

- Kevlar 149 for ropes applications.

The choice of using mild steel for structural part fulfils the following criteria:

- Proven technology: Steel welding and machining technologies are well understood and do not represent risk areas.

- Availability of material: Material can be procured in large quantities at low cost. (See RD29)

- Availability of Contractors: Industries operating in steel construction are numerous and widespread. This will generate fair competition among potential suppliers, assuring low costs.

- Formability: Steel structure can be retrofitted or repaired at low cost. Thus assuring flexibility of adding or modifying sub systems during the telescope operational life.

- Analysis accuracy: Analyses of steel structures are well understood and highly predictable. Thus assuring a good optimization of the telescope structure and minimise risks associated to safety during construction and during the whole telescope operational life.

- Good specific strength / specific stiffness ratio: While the specific stiffness remains one of the most important parameter in the telescope structure design, the magnitude of stresses

is not anymore negligible and the specific strength becomes also a major design parameter (see Figure 9-14).

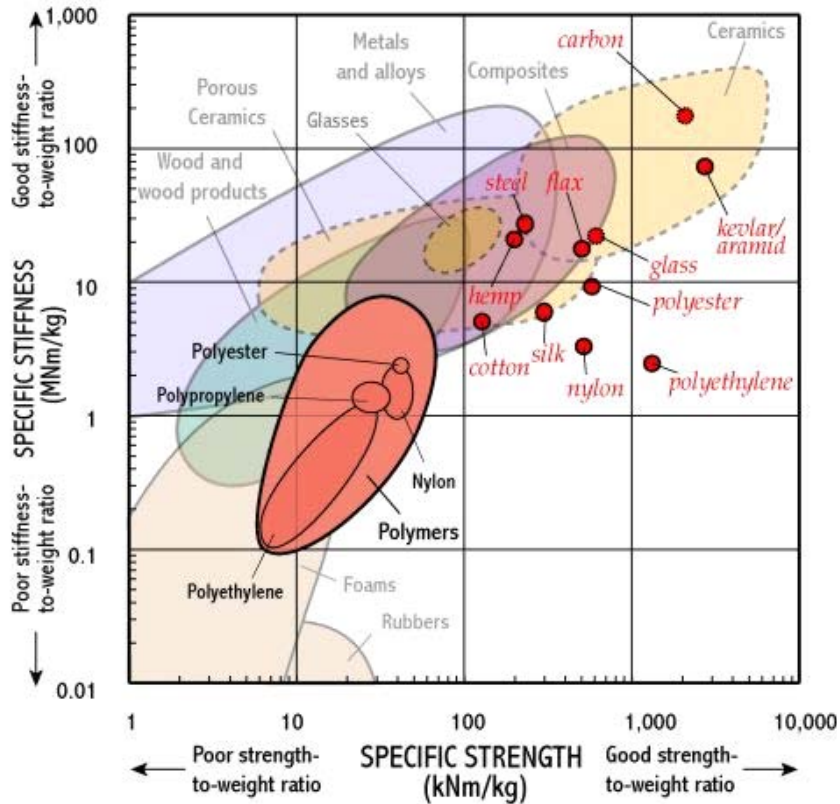- Good cost / performance ratio:

Figure 9-14: Structural materials stiffness and strength.

In the baseline design, composite material are only used for ropes applications (see section 9.4.4.2). Nevertheless designs options, which adopt partially composite material instead of steel, have been investigates and reported in section 9.5.

9.4.1.2   Structural element selection

The large majority of the mechanical structure elements are made from mild steel cylindrical pipes. The choice of using cylindrical pipes for structural part fulfils the following main criteria:

- Availability in large number of sizes and wall thickness. This makes an effective optimization of the structure.

- Formability, the pipes can be machined, welded and integrated in large structure at low cost. (See RD29)

- Cylindrical external surface offer less surfaces prone to dust deposition and make cleaning operation easier (see Figure 9-15).

- Smooth stress transition on the nodes.

- No sharp edges.

- Best wind drag coefficient

- Large external surface versus wall thickness. Low thermal inertia.

- Possibility of inner ventilation.

Telescope structure and kinematics

Figure 9-15: Typical welded node.

9.4.2   Fractal Design

From 2004 onward a so-called *Fractal Design* has been adopted for the telescope mechanical structure. This design is based on a six fold symmetry of the primary and secondary mirrors segments (see Figure 9-16). Each part of the telescope structure is a scaled down or scaled up replica of the mirror segment pattern. Similar to many "Natural fractals" like trees, clouds, ice crystal, rocks, etc. the OWL's Fractal Design turned out to be very efficient and uses the structural material in the most economical manner. The main advantages of this design approach and fabrications are:

- Standardisation of parts.

- Homogeneous distribution of load in the structure.

- Even load transfer from the optical element to foundation.

- Low mass and high static and dynamic performance.

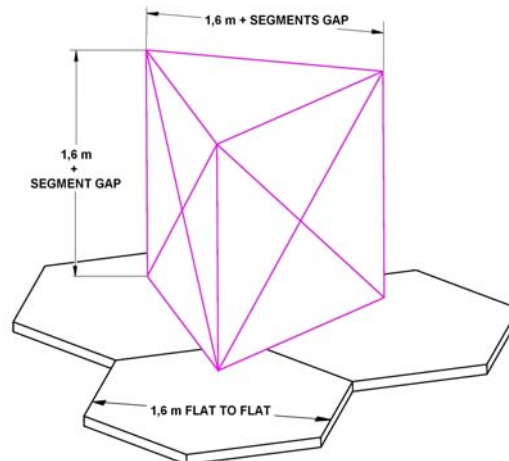- Simplicity in manufacturing transport and site assembly.

Figure 9-16: Base Fractal pattern.

9.4.2.1   Base module

From the segment hexagonal pattern, a base module has been derived (see Figure 9-17). It is made by cylindrical pipes which form a trusses structure. At the intersection of 2 or more pipes, standard nodes are realized using a minimum of different parts. Figure 9-18 shows the most complex node which is built up using only 3 different parts. Therefore the complete OWL mechanical structure can be assembled using the fairly simple base module geometry, or its integer equivalents.
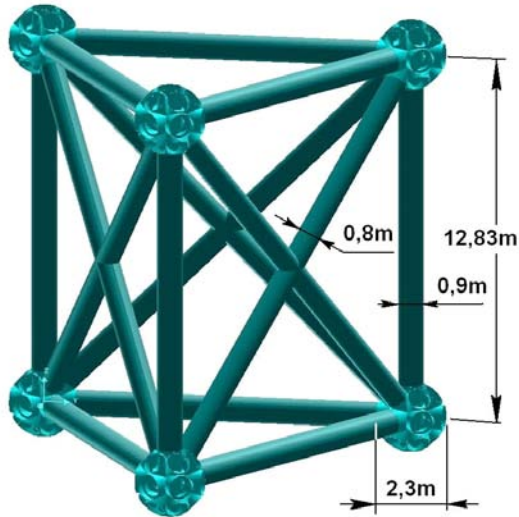
Telescope structure and kinematics
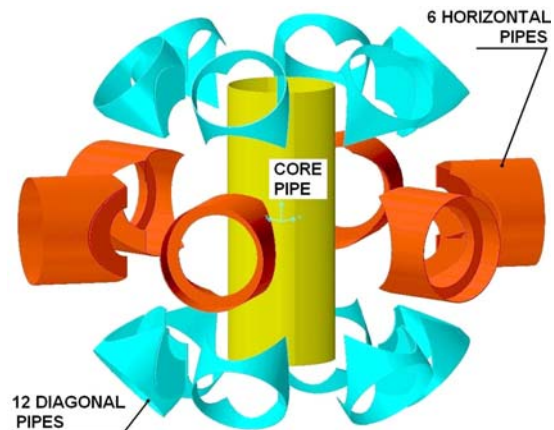
Figure 9-17: Base Module.

Figure 9-18: Node exploded view

9.4.3   Azimuth Structure.

The azimuth structure shown in Figure 9-19, is a steel trusses structure which copies the mirror segment hexagonal pattern. The trusses are made of cylindrical pipes.
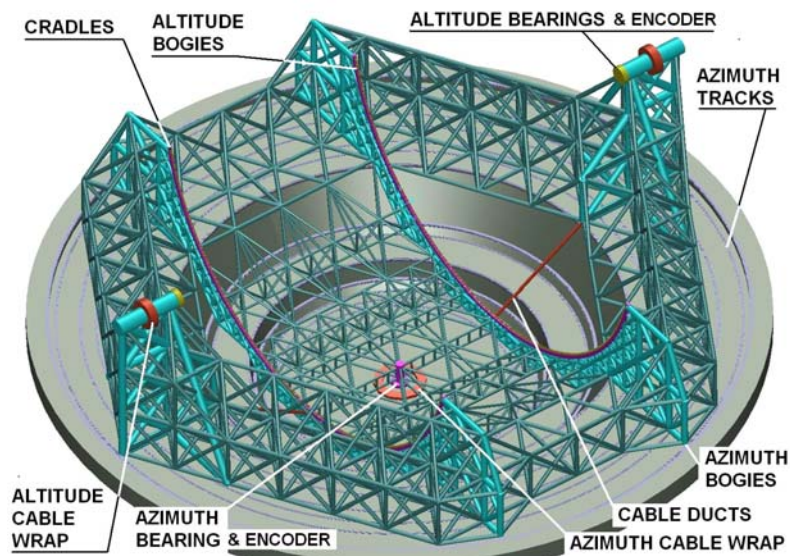
Figure 9-19: Azimuth Structure

Its major characteristics are:

* It is partially embedded in to the concrete foundation.

* One azimuth roller bearing, which constrains 3 translations DoF, defines the telescope azimuth axis and an absolute rotary encoder supply the position signal of the azimuth structure. The central bearing gives the absolute "X-Y-Z" reference to the azimuth structure

* The telescope altitude axis, at a height of about 38 m from the ground level, is defined by two roller bearing which constrain 3 translations DoF. Two absolute rotary encoders supply the position signal of the altitude structure.

- The azimuth rotation is realized by means of friction drives and bearings (azimuth bogies) which are attached to the azimuth structure and run on annular tracks embedded in the foundation.

- Two cradles supply the supporting structure for the altitude bogies.

- One azimuth cable wrap brings the fluid and electrical supplies and control signals from the technical rooms (shown in Figure 9-20) to the azimuth structure. Two altitude cable wraps further lead these supplies to the sub-systems located in the altitude structure.

Figure 9-20: Azimuth structure and foundation interface

9.4.4 Altitude Structure.

The altitude structure shown in Figure 9-21, is a steel trusses structure with the same six-fold symmetry as the mirrors. The trusses are made of cylindrical pipes.
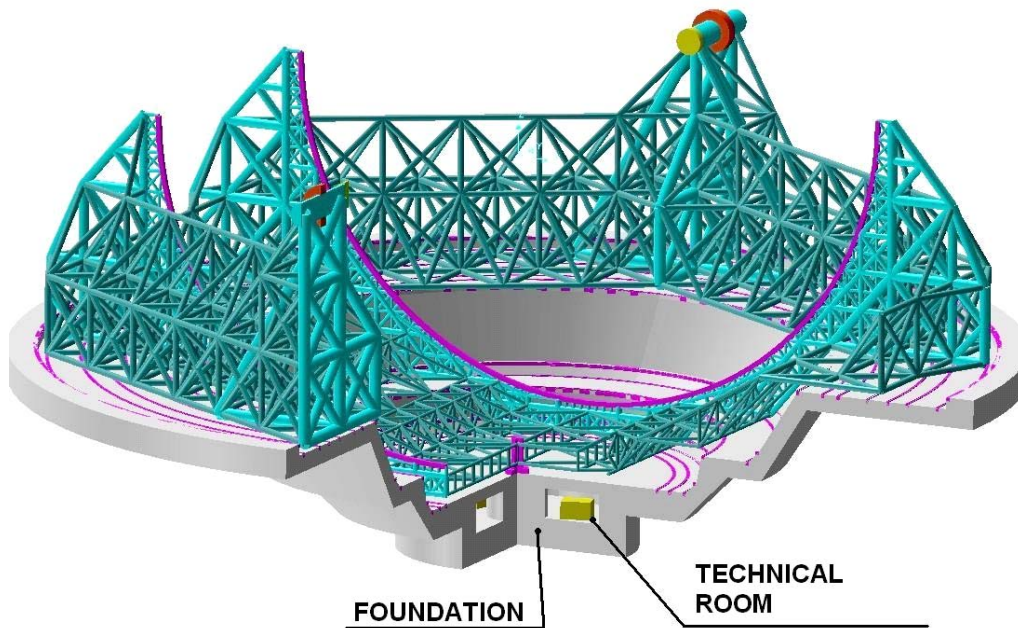
Its major characteristics are:

- It hosts all the optical elements.

- It has six focal stations.

- Supplies all the lift and access facilities to the optical elements.

- It supplies thermally insulated and clean environments for the optical elements and instrumentations.

- The altitude rotation is realized by altitude bogies, attached to the azimuth structure and running on the two altitude cradles.

- The telescope altitude axis is defined by two roller bearings which constrain 3 translations Degrees of Freedom (DoF). Two absolute rotary encoders supply the position signal of the altitude structure.
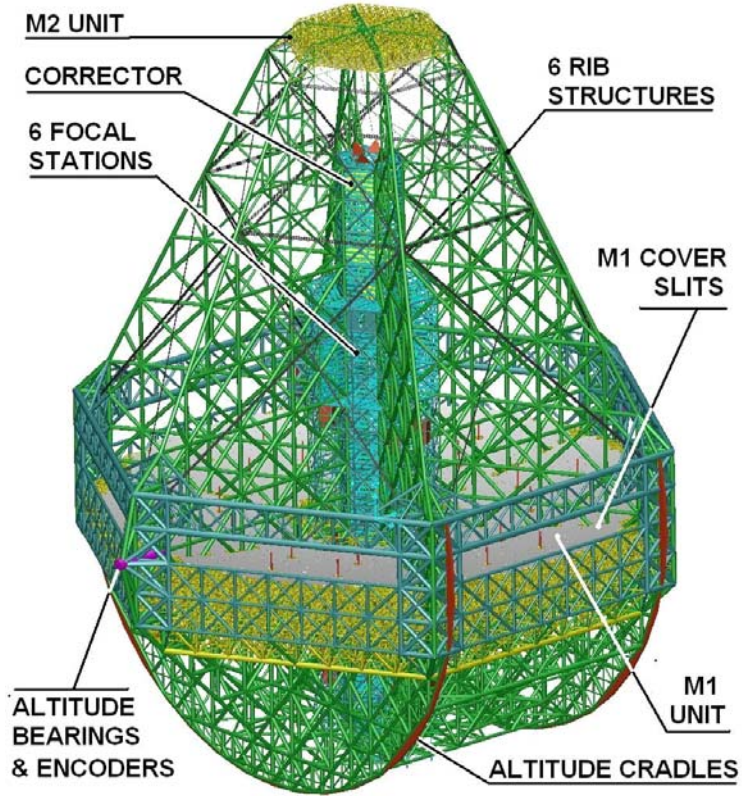
Telescope structure and kinematics

Figure 9-21: Altitude Structure

Figure 9-22: Top view

Telescope structure and kinematics

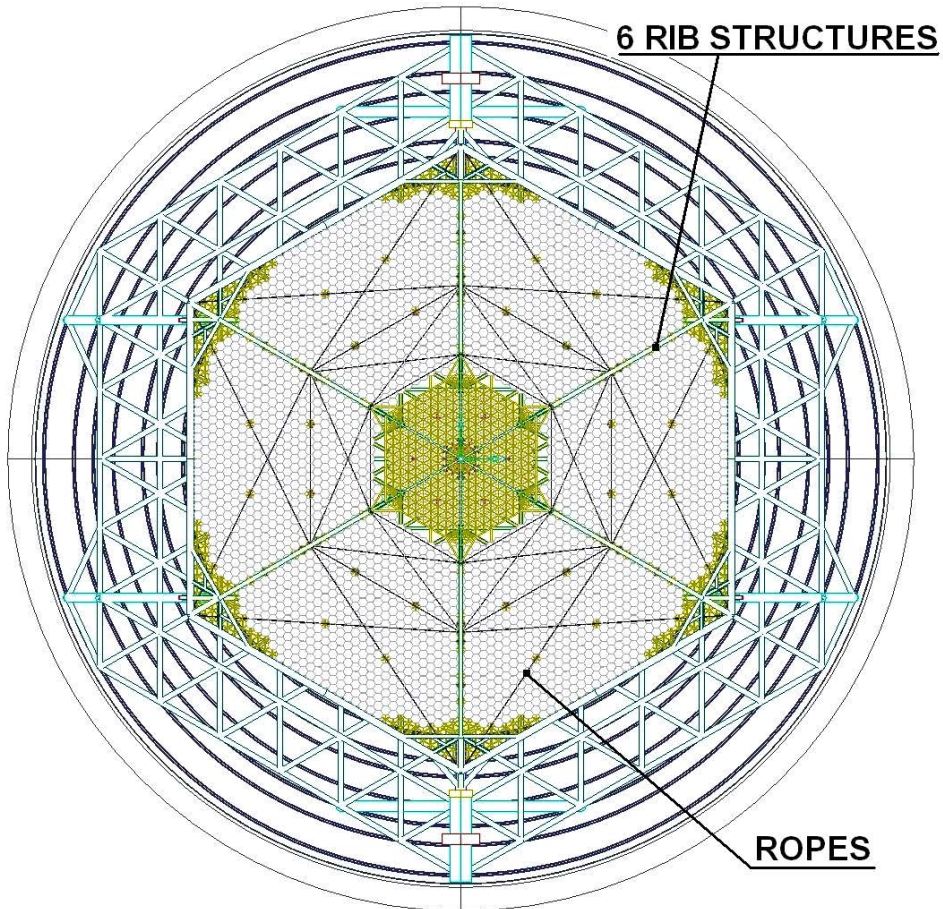### 9.4.4.1 Primary mirror obscuration

The light from the sky is obscured (see Figure 9-22) by the following parts:

- 6 Ribs structures. These structures connect the secondary mirror unit to the lower parts of the altitude structure where the kinematics is located. The maximum section across the light beams is about 900 mm. The Primary mirror obscured area by the 6 ribs structure is about 410 m^2.

- Torsion ropes constrain the rotation DoF of the secondary mirror unit along its optical axis. The area obscured by the torsion ropes is about 70 m^2

9.4.4.2 Structural ropes

The altitude mechanical structure made of steel pipe elements can constrain 5 Degrees of Freedom (DoF) of the secondary mirror. The DoF around its optical axis θz is constrained by a set of ropes, which are placed in rows parallel to the incoming light beam from the sky (see Figure 9-23). Thus the optical obscuration is minimized (see also appendix A-1.4).

Major Functions:

- Stabilize the rotation DoF of the secondary mirror.

- Stabilize slender structural elements located in the upper part of the Altitude Structure.

- Increase global mode frequencies of the upper part of the Altitude Structure.

It shall be noted that, the structural ropes are not essential for static or quasi static survival load cases (with exception of Maximum Likley Earthquake (MLE). The telescope does not collapse if complete rope sets are missing (e.g. Up-grades or maintenance). However the telescope will not have sufficient stiffness to meet performance requirements.

The most important criterion is stiffness in tension. Because it is important that the telescope does not flex too greatly under strong winds or during the rotation of the altitude structure, the stiffness (Young's modulus) must be high. In addition, the weight of the ropes themselves is also important. For this reason a specific stiffness - specific strength chart (see Figure 9-14) is useful for identifying suitable materials - the chart shows a selection of materials available as fibres.

Until recently steel cables have been used for tensioning type applications. Steel wire can have a very high tensile strength, but it is quite heavy. Recently very high specific stiffness and strengths have been obtained with synthetic fibres. These are now used in suspension bridges and made by incorporating fibres into a matrix to form a composite bundle. This is then twisted with others to form a rope. Similar solutions could be adopted for OWL tensioning ropes.

Essential rope properties are listed below:

- Creep properties (the gradual extension over time under a tensile load). The dimensional stability of the ropes over time minimizes the need of resetting the tensioning forces.

- Internal damping properties shall absorb vibrations generated by wind disturbance or by the telescope drives.

- Fatigue resistance to cyclic tension due to wind disturbance and gravity changes during the altitude structure rotations.

The OWL rope system will be integrated in a mechanical structure made of mild steel. Therefore the following critical problems shall be solved by the rope system:

- Matching of differential thermal expansion.

- Tensioning forces calibration and control.

Therefore the structural rope system consists of:

1. Ropes.

2. Thermal compensation and tension control devices.

3. Mechanical interfaces (see Figure 9-24).
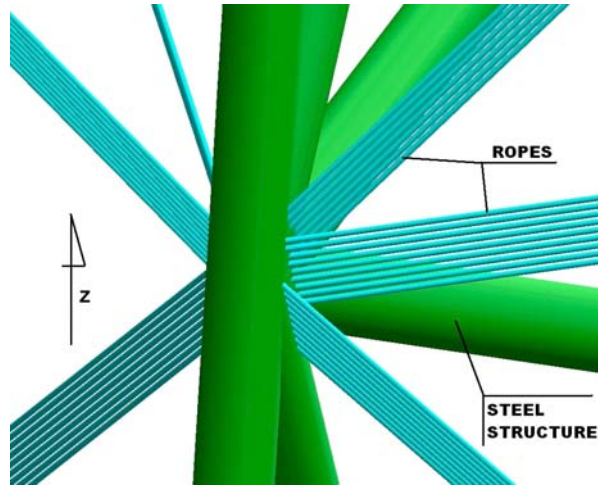
Figure 9-23: Sets of parallel rope
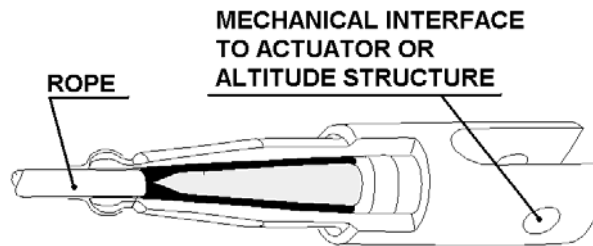
Figure 9-24: Rope mechanical interface

A dedicated study of rope implementation in ELTs including OWL is planned in the ELT Design Study. Further detail of the study "Structural ropes for ELT" can be found in the study Statement of Work (RD510).

9.4.4.2.1   Material selection

There are three grades of Kevlar available: Kevlar 29, Kevlar 49, and Kevlar 149. The table below shows the differences in material properties among the different grades. The Kevlar 149 has been selected.

Grade	Density g/cm^3	Tensile Modulus (GPa)	Tensile Strength (GPa)	Tensile Elongation (%)
29	1.44	83	3.6	4.0
49	1.44	131	3.6--4.1	2.8
149	1.47	186	3.4	2.0

Table 9-2: Kevlar available grades.

It is important not to expose Kevlar ropes to chemicals (e.g. soda of the recoating process) otherwise the Kevlar decomposes.

9.4.4.2.2 Wind on ropes

The ropes implemented in the altitude structure are vulnerable to wind induced vibrations and flutter. Due to constant section of the ropes vortex shedding can be generated (see Figure 9-25).

Figure 9-25: Wind vortex shedding.

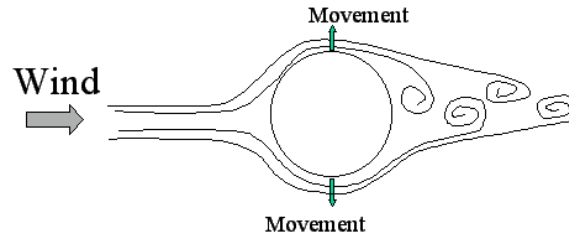The situation can be improved by increasing the damping in the system. Similar to the one reported in [34] for the cable stayed bridges (see Figure 9-26).
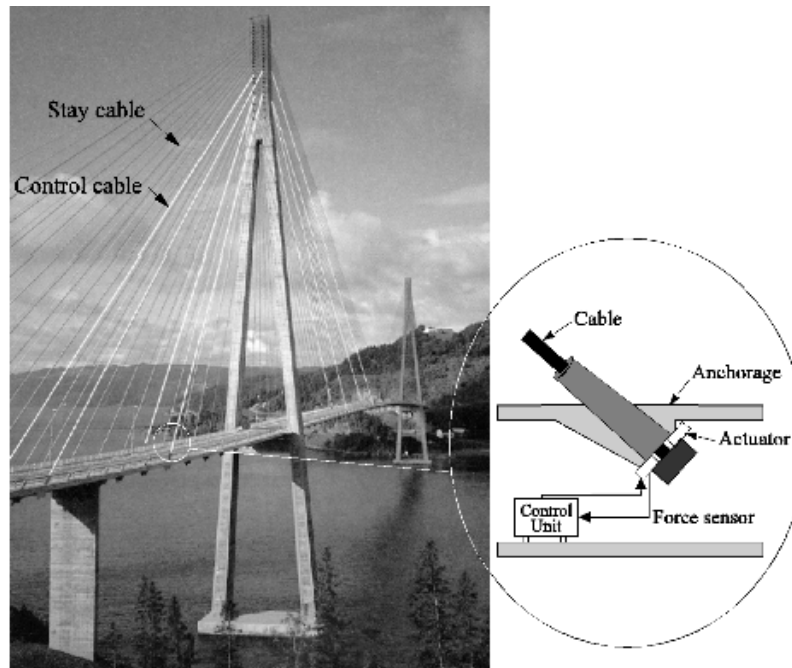

Figure 9-26: Cable damping system. (Courtesy of ULB).
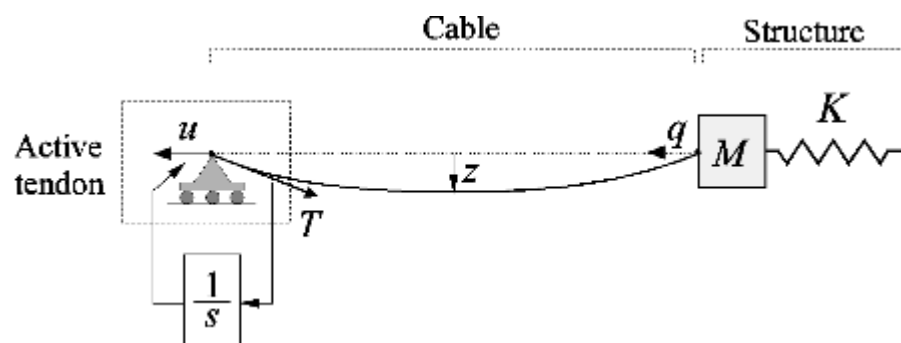
Figure 9-27: Active damping concept. (Courtesy of ULB).

Control strategy - The key feature of our control strategy is the use of a decentralized control system with collocated actuator/sensor pairs (displacement actuator and force sensor, see Figure 9-27). For this configuration, *Integral Force Feedback* (IFF) leads to guaranteed stability.

9.4.4.3   Focal Stations

At about mid-span between the primary and secondary mirrors 6 focal station are realised, placed symmetrically around the altitude structure optical axis. Figure 9-28, Figure 9-29 and Figure 9-30 show the layout dimension of the focal stations. The following allocations are foreseen:

- Focal station 1: Heavy scientific instrument (Attached to the structural element of the Focal Stations).

- Focal station 2: Light scientific instrument (Attached to the rotator).

- Focal station 3: Heavy scientific instrument (Attached to the structural element of the Focal Stations).

- Focal station 4: Light scientific instrument (Attached to the rotator).

- Focal station 5: Light scientific instrument (Attached to the rotator).

- Focal station 6: Technical instrument (Attached to the rotator).

Each Focal Station is equipped with a dedicated Adapter Rotator described in section 6. Accessibility to the focal station and instrument integration and maintenance are described in section 15.1.
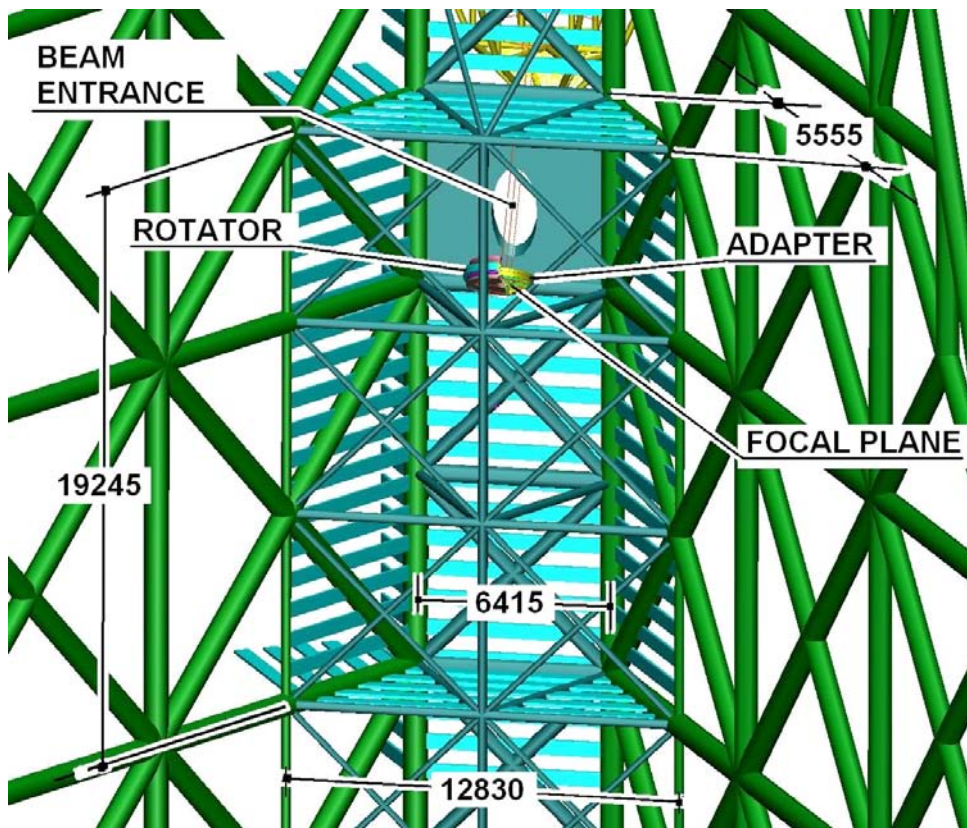
Figure 9-28: Focal station layout.
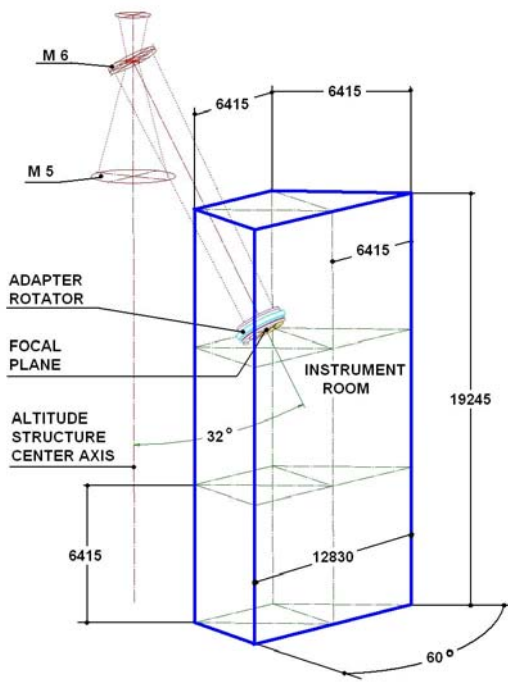
Figure 9-29: Focal station external dimensions.   *Figure 9-30: Focal station external dimensions. Side view.*
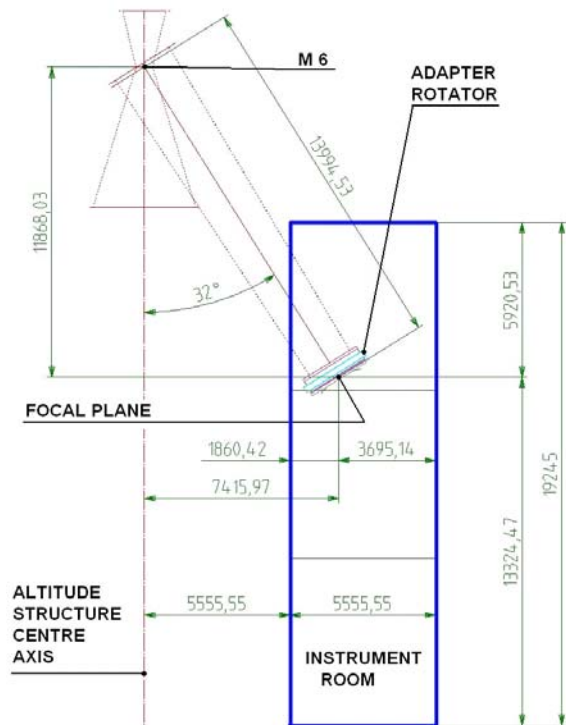
9.4.4.3.1   Alternative focal station.

For instrument aiming at very high stability, presumably fed with optical fibers of about 300 m length, an instrumentation station can be implemented in the technical rooms. Possible dimensions are indicated in Figure 9-31. Foundations which are mechanically de-coupled from the telescope foundation can be realized. No loads need to be transferred from the roof of the technical room to the telescope foundation.

Nasmyth-type stations fed by suitable optomechanical relays remain to be assessed in the design phase.
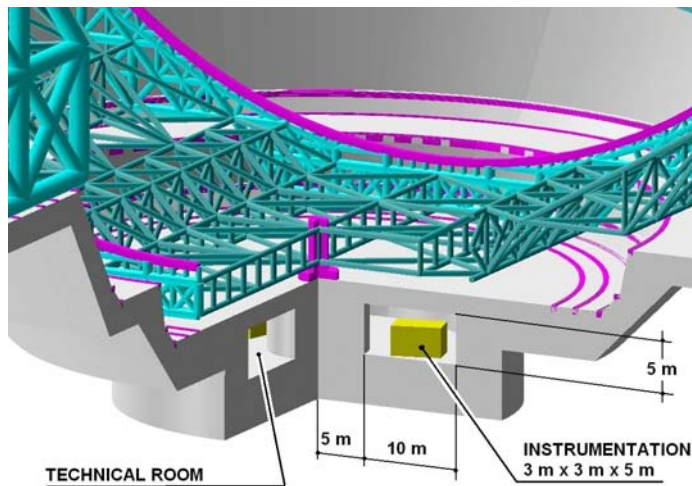
Figure 9-31: Fibre fed focal station.

9.4.5   Sub-Systems design.

9.4.5.1   Kinematics.

An essential function of the telescope altitude-azimuth mechanical structure is to provide a smooth, distributed and stiff transfer of loads to the site soil. The OWL telescope has its tracks embedded into the concrete foundation. The classical, traditional Fork / Tube concept standing on a pier has evolved into a Azimuth Structure / Altitude Structure concept embedded into a crater-like foundation. The smooth and even transfer of the loads from the optomechanical structures to the soil via the altitude structure, azimuth structure and concrete foundation can only be achieved using a large number of mechanical interfaces which shall also provide the kinematics of the telescope. The telescope is constrained in a hyper-static mode, which requires implementing accurate and reliable drive and bearing systems, thus avoiding concentration of stresses and deformation of the structural steel element and of the concrete foundation.

Different types of drives and bearings systems can be implemented between the azimuth structure and tracks, and between the azimuth-altititude structures. However a typical angular accuracy of few tenths of arcsec, must be well within the performance of the adopted solution, while interfaces and kinematics must ensure a homogeneous load transfer to the foundation.

9.4.5.1.1   Torque requirement.

The main axes drive systems are dimensioned to provide the following characteristics:

- Blind angle at zenith $\leq \pm$ 0,5 degree.

- Acceleration   0,1 degree s -2 (1,745 $\times$ 10-3 rad s-2).

- Maximum velocity   0,5 degree s -1 .

- Minimum tracking accuracy   1 arcsec.

9.4.5.1.2   Acceleration.

Altitude mass moment of inertia   1,121 $\times$ 10^{10} kg m^2.

Altitude required torque   19,6 MNm.

Azimuth mass moment of inertia   3,366 $\times$10^{10} kg m^2.

Azimuth Required torque   58,7 MNm.

9.4.5.1.3   Friction Drive & Bearing.

OWL performance and cost constraints require that different solutions be assessed. Several design iteration and trade off, indicate that merging drive and bearing functions into friction type mechanical devices ("bogies", shown in Figure 9-32, Figure 9-33 and Figure 9-34), reduces the complexity and cost of the design and allows to constrain the telescope in hyper-static mode, without jeopardizing the telescope operation.

The major design constrains in terms of feasibility and costs associated are listed below:

- Tracks alignment tolerances, cleanness and protection.

- Number of bearings.

- Cleanness and temperature control.

- Drive alignment tolerances, cleanliness and protection

- Inspection and maintenance operation.

- Stress concentration.
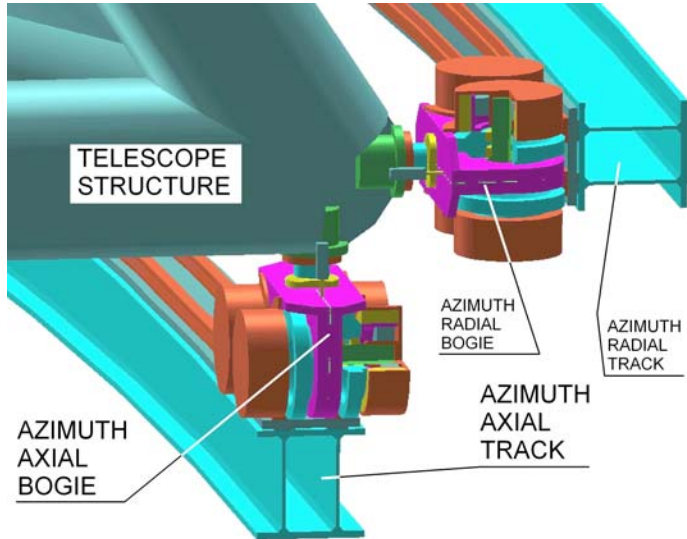
Figure 9-32: Axial and Radial Bogies.
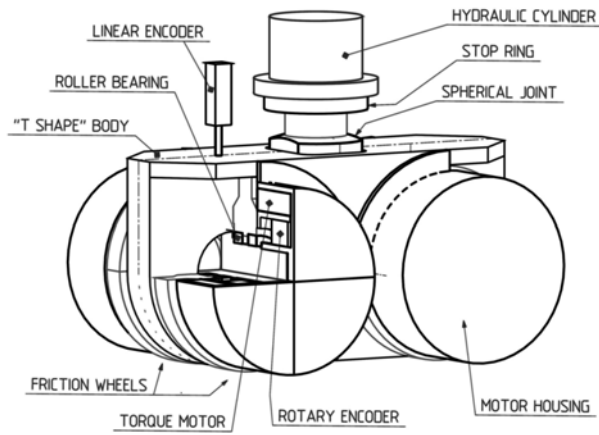
Figure 9-33: Bogie layout
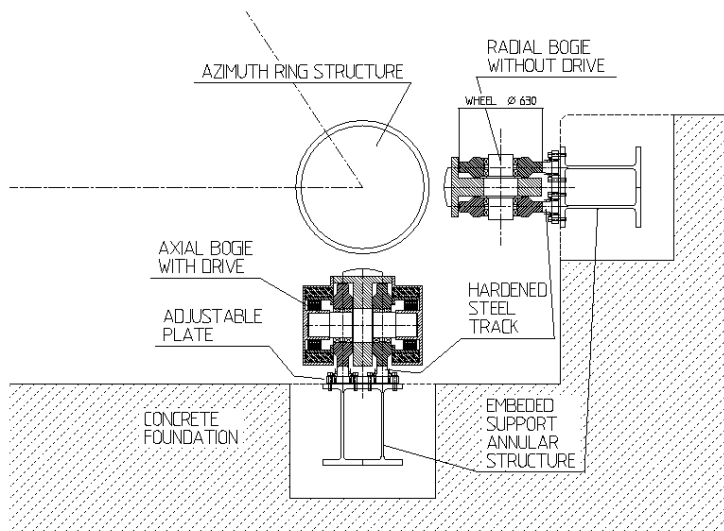
Figure 9-34: Axial And Radial Bogies cross section.

Telescope structure and kinematics

The large number of bogies, assures a smooth and homogeneous transfer of the loads to the site soil. Each bogie has 4 spherical or 4 cylindrical wheels, for the azimuth and altitude (cradle) flat tracks. Each wheel, with a diameter of 630 mm, is independently driven by a commercially available brushless ring torque motor, water cooled and equipped with an angular encoder. The required mean angular accuracy is 3 arcmin. at the wheel-motor axis. Each wheel has 2 self-aligning roller bearings.

In order to obtain homogeneous reaction forces on each bogie and consequently on the foundations, a "hydraulic whiffle tree" system is implemented, which consists of communicating hydraulic cylinders, their displacement being monitored by linear encoders. This whiffle tree system can be locked during observation to attain high dynamic performance.
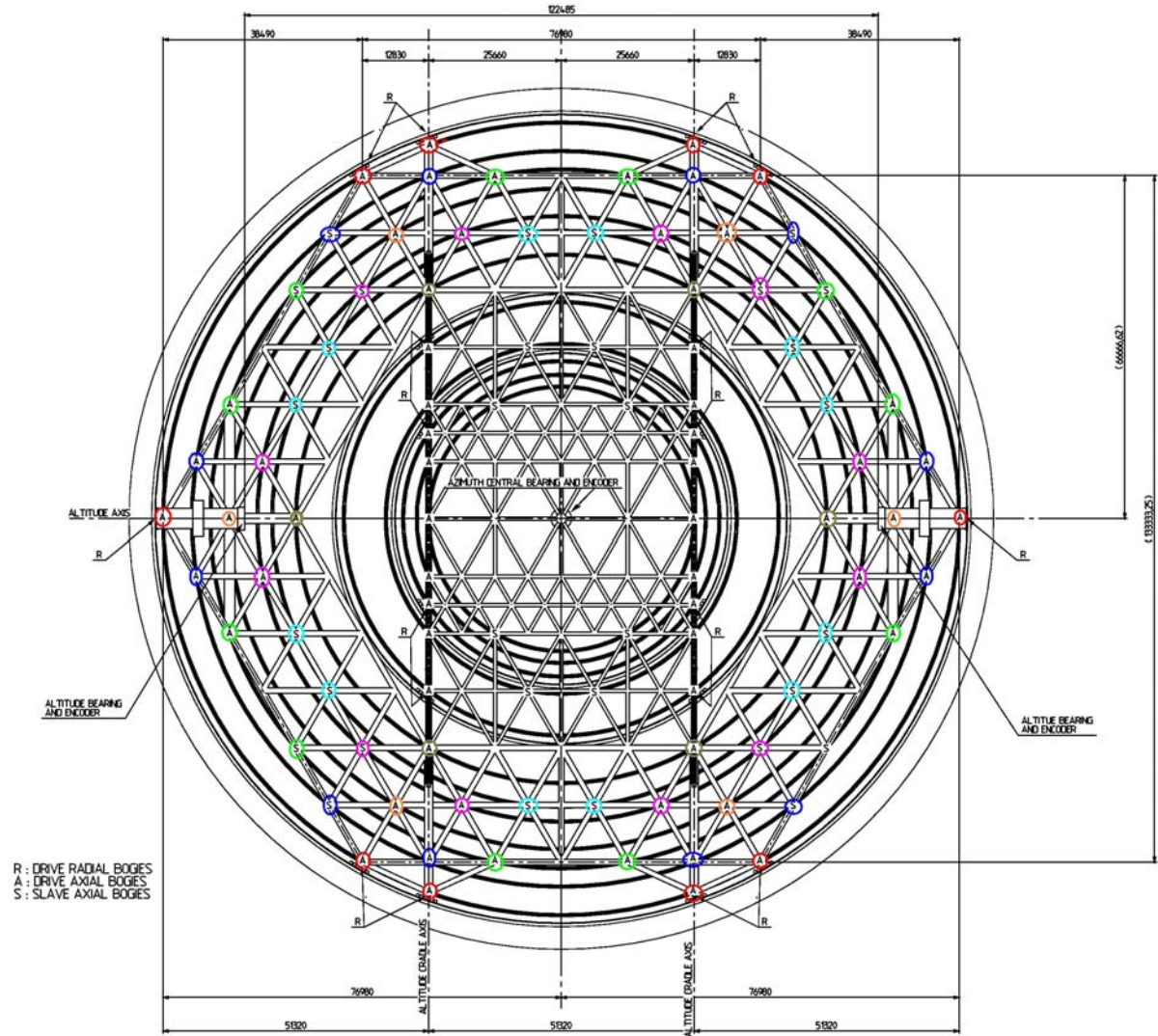
Figure 9-35: Azimuth bogies location.

Azimuth axis bogies system. - The azimuth structure integrates the azimuth bogies which are constrained by flexures (X and Y translation Degree of Freedom) and by Hydraulic jacks (Z translation DoF).

Technical solution implemented is shown in Figure 9-35 and consists of:

- Absolute "X-Y-Z" reference provided by the Azimuth central bearings

- 246 bogies attached to the azimuth structure.

Telescope structure and kinematics

- 192 axial bogies indicated with the letter "A" . The axial bogies support the entire mass of the telescope. This corresponds to about 80 tons per bogie.

- 54 radial bogies indicated with the letter "R". Each radial bogie is pre-stressed with a nominal force of 785 KN (These 54 radial bogies could be eliminated in the 2005 design).

- There are 12 axial tracks and 3 radial tracks (the 3 radial tracks could be eliminated in the 2005 design), shown in Figure 9-35. The mean track radius is 57.647 m. The reduction ratio Friction wheel / mean track radius is 1/183.

- The slip friction generated at the azimuth axis is 26,43 MNm.

- 32 slave bogies are indicated with the letter "S". These bogies do not have torque motor. Their function is to suppress local modes of the azimuth structure.

- In order to transmit the 1166 Nm peak torque of each drive motor the boogies shall be loaded with at least 20 tons.

Azimuth hydraulic wiffle tree - The main function of the hydraulic wiffle tree is to equalize the loads on the bogies. The key component hardware is described here below:

1. *Master bogies.*

   Six master axial bogies located at the 6 vertexes of the hexagonal shape of the azimuth structure.

   The stroke of the hydraulic cylinder of the master bogies, is controlled by the linear encoder (see Figure 9-33). An indicative hydraulic system diagram for double acting hydraulic cylinders is shown in Figure 9-36. However the bogies may also have single acting load return hydraulic cylinders, similar to "Pancake Locknut Cylinders". The final configuration will be defined after the breadboard test, see also Figure 9-38.

Figure 9-36: Computer controlled hydraulic cylinders of the master bogies

   A: Controller.

   B: Encoder.

   C: Sensor Cable.

   D: Valves (Needle, shut-off, check etc.) and pressure sensors.
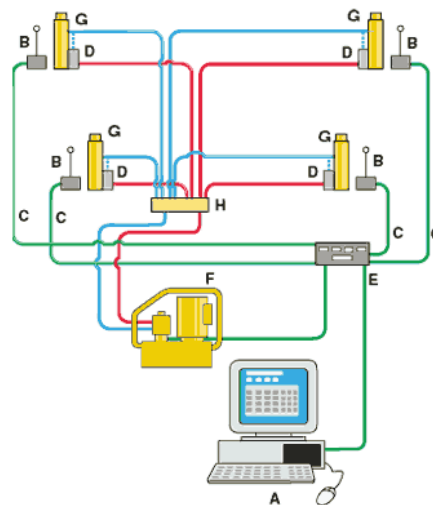
   E: Electro Box.

   F: Power Source.

   G: Hydraulic cylinder.

   H: Control Valve Manifold Assembly.

2. *Needle valves.*

    In order to compensate the low spacial frequency flatness tolerance of the axial tracks and the cylindricity tolerance of the radial tracks, all the hydraulic cylinders are connected together. Needle valves minimise the exchange of oil among the cylinders. Thus the high frequency dynamic performance of the telescope is kept. The needle valves have a low pass filter function.

3. *On-board leveling system.*

    The global horizontal flatness of the telescope is measured using a system which allows real time continuous measurements, similar to the one shown in Figure 9-37 and based on communicating vessels principle.

Figure 9-37: Communicating vessels measurement

Altitude axis bogies system.- Technical solution implemented:

- 154 bogies attached to the two cradles of the azimuth structure.

- 60 radial bogie located in the central parts of the 2 cradles, support the entire mass of the altitude structure. This corresponds to about 80 tons per bogie.

- 94 radial bogies located at the extremities of the 2 cradles. Each radial bogie is pre-stressed with a nominal force of 785 KN (about 80 tons).

- 2 identical cradle tracks attached to the altitude structure. The cradle track radius is 52 m. The reduction ratio Friction wheel / mean track radius is 1/165.

- The slip friction generated at the altitude axis is 14,14 MNm.

- In order to transmith the 1166 Nm peak torque of each drive motor the boogies shall be loaded with at least 20 tons.

Altitude hydraulic wiffle tree - The altitude hydraulic wiffle tree is based on the same principle of the azimuth hydraulic wiffle tree. The main differences are listed below:

- Absolute "X-Y-Z" reference supplied by the 2 altitude bearings.

- Grouping the bogies symmetrically with respect to the azimuth axis. This configuration allows to control the loads and the forces applied to the bogies with function of their vertical coordinate.

- Alternatively it may also be possible to have different hydraulic cylinder effective area with function of their vertical coordinate.

Friction - The friction assumptions are quite conservative. Improved surface qualities and accurate alignment can reduce considerably the friction. Measurements on the friction drive systems of the VLT show that the final performance of a friction drive system can be much better than that calculated during the design phase. In order to determine the correct value of the friction, prototypes of the bogie, shown in Figure 9-38, will be manufactured and tested. A

dedicated Friction characterization measurement campaign, is planned in the ELT Design Study (see appendix A-1.4). Further detail of the "Characterization of friction drive and bearings" can be found in the Statement of Work RD513 and Technical Specification RD514.
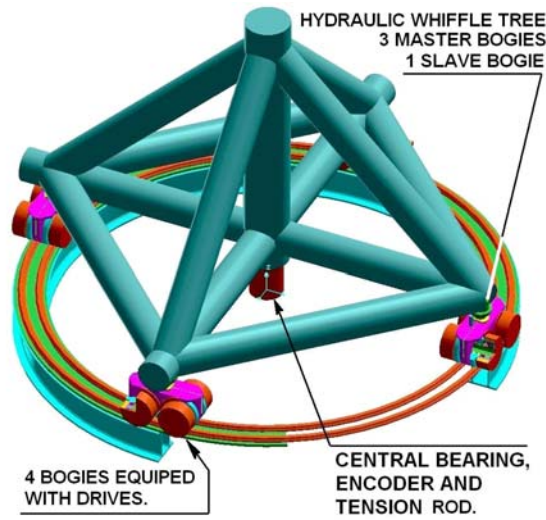
Figure 9-38: Bogies breadboard test setup

	Number of bogies.	Load per bogie [tons].	Number of wheels.	Load per wheel [tons].	Ratio wheel / track.	Number of mass loaded bogies.	Number of force loaded bogies.
Azimuth axis	246	76	984	19	1/183	192	54
Altitude axis	154	72	616	18	1/165	60	94

Table 9-3: Main axes friction drive and bearing topology.

	Nominal operational load per bogie [tons].	Minimum load per bogie [tons].	Minimum operational load per bogies [tons].	Maximum operational load per bogie [tons].	Survival load per bogie [tons].
Azimuth axis	80	15,09	20	150	240
Altitude axis	80	15,09	20	150	240

Table 9-4: Load cases.

	Total slip friction torque [MNm]	Yotal stick friction torque [MNm].	Roller bearings friction [MNm].	Total wind load torque [MNm].	Total acceleration torque [MNm].	Total required torque [MNm]
Azimuth axis	26.43	33.04	Negligible.	1.1	58.7	92.84
Altitude axis	14.14	17.7	0.15	7.1	19.6	44.55

Table 9-5: Main axes torque requirement.

	Torque motor type.	Continuous torque per motor [Nm]	Total continuous generated torque	Peak torque	Total peak torque

Telescope structure and kinematics

			[MNm].	[Nm]	[MNm].
Azimuth axis.	ETEL TMA 0530-050	859	**154.69**	1166	210
Altitude axis.	ETEL TMA 0530-050	859	**87.36**	1166	118.57

Table 9-6: Friction drive generated torque

The breadboard test will provide the following information:

- Stick and slip friction.

- Vertical and lateral stiffness.

- Pointing and tracking accuracy under wind disturbance.

- Performance of the hydraulic wiffle tree.

- Performance master and slave bogies concept.

- Performance of track misalignment compensation.

- Performance under load variations.

- Survival load case.

- Performance of the on-board hydrostatic leveling system.

- Test the control system.

- Test of alternative heavy-duty cycloidal drives.

- Induced vibration.

- Define maintenance criticality and concept.

- Identify suppliers.

- Costs evaluation.

9.4.5.1.4   Hydrostatic pads and direct drive.

During the 2002 Design iteration a detailed trade-off between Hydrostatic Pads and Direct Drive versus Friction Drive and Bearings has been performed.

	Direct drive & Hydrostatic bearing	**Friction Drive & Bearing (bogies)**
Azimuth tracks	87.3	12
Azimuth base plate	Not applicable	11
Azimuth understructure	15	12.8
Azimuth bearing	17.5	Not applicable
Azimuth drive	11.5	Not applicable
Azimuth bogies	Not applicable	21
Altitude cradle tracks	3.7	0.7
Altitude bearing	10	Not applicable
Altitude drive	4	Not applicable
Altitude bogies	Not applicable	4.5
Total	**149 MEuro**	**62 MEuro**

Table 9-7: Cost breakdown of OWL's drive and bearing systems

Telescope structure and kinematics

The following Table 9-7 compares the cost estimates associated to OWL's different drive and bearing systems. delivered ex works. Costs related to transport and integration on site are not shown.

Table 9-7 shows that the adopted solution of the telescope drive and bearing systems has a major impact on the total cost of the project. The difference in cost persists also for transport. integration on site and during the operational lifetime of the telescope in term of RAMS.

The main source of cost difference is the type of annular tracks. which have to be manufactured and aligned within the severe tolerance necessary to the hydrostatic bearings and direct drive systems. The values reported on the table are based on the 2002 design and extrapolation of the existing VLT systems

9.4.5.1.5   Magnetic Levitation.

Magnetic levitation (maglev) is a relatively new transportation technology in which non contacting vehicles travel safely at high speeds. while suspended. guided. and propelled above a guideway by magnetic fields. The guideway is the physical structure along which maglev vehicles are levitated. Figure 9-39. which show the Maglev system components applied to trains. depicts the three primary functions basic to maglev technology: levitation or suspension; propulsion; and guidance. In most current designs. magnetic forces are used to perform all three functions. although a nonmagnetic source of propulsion could be used.

These functions are also present in the drive and bearing systems of OWL. The similarity of functions can be better highlighted comparing Figure 9-39 and Figure 9-40 together.

The magnetic levitation bearings with integrated linear direct drives shall have the same functions as the friction drive and bearing systems tailored to OWL requirements. However some of the main critical requirements listed qualitatively in Table 9-8 differ from maglev transportation technology.

Radial and axial bearing forces.	Very High.
Tangential drive forces..	High.
Radial. axial and tangential stiffness.	Very High.
Accuracy	High.
Heat dissipation.	Low.
Energy consumption.	Low.
Induced vibrations.	Very Low.
System control.	Very High.
Electro Magnetic Compatibility	High
Reliability.	High.
Velocity.	Low.
Acceleration .	High.
Generated Friction.	Negligible.
Mechanical tolerances of the tracks.	Low.

Table 9-8: Maglev main requirements

To conclude this summary section. it can be stated that main major potential advantages of the maglev system applied to OWL. compared to other technology. are:

- Negligible friction.

- Low mechanical alignment tolerance of the tracks.

- Quasi perfect distribution of forces.

- High stiffness
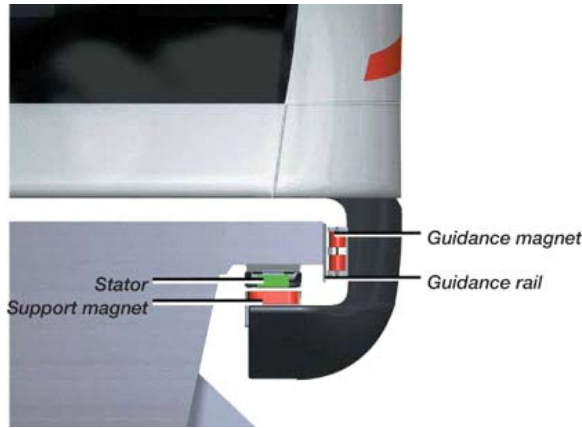
Figure 9-39. MagLev for trains
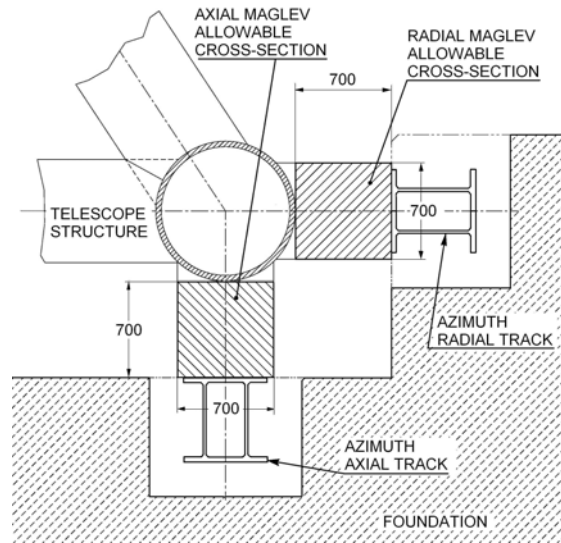
Figure 9-40. OWL MagLev available design location.

In the framework of the ELT Design Study. a dedicated study study will assess the feasibility and cost of the MagLev technology applied also to OWL main axes (see appendix A-1.4). Further detail of the study "Magnetically levitated systems and linear drives for ELT main axes" can be found in the study Statement of Work RD515.

This study will cover the following topics:

1. Conceptual design of the electro-mechanical system.

2. Generated forces vs. cost trade-off.

3. Stiffness vs. cost trade-off.

4. Gap vs. cost trade-off.

5. Conceptual design of the control system.

6. Define mechanical interfaces.

7. Analyses of performance.

8. Define maintenance criticality and concept.

9. Define suppliers.

10. Costs and schedule evaluation for a supply of ~ 300 meters of maglev system.

11. Final report.

Maglev generated forces - Each linear meter of the bearings and drives systems shall be able to generate as a minimum the forces reported in Table 9-9. during operation of OWL.

	Altitude Radial bearings & drives.	Azimuth axial bearings & drives	Azimuth Radial bearings & drives.
Linear Radial force [kN/m].	500	50	500
Linear Axial Force [kN/m].	50	500	50
Linear Drive Force [kN/m].	2	2	2

Table 9-9. Bearings & drives linear generate forces.

Telescope structure and kinematics

Maglev survival load case - During survival load case. the maglev system shall be able to generate forces which are 2 times the operational forces listed in Table 9-9.

Maglev minimum required stiffness - Each linear meter of the bearings and drives systems shall have as a minimum the stiffness reported in Table 9-10.

Characteristic	Altitude Radial bearings & drives.	Azimuth axial bearings & drives	Azimuth Radial bearings & drives.
Radial stiffness [N/mm/m].	20×10^6.	10×10^6.	20×10^6.
Axial stiffness [N/mm/m].	10×10^6.	20×10^6.	10×10^6.
Drive Stiffness [N/mm/m].	30×10^6.	30×10^6.	30×10^6.

Table 9-10. Minimum required stiffness.

9.4.5.2   Corrector.

The Corrector structure shown in Figure 9-41. is a steel trusses structure which copies the mirror segment hexagonal pattern. The trusses are made of cylindrical pipes.

It supports 2 Active mirrors (M3 and M4) and 2 Adaptive Mirrors (M5 and M6). It is equipped with a set of actuators which will supply alignment capabilities and can also compensate thermal and gravity deformation of the whole telescope structure in the x-y plane. The z axial bearing and actuator can re-focus the whole corrector.
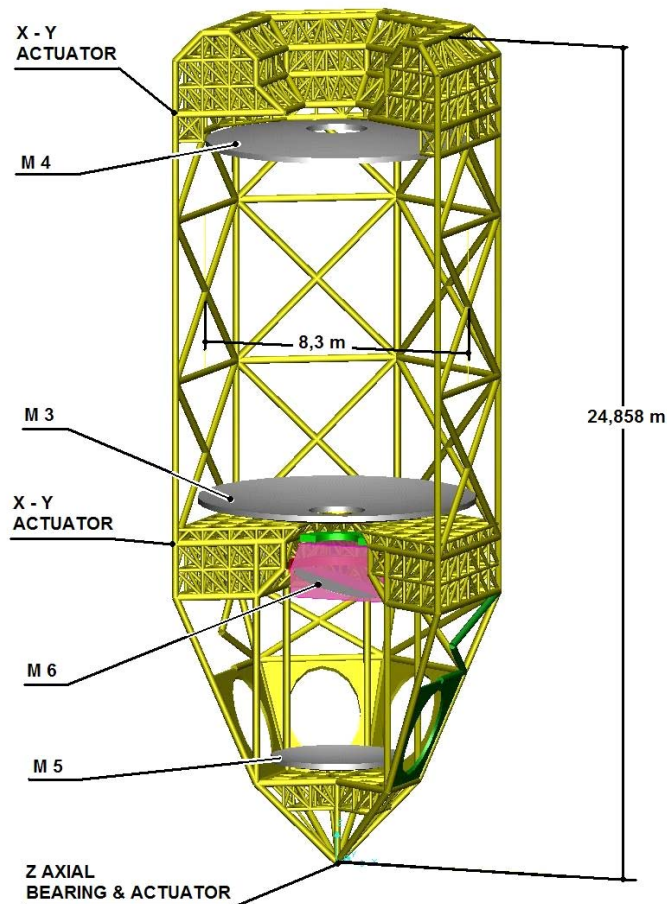
Figure 9-41: Corrector

9.4.5.3   M3 and M4 Unit

The M3 and M4 are 2 active mirror units with dimensions and mass similar to the VLT Primary mirror units. The baseline for the mirrors substrate is Glass Ceramic.

The corrector configuration allows:

- High stiffness of the 2 mirror cells.

- Comfortable design volumes around the mirrors.

9.4.5.4   M5 Unit

The M5 is an adaptive mirror unit with a 3.9-m adaptive shell. It provides active focusing. The baseline for the mirrors substrate is Glass Ceramic.

The corrector configuration allows:

- High stiffness of the mirror cell.

- Comfortable design volumes around the mirror.

9.4.5.5   M6 Unit

The M6 unit (see Figure 9-42 and Figure 9-43) is the most complex opto-mechanical unit in the corrector. It has a total mass of 4 tons. Its main functions are:

- Tip-tilt field stabilization. described in section 7.2.3. The field stabilization stage has a mass budget of 500kg.

- Adaptive optics. described in section 8.2.1.2.1.

- Directs the optical beam to the 6 focal station.
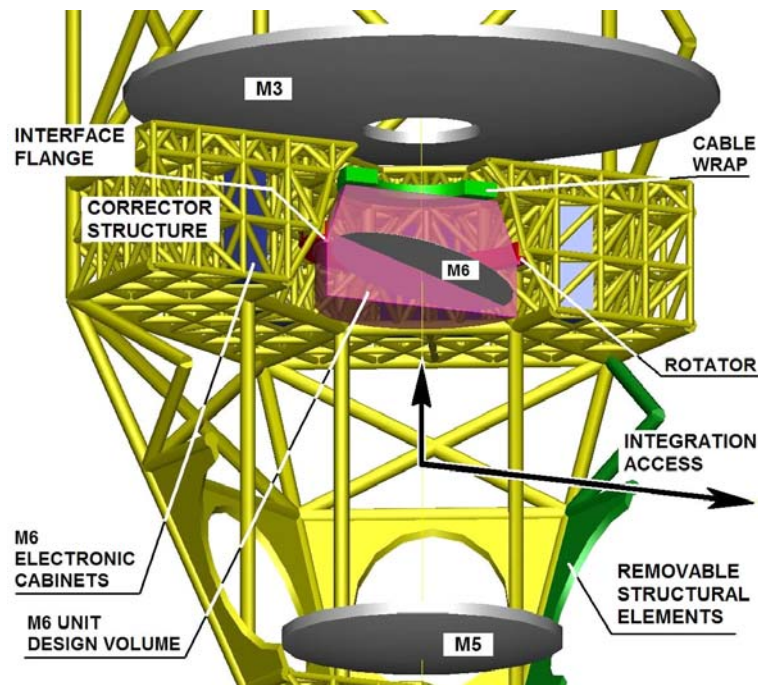
Figure 9-42: M6 lay out design and location

Telescope structure and kinematics
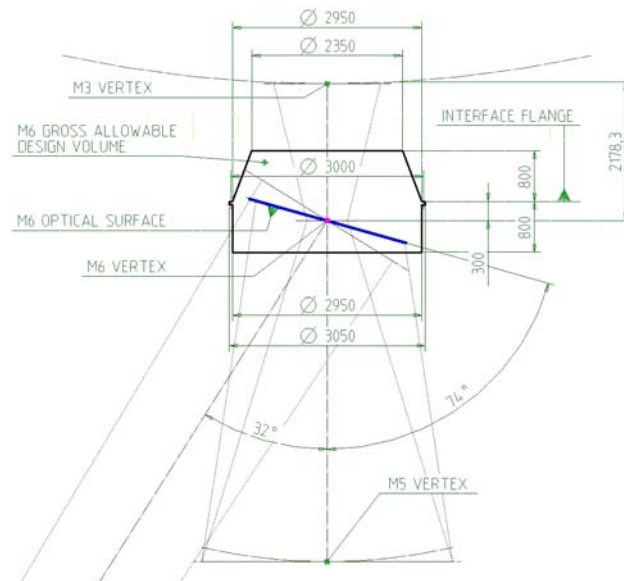
Figure 9-43: M6 unit overall dimensions.

9.4.5.5.1 Interface to the corrector.

The corrector is attached to a rotator bearing which is used to align the optical beam going out from the M6 to the 6 focal stations. The rotator bearing and its drive system are part of the corrector and provides the following interfaces:

- Mechanical

- Fluid and electrical supplies

- Signal

- Cable routing via a cable wrap.

9.4.5.5.2 M6 Unit design volume

Due to the intersection of several optical beams shown in Figure 9-44. the design volume shown in Figure 9-45 is restricted. This makes the inner design particularly challenging.

Figure 9-44: Optical bems intersection

Telescope structure and kinematics
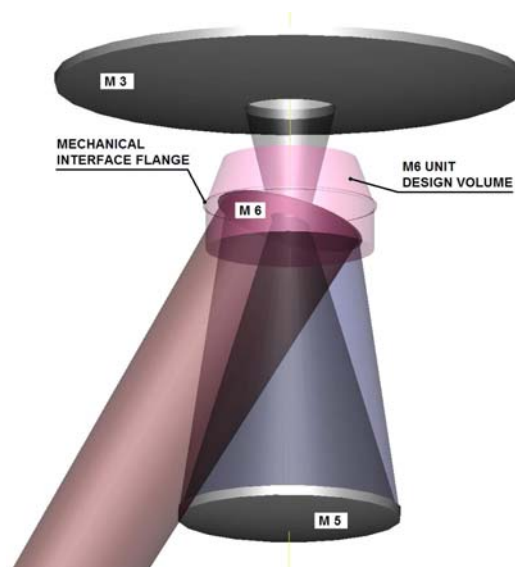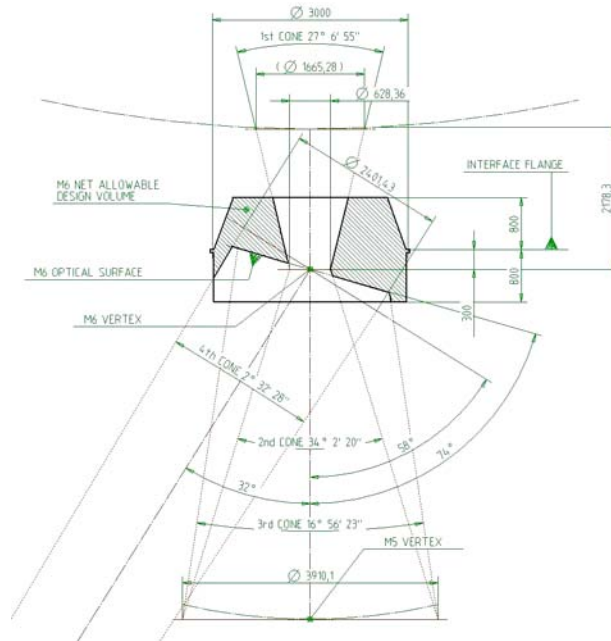
Figure 9-45: M6 available design volume.

9.4.6   Segments support system.

The surface of the OWL segmented mirrors must maintain the desired shape within an accuracy of a small fraction of the wavelength. This implies periodic re-adjustment of the piston and tip-tilt position of each segment at a frequency of a few Hz and within an accuracy of a few nanometers. The mirror shape is affected by external disturbances which can be classified in low and high temporal frequency:

- Low   Gravity and thermal variation.

- High   Wind buffeting.

The low temporal frequency disturbances imply a large stroke. typically several centimeters over time scale of several minutes or more. The high temporal frequency disturbances cause displacements of fractions of a millimeter. Therefore each segment is equipped with an active support (see Figure 9-46). including

- 1 Segment Support Structure

- 3 Position Actuators

  - Extractor

  - Coarse stage

  - Fine stage

- 18 axial support points whiffle tree system

- 1 Lateral support

  - Slave actuator

  - Membrane

- Hexagonal Segment

  - Edge sensors
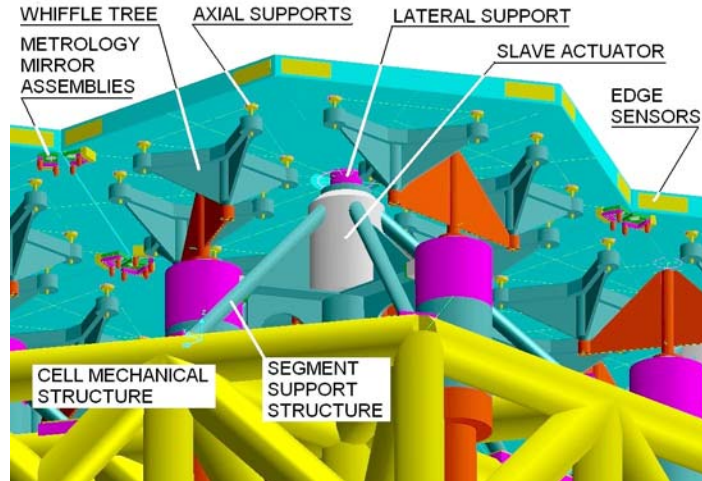
Figure 9-46: Segment support system.

9.4.6.1 Segment assembly.

The Position Actuators will be integrated into the mirror cell of the telescope mechanical structure and interface with the whiffle tree (see Figure 9-47). The whiffle tree distributes the axial loads of the hexagonal mirror segments. The Position Actuators may remain permanently mounted on the segment support structure.
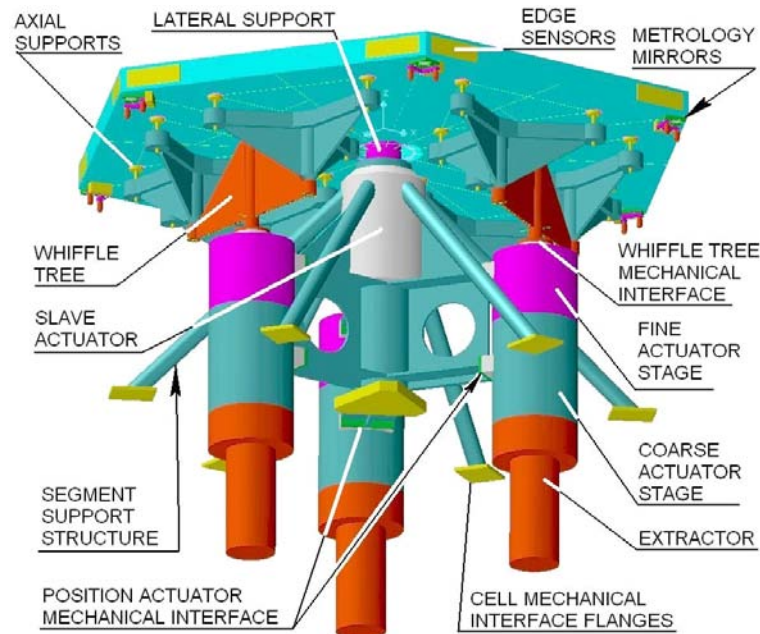
Figure 9-47: Hexagonal segment assembly

9.4.6.2 Extractors.

In order to simplify the handling of the hexagonal segments. each segment shall be extracted from the mirror (open configuration) using dedicated actuators called extractors. The extractor may also be integrated into the Position Actuator assembly. Once the segment is extracted from the mirror surface. a dedicated tool built in in the maintenance cover (see section 13.2.1.4 and 15.1.1.4) or in the M2 handling facilities (see section 15.1.1.6). will handle the segments to their way to the off-line maintenance facilities.

9.4.6.3   Position Actuators characteristics.

18 Position Actuator prototypes will be purchased in the frame of the ELT Design Study and tested on a Wind Evaluation Breadboard at the Observatory Roque de los Muchachos. La Palma (see section 9.4.7). Two types of actuators will have to be developed and manufactured:

- Position actuators for glass segments.

- Position actuators for lightweight Silicon Carbide segments.

The final Position Actuators performance specifications can be met using a two stages concept with coarse and fine stages or with a single stage concept. The required Position actuators performance are listed in the sections below.

9.4.6.3.1   Axial stiffness

The resonance frequency of a segment on its whiffle tree shall be at least 60 Hz. Therefore high axial stiffness is required for the Position Actuators.

The axial resonance frequency of a Position Actuator loaded with the masses indicated below shall be at least 120 Hz.

9.4.6.3.2   Load cases.

Compression Load

- Position Actuator for glass ceramic segments: 0 to 170 kg.

- Position Actuator for lightweight SiC segments: 0 to 60 kg.

- The continuous load changes are due to the rotation of the telescope altitude structure from horizon to zenith (around X axis).

Tension Load

- For the OWL secondary mirror. the Position Actuators are also compatible to tension loads equal to compression loads.

Wind load

- The wind buffeting on segments is a random process and it is defined by statistical parameters. An apprpriate description is the Power Spectral Density (PSD). Wind perturbation is characterized by the PSD of the wind speed. Based on which a theoretical model of the wind load perturbations can be obtained (Von Karman model). Assuming a mean wind speed of 10 m/s acting on the surface of each segment (1600 mm flat to flat) the RMS load is estimated to be 25 N (temporal values of wind load could reach values of 60 N).

9.4.6.3.3   Accuracy.

Two stages Position Actuator Concept

- Coarse stage   ± 0.05 mm   Goal ± 0.01 mm

- Fine stage   ± 5 nm   Goal ± 2 nm.

- Extractor   1 mm (open configuration)

One stage Position Actuator concept

- Accuracy   ± 5 nm   Goal ± 2 nm.

9.4.6.3.4   Stroke

The stroke of the Position Actuator shall compensate for the following sources of deformation:

- Gravity.

- Thermal.

- Track misalignment.

- Wind pressure on segments.

- Wind pressure on mechanics.

The strokes specified below consider the worst case assumption.

Two stages *Position Actuator* Concept

- Coarse stage   15 mm   Goal 30 mm

- Fine Stage   0.5 mm   Goal 1 mm

- Extractor   150 mm.

One stage PA concept

- Stroke   15 mm   Goal 30 mm

9.4.6.3.5   Closed Loop Bandwidth.

These specifications shall be met assuming a 100 Hz bandwidth of the metrology signal and an infinitely rigid support system.

Two stages PA Concept

- Coarse stage   0.5 Hz.

- Fine stage   10 Hz   Goal 20 Hz.

- Extractor (not applicable. only open and close configurations).

One stage PA concept

- Closed Loop Bandwidth   10 Hz   Goal 20 Hz.

9.4.6.3.6   Maximum tracking rate

During observation of an astronomical object. OWL altitude structure can reach a maximum angular velocity of 15 degrees per hour. During this operation the PA shall compensate for the deformation of the altitude structure due to gravity acceleration (see coarse stage stroke goal 30 mm). This deformation follows cosine function during the altitude rotation. e.g. minimum at zenith maximum at horizon.

PA Maximum tracking rate: 0.0025 mm/s.

Accuracy ± 5 nm. Under wind disturbance as per section 9.4.6.3.3.

Accuracy goal ± 2 nm. Under wind disturbance as per section 9.4.6.3.3.

9.4.6.3.7   Maximum slewing rate

When OWL goes from one astronomical object to the next or during maintenance operations. the altitude structure of the telescope can reach a maximum velocity of 0.1 degree/s. During these operations the PA shall compensate for the deformation of the altitude structure due to gravity acceleration (see coarse stage stroke goal 30 mm). This deformation follows cosine function during the altitude rotation. e.g. minimum at zenith maximum at horizon. The PA shall maintain the mirror segment within the range of the edge sensors ± 0.5 mm. This deformation follows cosinus function during the altitude rotation. e.g. minimum at zenith maximum at horizon.

PA Maximum slewing rate: 0.06 mm/s.

Accuracy ± 0.1 mm.

9.4.6.3.8 Heat dissipation.

During operation. the external surface of the PA and of its electronic cabinets shall not exceed 1 ºC above ambient temperature at 0 m/s wind velocity.

Active cooling of the PA is regarded as an increase of complexity and shall be avoided.

Active cooling of the PA electronic cabinets is regarded as an increase of complexity and shall be avoided.

9.4.7 Wind Evaluation Breadboard

In order to define the objectives for the control of wind buffeting disturbance on OWL segmented mirrors. an electro-mechanical set-up called Wind Evaluation Breadboard will be realised in the frame of the FP6. which will simulate the real operational constrains applied to large segmented mirrors. Further detail of the "Wind Evaluation Breadboard" can be found in the Statement of Work RD507. and Technical Specifications RD503.

For the WEB the following critical sub-systems will be procured:

- 18 Position Actuator Prototypes. described in RD502 and RD503.

- 24 Edge Sensors. described in RD504 and RD505.

9.4.7.1 WEB layout.

The main WEB sub-systems and components shown in Figure 9-48. are listed below.

1. Seven hexagonal panel assemblies.
    1.1. Aluminium hexagonal panels.
        - 3 heavy type.
        - 3 lightweight type.
        - 1 master central panel
    1.2. Segment Support Structure.
    1.3. Metrology mirrors assemblies.
    1.4. Support and Phasing system.
        - 18 axial support points structure (Whiffle Tree).
        - 1 lateral central support point structure.
        - 1 slave actuator.
        - Torsion rods.
        - Fine actuators.
        - Coarse actuators.
        - Edge sensors.
        - Extractor.
2. Cell.
    2.1. Trusses structure.
    2.2. Hinges.
3. Base frame.
    3.1. Structure.
    3.2. Pads.
    3.3. Altitude Tilt actuator.
    3.4. Azimuth actuator.
4. Rear support structure.

Telescope structure and kinematics

5. Wind Skirt board.

6. Track.

7. Optical metrology set-up.

    7.1. Control Electronic.

    7.2. Hardware.

8. Software.

9. Civil engineering sub-systems

    9.1. Enclosure.

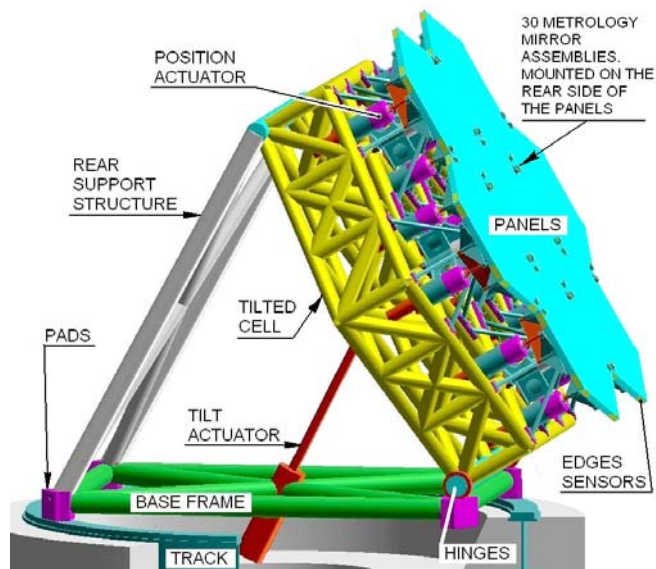   9.2. Foundation.

Figure 9-48: Layout of WEB.
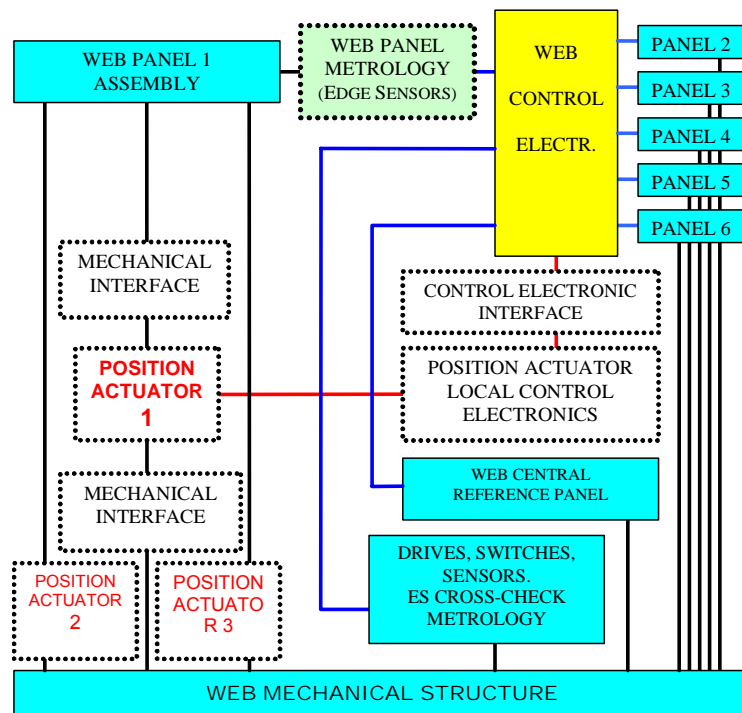

Figure 9-49: WEB Functional Layout.

Telescope structure and kinematics

Figure 9-49 show the functional layout of WEB and the interface between:

- WEB structure and kinematics
- Position actuators
- Position Sensors
- Metrology
- Control Electronics

9.4.8 Internal Metrology

Several internal metrology systems can be integrated in the telescope structure. These systems have the function of supplying absolute reference and measurements during stand-by and observation and maintenance modes. The main intended use of the internal metrology is to actively compensate the low frequency telescope deformation due to gravity and thermal disturbances.

The following telescope sub-systems are monitored by the internal metrology within a typical accuracy of 0.5 to 1 mm along the X-Y-Z axes. at low frequency rate (0.01 Hz) and over a maximum range of 160 m:

- Primary mirror.
- Secondary mirror.
- Corrector.
- Azimuth structure (horizontal level only).

Off-the shelf industrial products meet the requirements. Such products include

- Fibre optic based extensometer RD504.
- Laser tracker.
- Hydrostatic levelling system (see Figure 9-37).

9.4.9 Thermal control and design provision

9.4.9.1 Thermally controlled volumes

The following volumes shown in Figure 9-50. are thermally controlled during the day:

- Primary mirror: Total volume 102845 m3.Only for glass ceramic mirror substrate.
- Secondary mirror: Total volume 4115 m3.. Only for glass ceramic mirror substrate.
- Corrector: Total volume 4801 m3.
- Focal stations: Total volume 6172 m3.

These locations can be air conditioned via conduits which can be connected to the cooling facility located in the technical room. These connections can be realised in the vertical and horizontal parking positions.

Telescope structure and kinematics
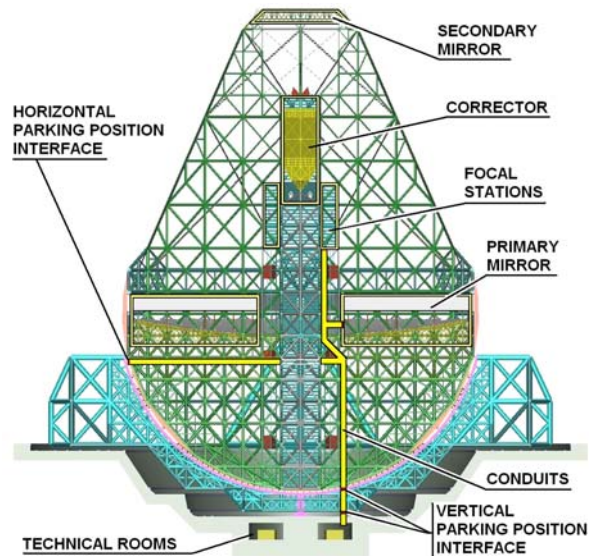
Figure 9-50: Air conditioning layout

9.4.9.2   Passive thermal control of the mechanical steel structure.

The mechanical steel structure of the telescope does not need to be thermally controlled. The large heat exchange area of the mechanical elements. along with their thin wall thickness. assures a very low thermal inertia. Experimental data (see section 5.4.1.3) and analysis show that the mechanical steel structure can enter in to temperature regime with the ambient air within few minutes after sunset.

If necessary the fractal design made of cylindrical pipes (see Figure 9-51) also allows an inner air flow. thus further reducing the thermal inertia of the telescope mechanical structure.

The inner air volume contained in the mechanical structural pipes is:

• Azimuth structure 20480 m3.

• Altitude Structure 18235 m3.

• Total volume 38715 m3.

The total volume of OWL structural pipes corresponds to about one VLT enclosure volume.

Figure 9-51: Inner ventilation.

9.4.10   Safety

The telescope structure concept has embedded safety provisions in the design. against hazards which can be generated during transport and integration (see section 13.2.2) as well as during maintenance and operation (see section 15.1.2). Particular attention has been paid to:

Telescope structure and kinematics

o Environmental hazards during integration.

o Human access to subsystems during maintenance and.operation.

9.4.11   Mass & Moment breakdown.

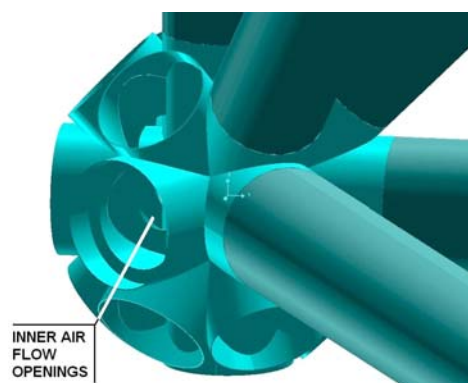The mass and moment breakdowns are given in Table 9-11 and Table 9-12.

SUB-SYSTEMS.	Corrector [Tons]	Altitude structure [Tons].	Total Mass. [tons].
M1 - 3048 glass ceramic hexagonal segments.		1158.2	
M1 whiffle tree and actuators.		304.8	
M2 - 216 glass ceramic hexagonal segments.		82.08	
M2 whiffle tree and actuators.		21.6	
M3 and actuators.	31.5		
M4 and actuators.	30.5		
M5 and supports.	8.25		
M6. tip-tilt cell and actuators.	4		
Corrector steel pipes structure.	57		
Total corrector unit.	131.85	131.85	
Instrumentations (6 instruments).		90	
Altitude structure steel pipes and kevlar ropes.		7242	
Total altitude structure.		8918.63	8918.63
Total azimuth structure.			5415.9
Miscellaneous (electronics. cabling. piping. stairs. lifts. cat-walks. paint. welds etc.)			500
Total telescope rotating mass.			14834.53
Azimuth tracks.			~ 4500

Table 9-11: Telescope mass breakdown

AXES	MASS MOMENT OF INERTIA [KG M^2].
Altitude.	1.123×10^{10}
Azimuth	3.368×10^{10}

Table 9-12: Mass moment of inertia

9.5   Structural analysis

Structural analyses have been performed to assess the feasibility of the structural baseline design. The analyses are based on a set of global FE Models of the 2004 (see 9.3.6) OWL structure representing the altitude angle configurations 0º. 30º. 60º and 90º from zenith. Some analyses and analyses studies presented herein are based on the 2002 design (see 9.3.5) of OWL. Each configuration forms a different geometry with different number of interface bogies between altitude and azimuth structure. The FE Model in the zenith configuration is shown in Figure 9-52 and the side view of the 60º model including the boundary conditions is displayed in Figure 9-53.

The 2004 FE model comprises about 146000 elements and 40000 nodes representing 238000 degrees of freedom. The framework structure is modelled with pipe elements and the ropes with link elements. The latter transmit only longitudinal forces and no moments. The primary mirror segments as well as the mirrors M3 to M6 are represented as distributed mass elements which are connected to the cell structures by appropriate beam elements. The secondary mirror segments are modelled as shell elements connected to the M2 cell structure by appropriate beam elements. The mass of the M2 elements correspond to the real mass of the segments and their support system. The mirrors supporting structures are not modeled in detail. but their stiffness and mass is taken into account. The mirrors used in the baseline models are based on Zerodur material.

The altitude and the azimuth bogies are modelled as beam elements that represent the stiffness and mass assumptions described in RD33. RD13. The contact stiffness between the bogies' wheels and the rails has been taken into account. The connection of the altitude bogies in lateral x-direction is simulated only for the dynamic analyses. because in this case lateral forces are transmitted due to the friction of the bogies' wheels. In the static and stress analyses this degree of freedom connection is released. The hydraulic whiffle-tree system which provides a smooth reaction force distribution among the bogies is not simulated in the FE models presented herein. This is considered to be a conservative assumption in terms of stresses in the regions close to the bogies.

The mass budget of the FE Model corresponds basically to the mass breakdown listed in Table 9-13. A mass and mass moment of inertia summary extracted from the FE Model in zenith configuration is provided in Table 9-13. In order to take into account the "miscellaneous" additional mass allocation of 500 tons. the density of the steel has been adapted accordingly.
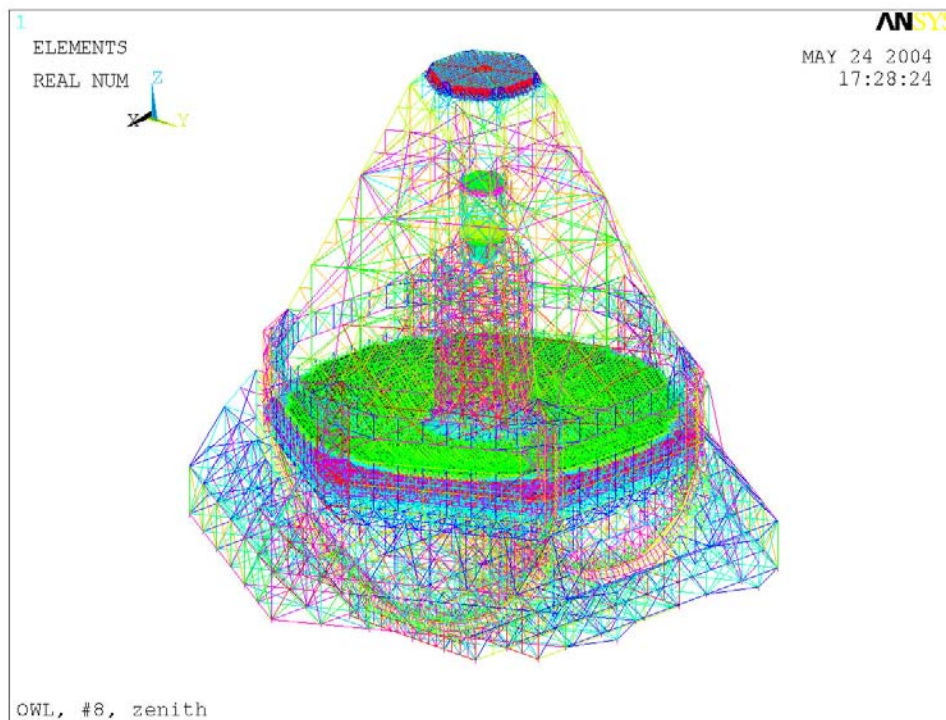

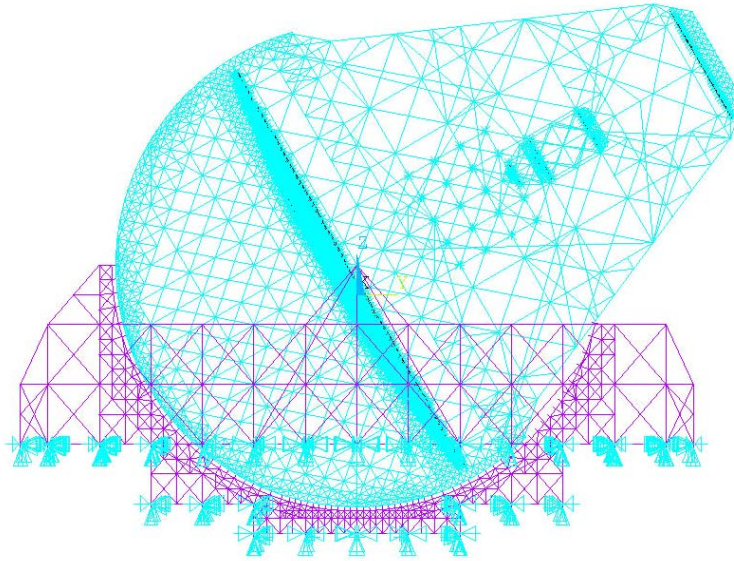*Figure 9-52: FE Model of OWL in zenith configuration.*

Figure 9-53: Side view of FE Model of OWL 60º from zenith.

Structure	Mass [ton]	Mass moment of inertia [kgm^2 *10^{10}]	CoG[66] [m]	Remarks
Altitude	8919	1.123	-0.370	Inertia of altitude structure about altitude axis
Azimuth	5416	3.368	-30.060	Inertia of complete structure about azimuth axis
Total	14287		-11.625	

Table 9-13: Mass and inertia budget of the FE model in zenith configuration.

The ground is assumed to be infinitely stiff and the model is fixed at the lower end of the azimuth bogies in the longitudinal directions. The influence of the foundation and soil stiffness to the telescope performance has been studied and is described in section 9.5.4.3.

The structural models used are adapted to the particular analyses for which they have been used and are accurate enough to provide a good representation of the structural behaviour in terms of displacements and frequencies. Local effects and stresses are usually simulated in the global models less accurately and will be evaluated with detailed local models if needed.

9.5.1   Analysis tree

The analysis tree shown in Figure 9-54 provides an overview of most of the analyses carried out during phase A. The flow chart describes the hierarchical order and the interconnections between requirements. design. analyses and results in a systematic way. Details of other disciplines and related interconnections like optics and control are not shown in this flow-chart.

---

[66] z coordinate with respect to altitude axis.
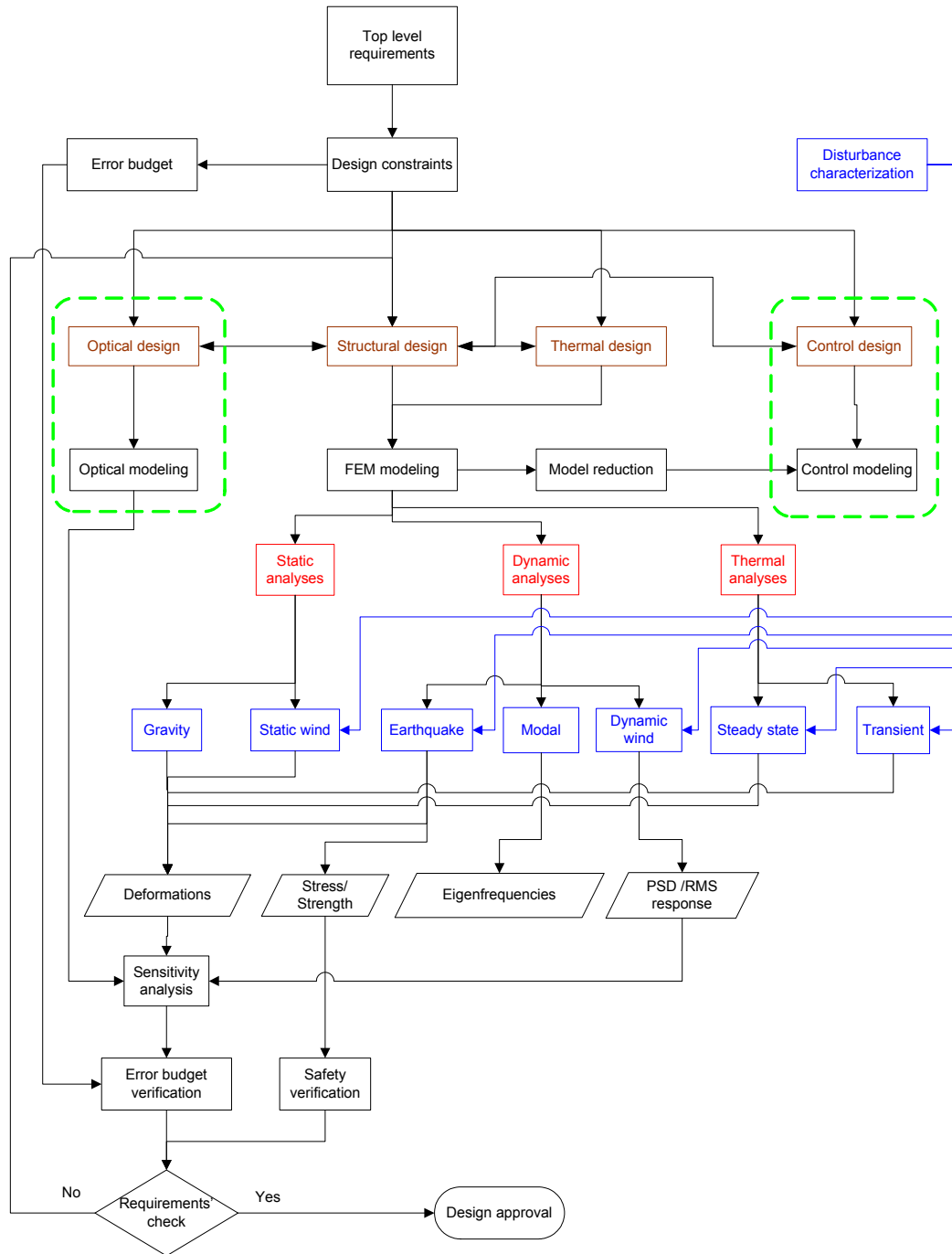
Figure 9-54. Analysis tree flow chart.

9.5.2   Static Analysis

The static analyses are based on the global FE models described above and aim at calculating the deformations and stresses under operational conditions like gravity and static wind load. The deformations of the optical components are used to define the required maximum range of the segment position and corrector actuators which are supposed to correct the static misalignments. In addition the rigid body (rb) displacements and rotations of the optical components are calculated based on a best-fit approach and multiplied with the optical sensitivity matrix to evaluate the individual influence of each mirror on the image motion error budget (see section 6.3.5). This will be very useful for further design improvements and optimisation studies in phase B.

9.5.2.1   Gravity

This section describes the analyses performed to evaluate the absolute and differential deformations due to gravity for the maximum operational altitude angle ranging from zenith to 60º. The gravity analyses include a certain initial vertical shift between the Altitude and Azimuth structures at the level of the main bearings. This shift of 15 mm has been preliminary optimised in a separate analysis run in such a way to transfer more load of the weight of the altitude structure through the main bearings and to reduce the maximum stress due to gravity.

The appropriate global 2004 models for zenith and 60º configuration have been analysed separately to calculate the differential displacements when the telescope is turning from zenith to 60º. Table 9-14 lists the differential global mean displacements of the optical elements in terms of piston. tilt and decenter. The differential piston and tilt between M2 and M1 is calculated to be 3.4 mm and 13.1 arcsec. respectively. These quasi-static errors will presumably be compensated for by the corrector actuators. As the secondary mirror is flat. its lateral decentre is irrelevant.

In order to define the required strokes of the segment position actuators. the local PTV displacements of the M1 and M2 segments have been evaluated and the worst case values are summarized in columns PTV of Table 9-14. Hence. the total required coarse segment actuator stroke results in 11 mm which includes 10.1 mm from the M1 piston and 0.9 mm contribution from the mirror segments tilt. i.e. 147 arcsec tilt corresponds to 0.9 mm actuator piston assuming an actuator distance of 1.2 m.

Mirror	Piston [mm]		Tilt [arcsec]		Decenter [mm]	
	rb	PTV	rb	PTV	rb	PTV
M1	7.8	10.1	0.3	147.1	13.2	8.8
M2	11.2	2.8	13.4	132.7	30.8	1.1
M3	12.0	2.1	-43.6	25.6	22.9	0.4
M4	13.0	1.7	-35.4	82.3	24.7	0.8
M5	11.1	1.7	-57.0	159.5	21.8	0.3
M6	12.1	0.6	-43.4	20.7	22.7	0.3
M2 - M1	3.4		13.1		17.6	

Table 9-14: Differential rigid body motions of the optical elements due to gravity.

The displacement distribution of the telescope under gravity load is displayed in Figure 9-55 and Figure 9-56 for the zenith and 60º configuration. respectively.

Fairly high stresses occur in the framework structure under gravity load. The maximum von Mises stresses in the order of 250 MPa occur in a region below the M1 segment supporting structure. In order to meet the stress safety requirements. several measures can be taken:

- Reinforce the framework structure in the critical areas by increasing the cross sectional areas of the beams

- Modify the topology of the framework structure in the critical regions (this has been already done in the 2005 model)

- Use higher strength steel in the critical areas. e.g. St52 instead of St37

The yield strength limits of the steel materials used are 240 MPa for St37 and 327 MPa for St52 and the ultimate tension strength limit of the steel cables is 1500 MPa.

It is foreseen to carry out an optimisation analyses campaign during phase B of the project. to evaluate the optimum beam cross-sections as well as optimum pretension of the ropes under various load scenarios.
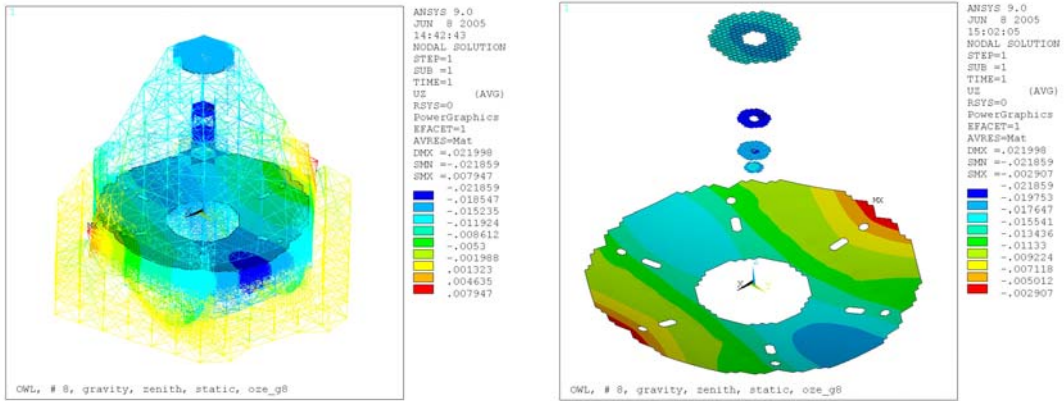
Figure 9-55: Vertical uz displacement distribution due to gravity for zenith configuration. Complete structure (left) and mirrors M1 to M6 (right).
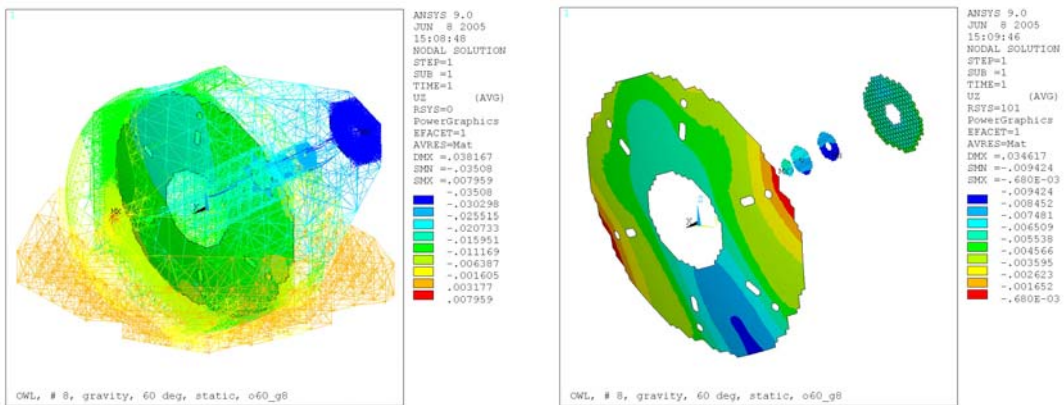

Figure 9-56: Displacement distribution due to gravity for 60º configuration. Complete structure in global vertical uz direction (left) and mirrors in normal displacements (right).

9.5.2.2   Steady State Wind

To estimate the influence of the steady state contribution of the wind loading. the deformation of the telescope has been calculated for a mean wind speed of 10 m/s. The corresponding pressure load distribution as described in section 5.4.1.1 is based on a wind speed profile and drag coefficients defined in standard norms. Three different altitude configurations (zenith. 30º and 60º) of the 2004 model have been investigated by applying pressure equivalent static forces. The rigid body displacements and rotations as well as the PTV errors of the optical elements were evaluated and the worst case values are listed in Table 9-15 for M1 and M2 in terms of piston. tilt and decenter. The maximum piston and tilt error occur for the 60º configuration and are -0.41 mm and 1.3 arcsec. respectively. These errors will presumably be compensated for by the fine segment position actuators. According to the PTV displacements of the M1 and M2 segments the required stroke of the fine segment position actuators is minimum 0.6 mm. Due to the small rigid body deformations of 0.4 mm a compensation of these errors with the fine segment position actuators will be investigated in the next phase.

Figure 9-57 shows the deformation of the optical elements for the 60º altitude configuration. The colours indicate the mirrors' normal displacements in meter.

Mirror	Piston [mm]		Tilt [arcsec]		Decenter [mm]	
	rb	PTV	rb	PTV	rb	PTV
M1	-0.29	0.60	1.30	4.57	-0.18	0.11
M2	-0.41	0.16	1.21	6.32	-0.80	0.03

Table 9-15: Worst case rigid body and PTV motions of M1 and M2 segments due to static wind.

```
ANSYS 8.1
MAY 20 2005
14:57:19
NODAL SOLUTION
STEP=1
SUB =1
TIME=1
UZ        (AVG)
RSYS=20
PowerGraphics
EFACET=1
AVRES=Mat
DMX =.935E-03
SMN =-.635E-03
SMX =-.304E-04
        -.635E-03
        -.567E-03
        -.500E-03
        -.433E-03
        -.366E-03
        -.299E-03
        -.232E-03
        -.165E-03
        -.975E-04
        -.304E-04
OWL, # 8, 60 deg, locked, wind, static, ow60_w8
```
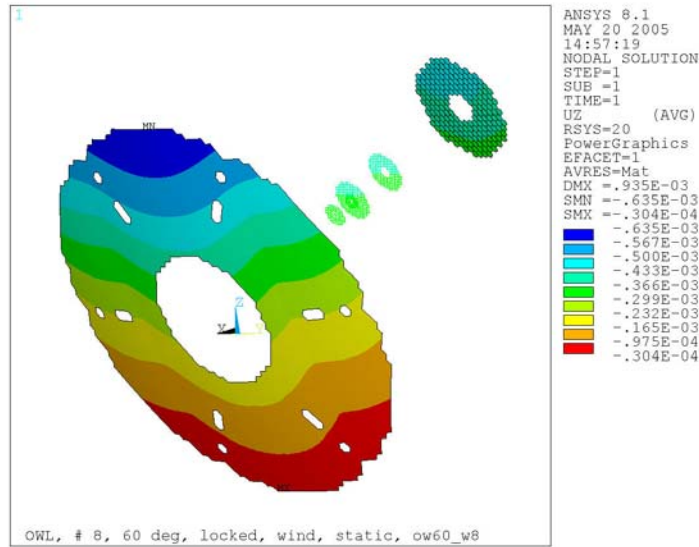
Figure 9-57. Normal displacement distribution of optical elements under static wind at60º.

9.5.3   Thermal analysis

The purpose of the thermal analyses described in this section is to predict temperature distributions of the OWL structure due to a set of nominal and accidental load case scenarios defined in section 5.4.1.3. The appropriate analysis results are used to assess the maximum segment position actuator ranges for maintaining the initial optical alignment requirement. The thermal analyses carried out are supposed to cover the following load conditions:

- The enclosure is closed and the telescope experiences a uniform temperature increase (nominal).

- The enclosure is closed and the telescope is exposed to a linear temperature gradient from bottom to top (nominal).

- The enclosure cannot be closed during the day and the telescope is exposed to direct sun radiation and outside air (accidental). This case covers also the thermal conditions during the installation process of the framework structure.

In the analysis models the thermal compensation system of the structural ropes. as well as the whiffle-tree systems of the altitude and azimuth bogies are not activated. Since this situation may occur in accidental cases like malfunctioning or failure of these systems. the effect on the thermal stresses are investigated and considered as worst case scenarios.

Based on the existing structural FE Model of OWL (2004 version) a simplified thermal FE model has been built which is able to calculate the steady state temperature distribution caused by sun radiation and natural convection with ambient air temperature. The convection coefficients and heat flux input load have been adapted to obtain the maximum temperature measured in the thermal experiments of a steel pipe on Paranal (see section 5.4.1.3). The thermal computations carried out until now are steady state analyses with conservative assumptions. but the thermal models allow performing transient analyses too. The accidental load cases comprise 17 different load configurations when the Enclosure is exposed to sun radiation during the day. Three different altitude angle configurations are combined with six different sun directions. After the calculation of the temperature distribution with the thermal FE model the appropriate displacements and stresses were computed with the structural FE model of OWL with the boundary conditions applied for the modal analysis.

Details about the thermal FE model. the analysis assumptions and results can be found in RD50.

The first nominal load case simulates a uniform temperature change of 10 °C (see 5.4.1.3. site 2) with respect to the reference (stress-free) temperature applied to the complete structure. This

load case represents a fairly conservative assumption. i.e. the temperature inside the enclosure follows directly the outside ambient air temperature. Due to this temperature change the M2 unit moves 17 mm in vertical z-direction (see Figure 9-58). This complies very well with a simple hand-calculation of a steel beam elongation with an equivalent length length of 147 m. The maximum radial displacement at the level of the primary mirror segments is calculated to be 7 mm at the outer edge. Hence. the maximum radial offset between two mirror segments is about 0.3 mm. This is well within the specified value of 4 mm.
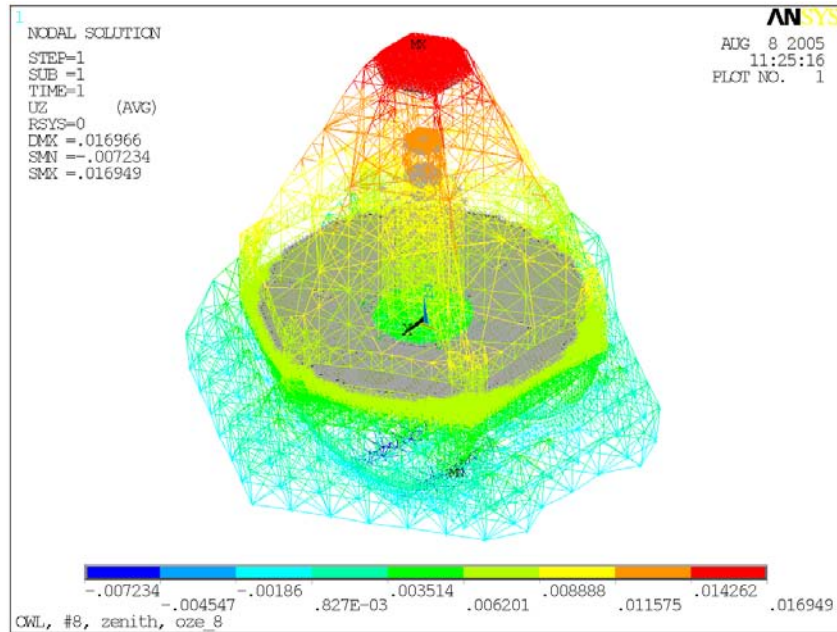
Figure 9-58: Vertical z-displacement distribution due to uniform temperature change of 10° C.

The corresponding von Mises stress distribution in the steel structure is displayed in Figure 9-59 with a maximum value of about 60 MPa occurring in the top region of the altitude bogies. The general stress level in the structure is fairly low. Stress peaks occur only in the overconstrained support and interface regions (bogies and structural ropes interfaces).

Figure 9-59: Equivalent stress distribution due to temperature change of 10° C.

Telescope structure and kinematics

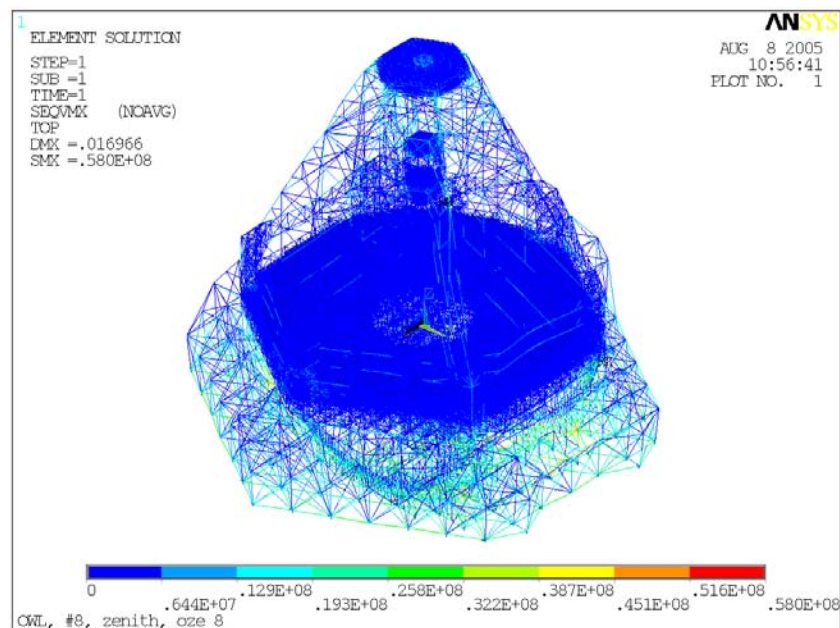The second nominal load case represents a linear temperature gradient of 10 °C from bottom to top. The appropriate displacement and stress results are much smaller than those of the first nominal load case.

Thermal accidental load conditions may happen if the enclosure cannot be closed during daytime. To simulate these cases the heat flux of the sun radiation has been applied in a simplified linear way by calibrating the external heat flux and the convection coefficient such to obtain in an equivalent pipe model the maximum measured temperature in the pipe experiment described in section 5.4.1.3.

Figure 9-60 shows a typical temperature distribution due the sun radiation direction at 60° altitude and 0° azimuth angle. The ambient temperature is 20 °C and the telescope is pointing to zenith. The maximum temperature is calculated to be 41 °C which complies with the highest average temperature measured in the pipe experiment on Paranal. The colder (blue) parts of the structure are located in the shadow of M1 and M2 which is taken into account in the analysis. As displayed in the deformation plot in Figure 9-61 this unsymmetric load scenario causes a global tilt of 45 arcsec of the secondary mirror unit with a maximum displacement of 27 mm in vertical direction. The differential displacement between M1 and M2 is 22 mm. which is confirmed by an equivalent hand-calculation assuming a temperature change of 20 °C in the structure between M1 and M2 (length 96 m).The resulting equivalent stresses in the framework structure are shown in Figure 9-62 with a maximum value of 163 MPa. Like in the other load cases the general stress level is fairly low and the peaks occur only in the overconstrained regions already mentioned before. The worst case tensile stress calculated for the structural ropes is 47 MPa due to thermal loading.
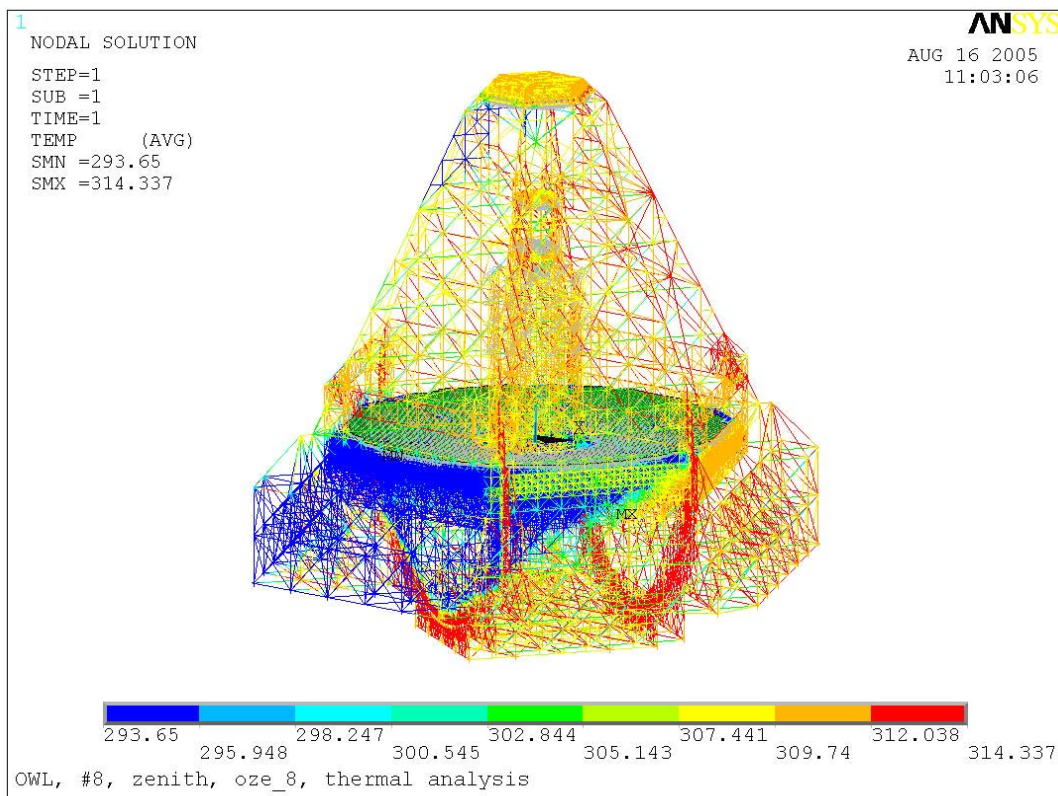
Figure 9-60: Temperature distribution due to sun radiation at 60° altitude angle.

For all load cases investigated until now a maximum stress of 182 MPa has been calculated. which is still below the allowable limit stress even under several conservative assumptions appearing simultaneously.

The overall maximum relative displacement between M1 and M2 is 25 mm for an altitude angle of 30° and a sun direction angle of 60°. This error occurs during the day and doesn't need to be compensated as long as the segment phasing is kept.

Figure 9-61: Vertical (uz) displacement distribution due to sun radiation at 60° altitude angle.

Figure 9-62: Equivalent stress distribution due to sun radiation at 60° altitude angle.

9.5.4 Dynamic Analysis

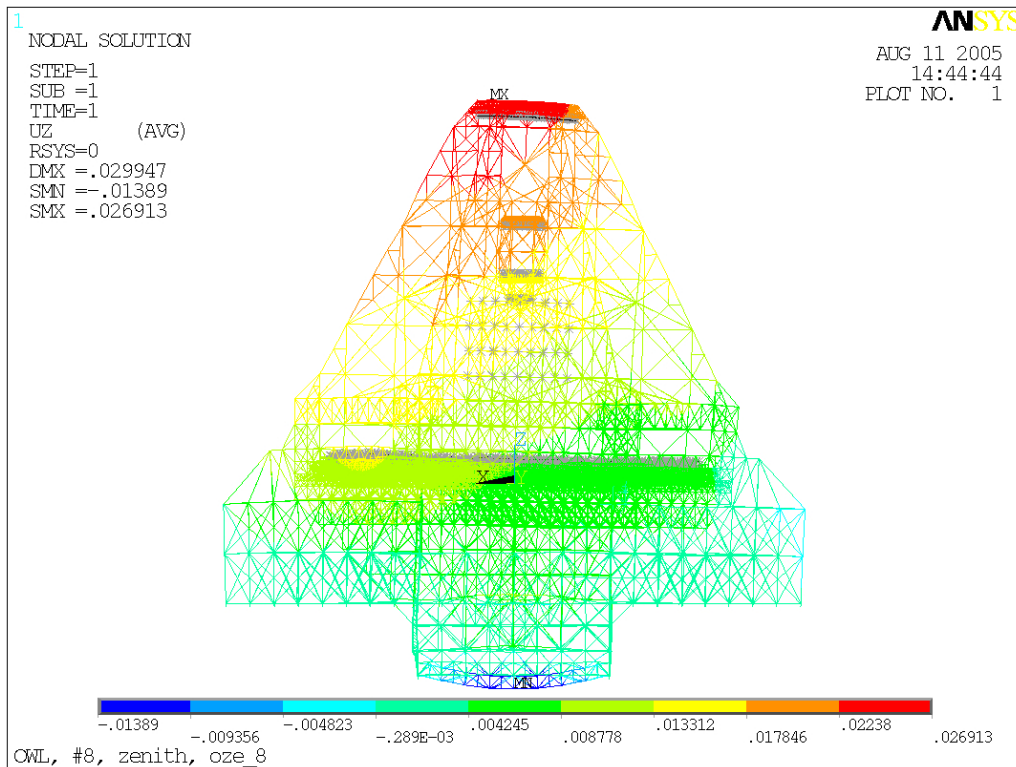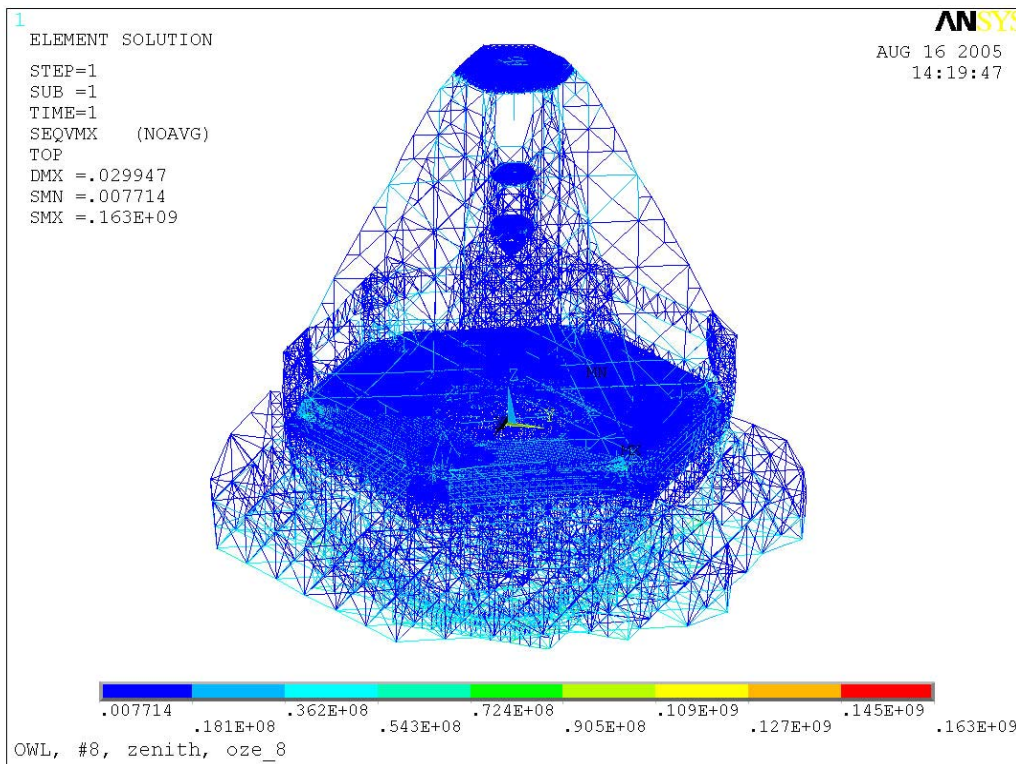The basic scope of the dynamic analyses is to predict the dynamic behaviour of the telescope structure. The modal analysis aims at calculating the natural frequencies and mode shapes. The dynamic wind load analysis described in this section is able to evaluate the open loop response of the optical subsystems in terms of global RMS deformation due to the wind load spectrum defined in section 5.4.1.1

9.5.4.1 Modal

In order to assess the response to dynamic loading and the bandwidth limitations for the various control systems of OWL. it is important to calculate the eigenfrequencies. mode shapes and corresponding effective masses of the OWL structure. Therefore. modal analyses have been carried out with the global 2004 FE models for various altitude configurations. The lowest 2000 modes have been calculated for the zenith configuration to cover frequencies up to 16.8 Hz. Until now 700 modes (~11 Hz) have been computed for the other configurations. A summary of the predominant eigenfrequencies. effective masses and mode shapes is provided in Table 9-16.Table 9-17 and Table 9-18 for the 0º. 30º and 60º altitude configurations. respectively.

Mode	Frequency	Effective mass / inertia in % of total						Mode shape
		MX	MY	MZ	IXX	IYY	IZZ	
1	1.59	67	-	-	-	2	-	Cross elevation
2	**2.58**	**-**	**30**	**-**	**29**	**-**	**-**	**Altitude locked rotor**
3	**2.86**	-	-	-	-	-	**44**	**Azimuth locked rotor**
6	3.67	-	35	-	12	-	-	2nd alt. locked rotor (counter motion)
7	3.93	**-**	**-**	11	**-**	**-**	**-**	Piston M2
9	**4.03**	-	-	**46**	-	-	-	**Piston altitude structure**
260	**7.32**	-	-	**0.1**	-	-	-	**Piston M2 unit structure**

Table 9-16: Eigenfrequencies and effective masses of zenith configuration.

Mode	Frequency	Effective mass / inertia in % of total						Mode shape
		MX	MY	MZ	IXX	IYY	IZZ	
1	1.55	67	-	-	-	2	-	Cross elevation
2	**2.49**	**-**	**27**	**-**	**31**	**-**	**-**	**Altitude locked rotor**
3	**2.92**	**-**	**-**	**-**	**-**	**-**	**42**	**Azimuth locked rotor**
6	3.83	-	30	3	10	-	-	2nd alt. locked rotor (counter motion)
7	**3.92**	**-**	**-**	**47**	**-**	**-**	**-**	**Piston Altitude structure**

Table 9-17: Eigenfrequencies and effective masses of 30 º configuration.

Mode	Frequency	Effective mass / inertia in % of total						Mode shape
		MX	MY	MZ	IXX	IYY	IZZ	
1	1.56	67	-	-	-	2	-	Cross elevation
2	**2.06**	-	28	1	32	-	-	**Altitude locked rotor**
3	**2.83**	-	-	-	-	1	**39**	**Azimuth locked rotor**
6	**3.63**	**-**	**18**	**28**	**28**	**-**	**-**	**Piston and Altitude bending**
7	3.78	-	14	22	22	-	-	2nd piston and alt. rotor (counter m.)

Table 9-18: Eigenfrequencies and effective masses of 60 º configuration.

The lowest natural frequency for all configurations is the cross elevation mode at about 1.6 Hz. which is a lateral motion of the Altitude structure along the altitude axis. This mode is dominated by the stiffness around the altitude cradles and has been already increased significantly by changing the design topology in this region in the 2005 model. The most important modes in terms of main axis controllability are the locked rotor frequencies about the altitude and azimuth axis. respectively. While the Azimuth locked rotor frequency is above 2.8 Hz for all configurations. the Altitude locked rotor frequency decreases from 2.58 Hz at zenith down to 2.06 Hz at 60º from zenith. This performance reduction is caused by the reduced number of altitude bogies in contact. The lowest piston mode of the M2 structure is calculated to be 3.9 Hz for the zenith and 3.6 Hz for the 60º configuration. The piston mode of the M2 unit structure occurs at 7.3 Hz in the zenith configuration and will be excited by the wind load. The mode shapes of the predominant eigenfrequencies for zenith configuration are shown in Figure 9-63. Figure 9-64. Figure 9-65 and Figure 9-66. respectively. As already mentioned a significant improvement of the dynamic performance in terms of locked rotor eigenfrequencies has been obtained. i.e. more than 20 % frequency increase compared to the former design iteration (2002).
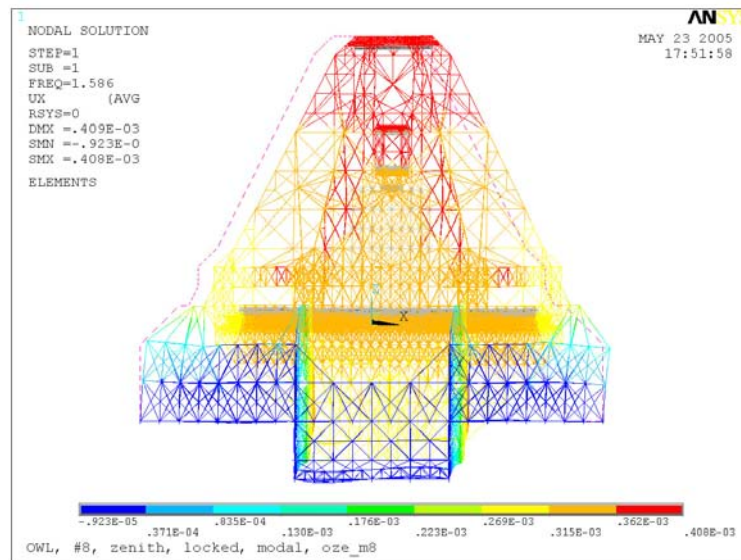
Figure 9-63: Mode shape of first eigenfrequency in zenith configuration at 1.59 Hz.
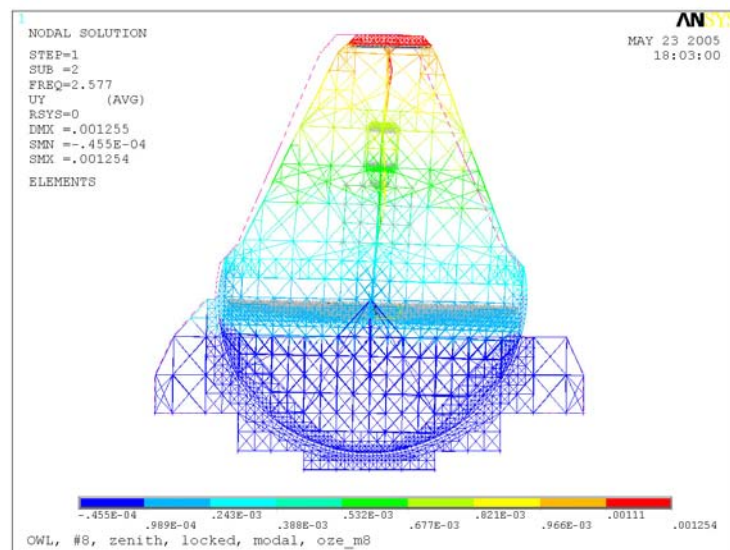

Figure 9-64: Altitude locked rotor mode shape in zenith configuration at 2.58 Hz.
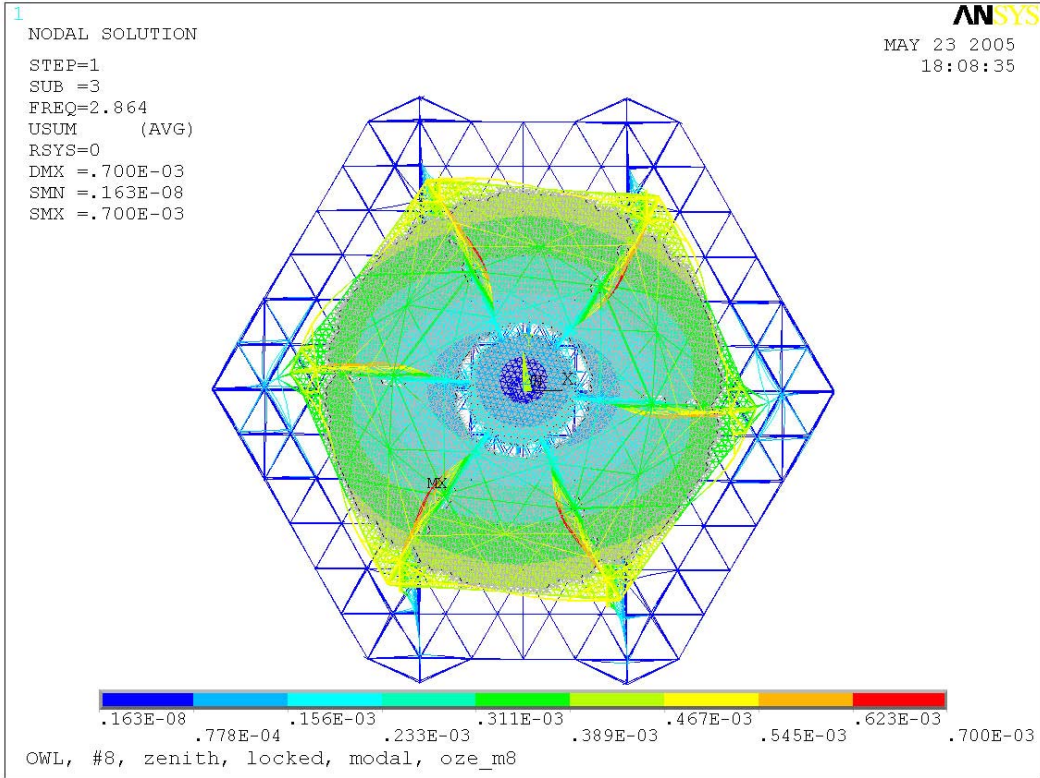
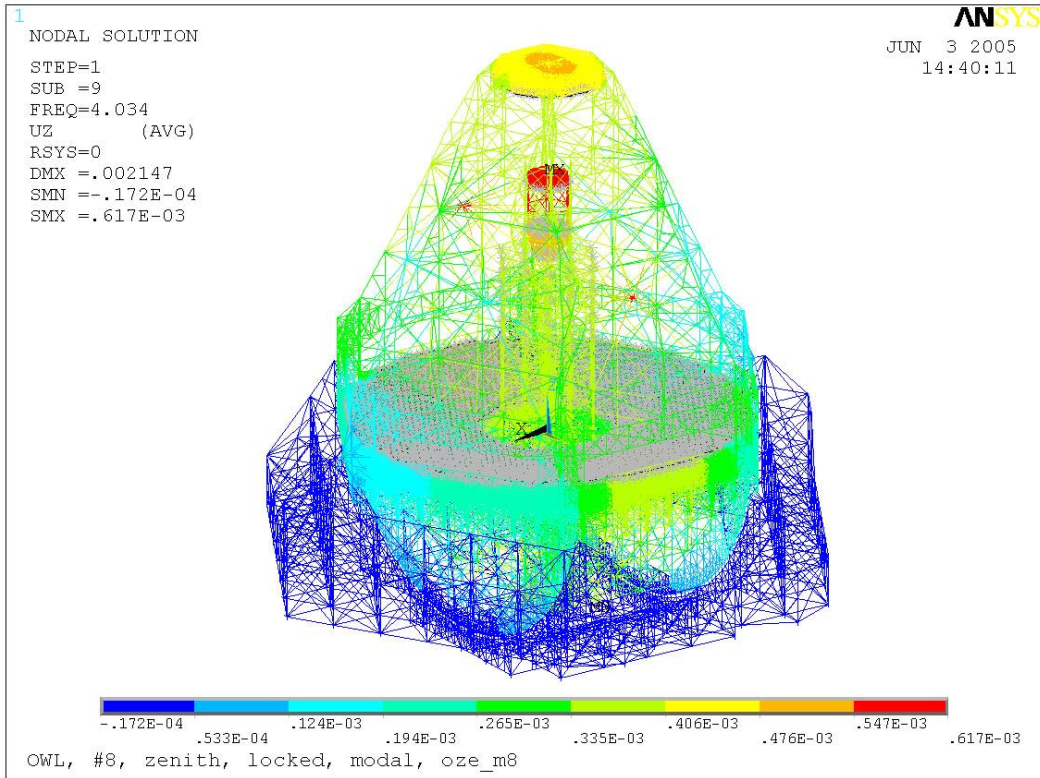*Figure 9-65: Azimuth locked rotor mode shape in zenith configuration at 2.86 Hz.*

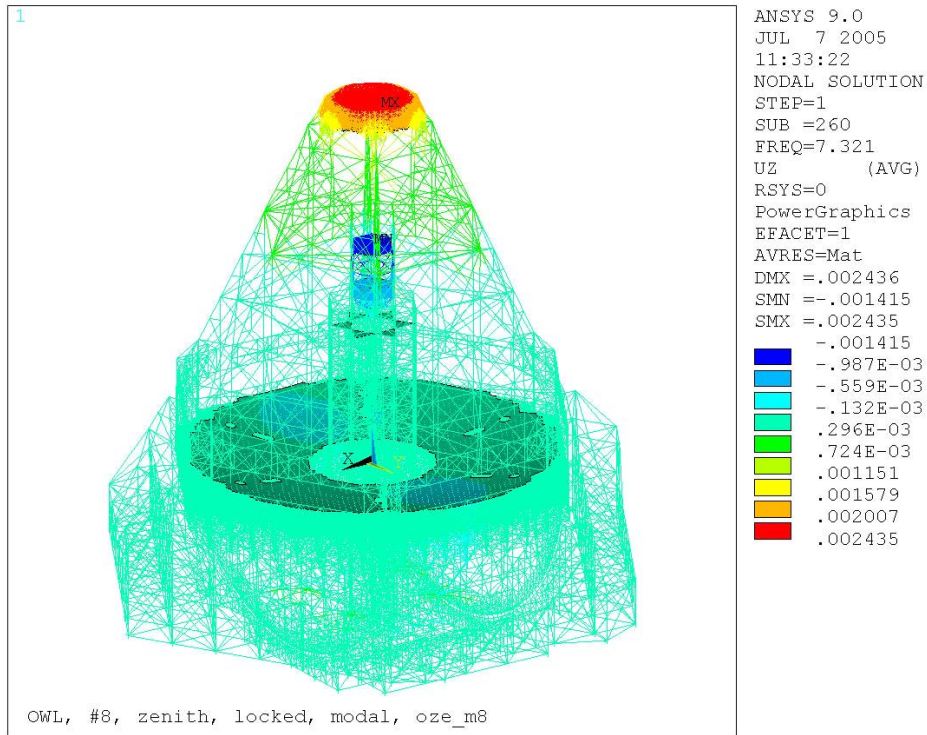*Figure 9-66: Piston mode of altitude and corrector structure at 4 Hz.*

Figure 9-67: Piston mode of M2 unit structure at 7.3 Hz.

In order to evaluate the dynamic behaviour of the M1 and M2 cell structures. the corresponding parts of the global FE model have been extracted and modal analyses performed. The M1 cell structure has been fixed at the altitude bogies and the main bearings and the M2 cell structure at the interface to the upper interface part of the altitude framework structure. Both the models are shown in Figure 9-68.

Figure 9-69 displays the lowest piston mode of the M1 cell structure alone. It forms a kind of spherical shape and occurs at 5.1 Hz. This mode corresponds to the 4 Hz piston mode computed in the global model. The lowest piston mode of the secondary mirror cell structure alone occurs at 7.75 Hz forming a spherical shape. The corresponding mode of the global model occurs at 7.3 Hz
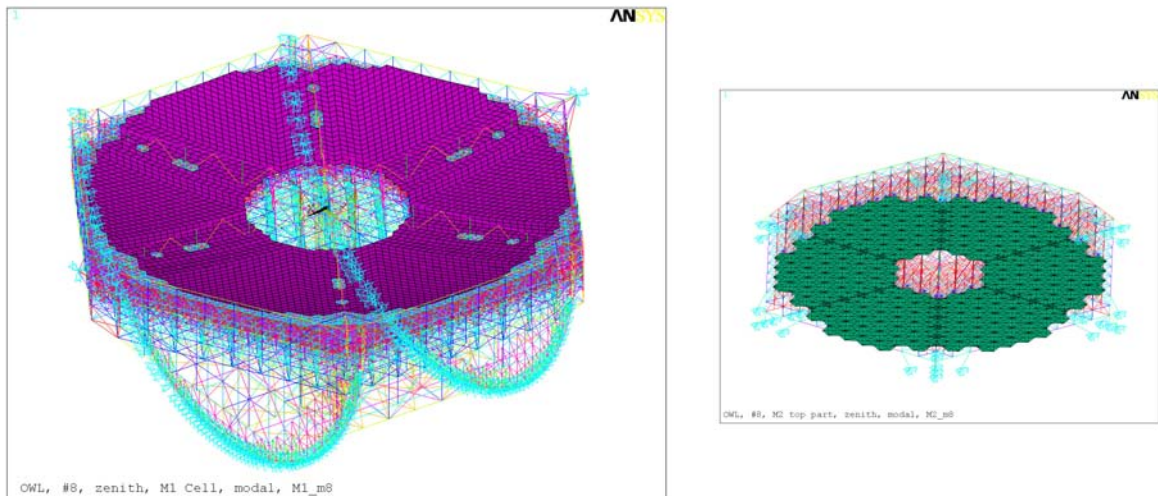

Figure 9-68: FE models of M1(left) and M2 cell (right) structures. respectively.
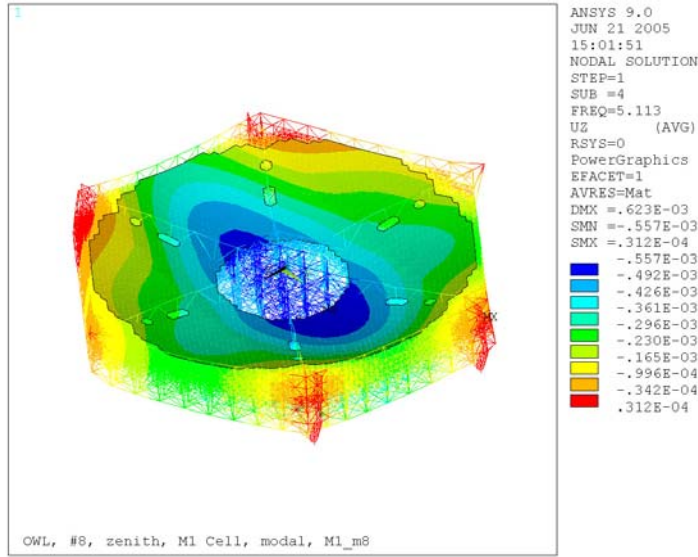
```
ANSYS 9.0
JUN 21 2005
15:01:51
NODAL SOLUTION
STEP=1
SUB =4
FREQ=5.113
UZ        (AVG)
RSYS=0
PowerGraphics
EFACET=1
AVRES=Mat
DMX =.623E-03
SMN =-.557E-03
SMX =.312E-04
     -.557E-03
     -.492E-03
     -.426E-03
     -.361E-03
     -.296E-03
     -.230E-03
     -.165E-03
     -.996E-04
     -.342E-04
      .312E-04
```

OWL, #8, zenith, M1 Cell, modal, M1_m8

Figure 9-69: Piston mode of M1 Cell structure alone at 5.1 Hz.


```
ANSYS 9.0
JUN 21 2005
11:54:54
NODAL SOLUTION
STEP=1
SUB =187
FREQ=7.755
UZ        (AVG)
RSYS=0
PowerGraphics
EFACET=1
AVRES=Mat
DMX =.00498
SMN =-.203E-03
SMX =.004907
     -.203E-03
      .365E-03
      .933E-03
      .0015
      .002068
      .002636
      .003204
      .003771
      .004339
      .004907
```

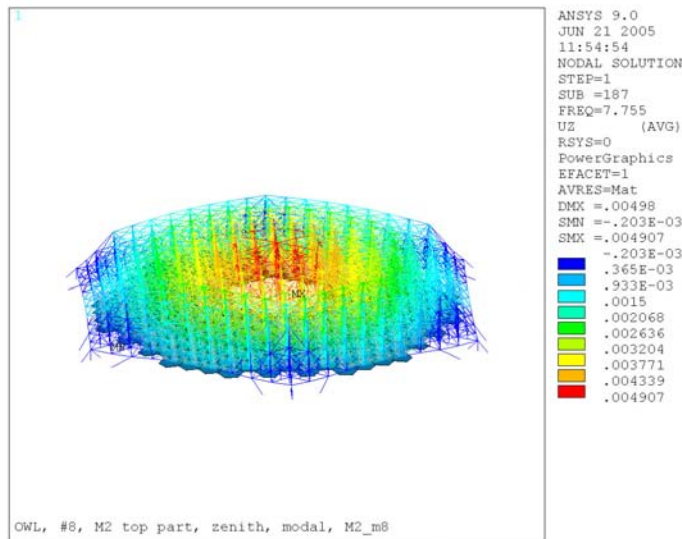OWL, #8, M2 top part, zenith, modal, M2_m8

Figure 9-70: Piston mode of M2 cell structure alone at 7.8 Hz.

Figure 9-71 shows the natural frequencies versus the mode number for the zenith configuration. The 2000 frequencies are closely spaced and distributed in the range between 1.6 and 16.8 Hz. The first flat plateau represents about 200 modes at 6.3 Hz with very small effective mass contributions. The second plateau occurs at about 8 Hz and covers about 40 modes. All these modes are related to local rotational oscillations of the M2 mirror segments about the vertical axis and are caused by missing restraining devices in the model. These devices will be implemented in the next update of the FE model. Most of the modes above 14.6 Hz (mode 833) are local bending modes of the beams that represent in a simplified way the whiffle tree supporting structure of the M1 segments. Therefore. only a small frequency increase above 14.6 Hz is recognized. Since these (cantilever) beams are underestimating the lateral stiffness connection of the M1 segments. a more accurate modelling will be carried out in the next phase. Nevertheless. these modelling deficiencies have negligible influence on the FE analysis results presented herein.

The diagram in Figure 9-72 displays the three effective mass components associated with each frequency. It can be seen from this diagram and from the effective mass tables. that the first 10 modes (4.1 Hz) contain more than 50 % of the accumulated effective mass in all three

directions. The effective masses for frequencies up to 10 Hz (first 400 modes) accumulate in the three component directions to 78 %. 75 % and 63 %. respectively. The additional effective mass increase achieved for the modes between 400 and 2000 is only 8 % in all component directions.
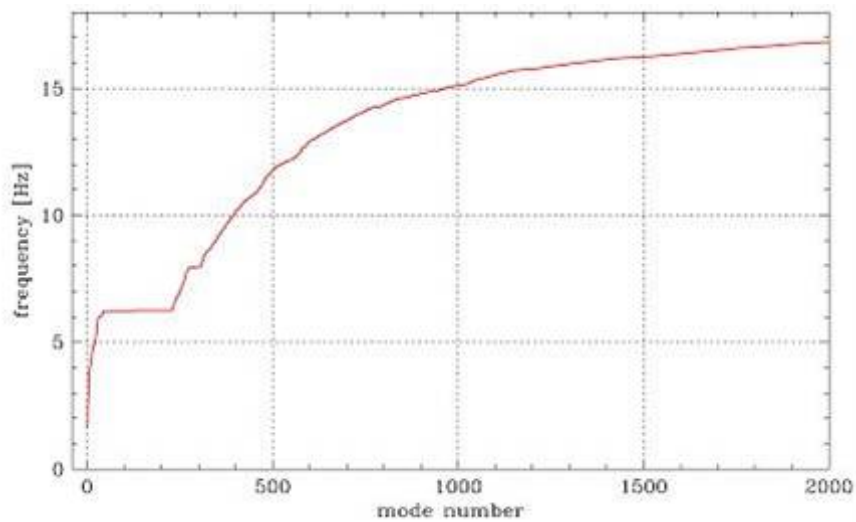
Figure 9-71: Natural frequencies versus mode number.
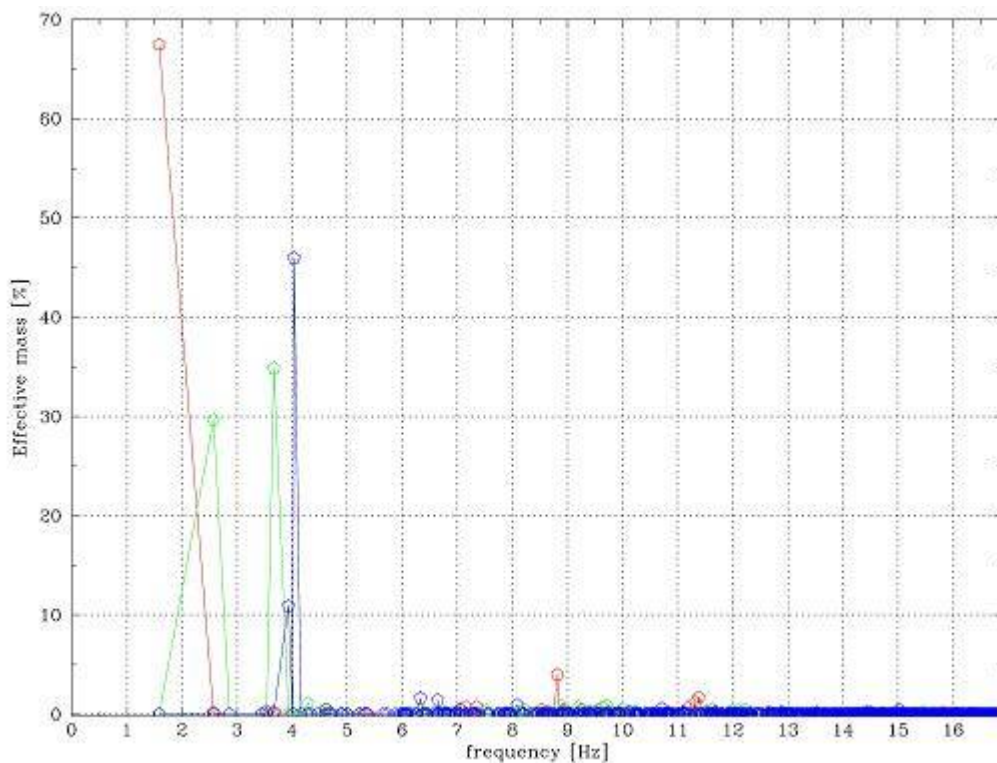
Figure 9-72: Effective masses versus frequency.

9.5.4.2   Dynamic Wind Load

The scope of the analysis study presented in this section is to investigate the global (macro scale) effect of the dynamic wind load contribution on the deformations of the segmented mirrors M1 and M2. respectively. The local (micro scale) dynamic behaviour between individual segments has been studied as well by applying the appropriate wind load to individual segments only by increasing the number of loaded segments stepwise. As the analyses account for frequencies up to 10 Hz. results represent the behaviour of the supporting M1 and M2 cell

structures. The much higher eigenfrequencies of the segment supports are not considered. The results have to be interpreted as open loop response to dynamic wind load excitation. They are indicative and form a conservative limit of the expected displacements which have to be corrected by the control loops. For the assessment of the effect of the wind disturbance on the closed loop phasing error it is referred to the appropriate simulations described in section 7.5.

The dynamic wind load characterization as defined in section 5.4.1.1 forms the load scenario for the Random Vibration analyses of the global FE model of OWL. This analysis method is used in place of time-history analysis to determine the response of a structure to random or time-dependent loading conditions such as wind loads. This technique allows evaluating statistics of the mirrors' deformation shapes and frequency dependant amplitudes. The Random Vibration analysis procedure is probabilistic in nature and is based on computing statistics of each modal response and then combining them. Using the theory of random vibrations. the response displacement PSD can be calculated from the input pressure PSD. With this response statistical output data like mean square response and 1σ values are derived.

9.5.4.2.1   Macro scale wind effect on segmented mirrors

Until now the zenith configuration of the 2004 FE model has been investigated by assuming the pressure load scenario of the 60° configuration which is considered to be the worst case wind load (see section 9.5.2.2). The wind load pressure has been applied only to the segmented mirror surfaces M1 and M2. The effect of the dynamically loaded framework structure will be studied in a later phase. The modal response is obtained from the modal analysis results for the lowest 400 modes that represent all frequencies up to 10 Hz. Based on the modal response and the input pressure PSDs the Random Vibration analysis has been performed by combining those modes which exceed a certain threshold value of their covariance ratio. i.e. the more the modes are separated the smaller are their contributions due to the interaction between them.

The following analysis assumptions have been used:

- For each mirror surface uniform input PSDs were applied to all nodes.

- The pressure PSDs applied to M1 and M2 are described in section 5.4.1.1. They take into account different wind velocities on M1 (10 m/s) and M2 (14 m/s) according to the wind profile and are fully correlated within each mirror.

- The pressure PSDs of M1 and M2 are uncorrelated to each other.

- For the calculation of the pressure PSD a conservative pressure (drag) coefficient of 1.0 was used.

- Constant damping ratio of 1 % to the full structure.

The distribution of the mirrors' surface deformation over the simulated frequency range has been evaluated in terms of the standard deviation 1σ. The contour plot in Figure 9-73 represents the 1σ deflection of M1. It is very similar to the mode shape of the main piston mode at 4 Hz and superimposed by a global tilt caused by the altitude locked rotor mode at 2.6 Hz. This behaviour is confirmed by the 1σ response PSD plot of the maximum and minimum displaced nodes of M1 as shown in Figure 9-75. The M1 deflections are clearly dominated by the main piston mode. whereas the highest peak in the M2 curve occurs at about 7.3 Hz which represents the piston mode of the M2 unit structure (see Figure 9-74). The locked rotor mode at 2.6 Hz is clearly visible on M1. but appears only marginally on the M2 curve (see Figure 9-76).

A comparison of the 1σ surface deflections of M1 and M2 for various frequency bands is summarised in Table 9-19. Due to the high wind energy content in the low frequency range the low band up to 1 Hz contains by far the highest contribution of 16.4 μm for M1 and 51 μm for M2. respectively. The open loop 1σ displacements for frequencies between 1 and 5 Hz become 304 nm for M1 and 1.4 μm for M2. It should be noted. that these deflections are of global nature and are supposed to be corrected mainly by the non-segmented mirrors.

Independent hand-calculations of the 1σ response PSDs agree quite well with the FE Analyses results for frequency bands up to 5 Hz. Higher frequencies are hardly comparable. because the hand calculation structure is based on a single spring-mass system with the locked rotor resonant frequency at 2.6 Hz for M1 and the main piston frequency at 3.9 Hz for M2.
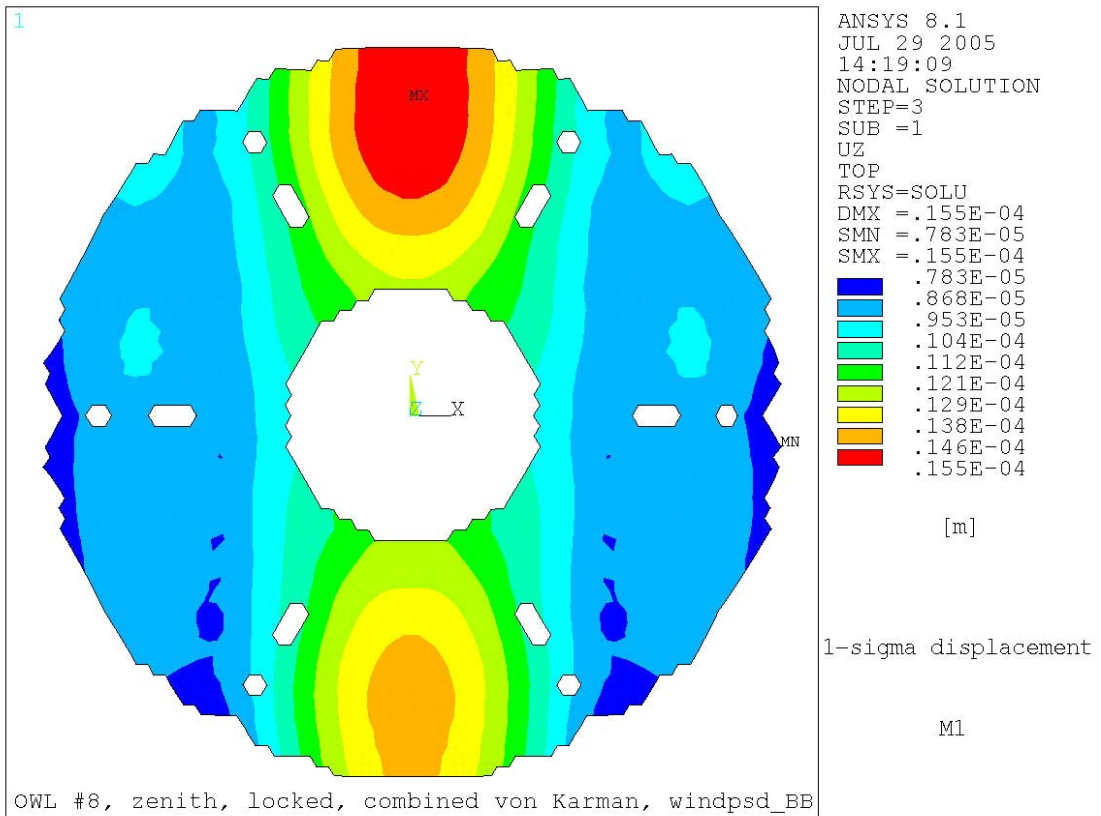
Figure 9-73: 1σ normal displacement distribution of M1.
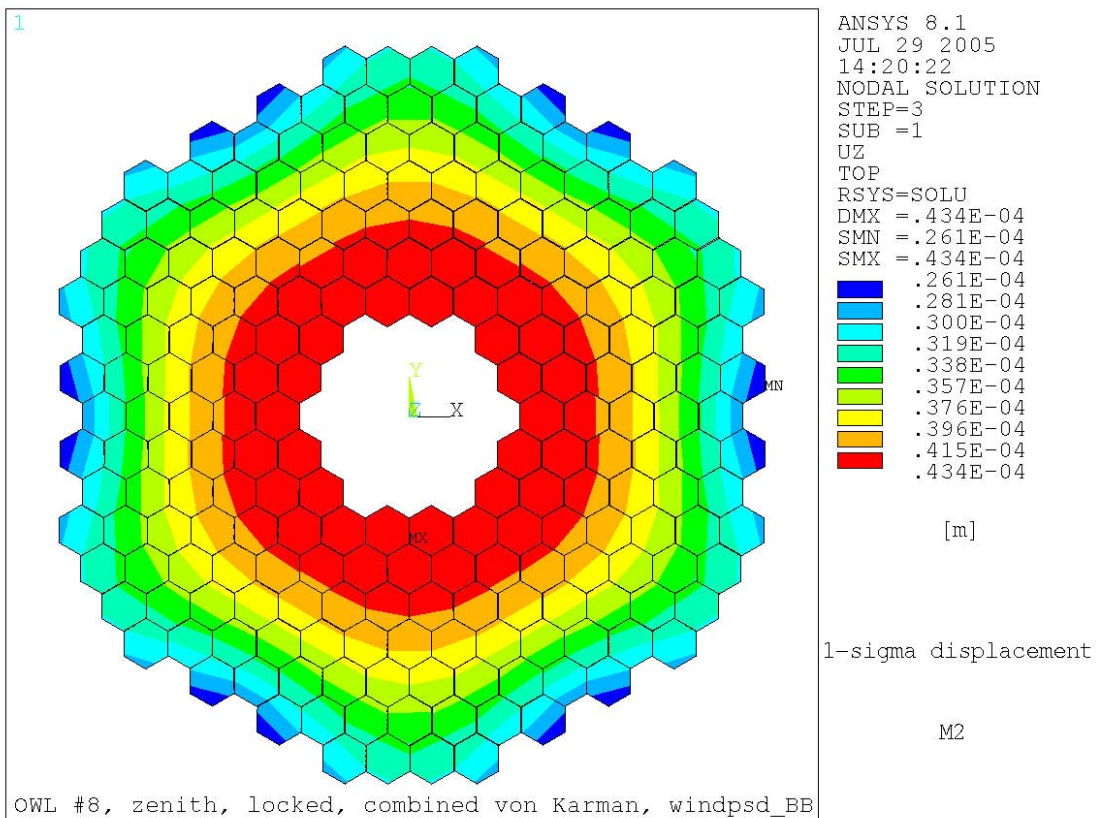
Figure 9-74: 1σ normal displacement distribution of M2.

Figure 9-75: 1σ response PSD of piston displacement of M1
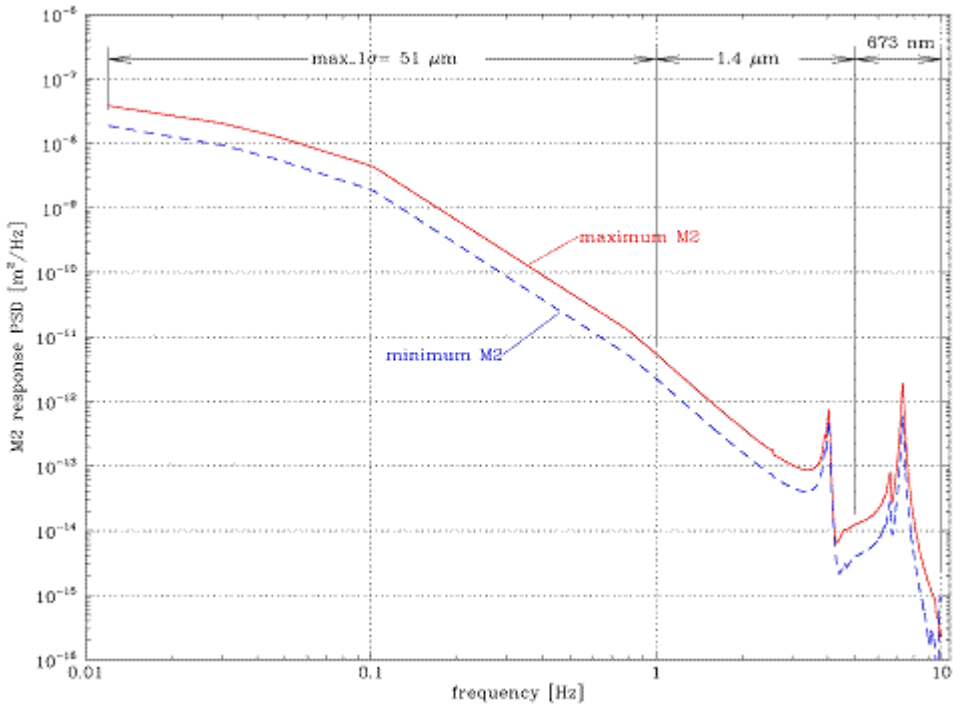
Figure 9-76: 1σ response PSD of piston displacement of M2.

Mirror	1σ displacement in [μm]			
Frequency range [Hz]:	0.012 to 1	1 to 5	5 to 10	full range
M1 (v_{mean}=10 m/s)	16.4	0.304	0.064	16.4
M2 (v_{mean}=14 m/s)	51.0	1.408	0.673	51.0

Telescope structure and kinematics

Table 9-19: 1σ maximum piston displacement of M1 and M2 due to von Karman wind load spectra applied to complete mirrors area.

9.5.4.2.2   Micro scale wind effect on phasing error

In order to assess the differential piston between two segments (phasing error measured by the segment edge sensors) under wind load. a series of PSD analysis has been carried out by loading only part of the M1 and M2 segments with the appropriate wind force spectra. Starting with the loading of only one segment the loaded area was stepwise increased until the full M1 and M2 area was loaded. For each analysis run the input PSD spectra were adapted to the loaded area in terms of the aerodynamic attenuation. The appropriate input PSD spectra applied for M1 and M2 are described in section 5.4.1.1.1.2. All the segments piston values have been compared with their neighbour segments to evaluate the maximum differential piston. Hence. this value can be interpreted as the maximum expected open loop 1σ phasing error. The resulting maximum differential 1σ piston displacements between two M1 and two M2 segments. respectively are summarised in Table 9-20 for various frequency bands. The associated absolute piston displacements are listed as well.

The absolute segment piston of M1 becomes 239 nm for frequencies between 1 and 5 Hz. whereas the differential piston becomes in the worst case only 16 nm for the same frequency band. For the frequency range between 5 and 10 Hz the differential piston is calculated to be only 3 nm. This is also an indication. that local modes of the M1 cell structure underneath the mirror segments are only slightly excited by frequencies below 10 Hz. To further illustrate these results the response PSD of the absolute and differential displacements for the worst case are shown in Figure 9-77. It represents a loaded area of 836 m^2. i.e. 75% of a 60° petal of M1. The response PSD demonstrates. that the energy content of the frequencies above 5 Hz is fairly small.

The resulting 1σ piston displacements of the M2 segments are much higher than those of the M1 segments. In the frequency range between 1 and 5 Hz the absolute piston becomes 1.46 µm and the differential piston about 210 nm in the worst case. For frequencies between 5 and 10 Hz the maximum differential piston is calculated to be 110 nm. This value is obtained when the full M2 area is loaded. It is obvious from the appropriate PSD response displayed in Figure 9-78. that the M2 unit piston mode at 7.3 Hz is significatnly excited and is the main contributor to this response.

Hence. the main reasons for the larger displacement response of M2 compared to M1 are the higher wind load (twice as high) and the lower stiffness of the M2 cell structure. To improve this situation. several design measures can be taken and will be investigated in the next phase:

- Improve the stiffness of the M2 cell structure to increase the M2 unit piston frequency.

- Use Silicon Carbide mirror segments.

- Include passive or active damping.

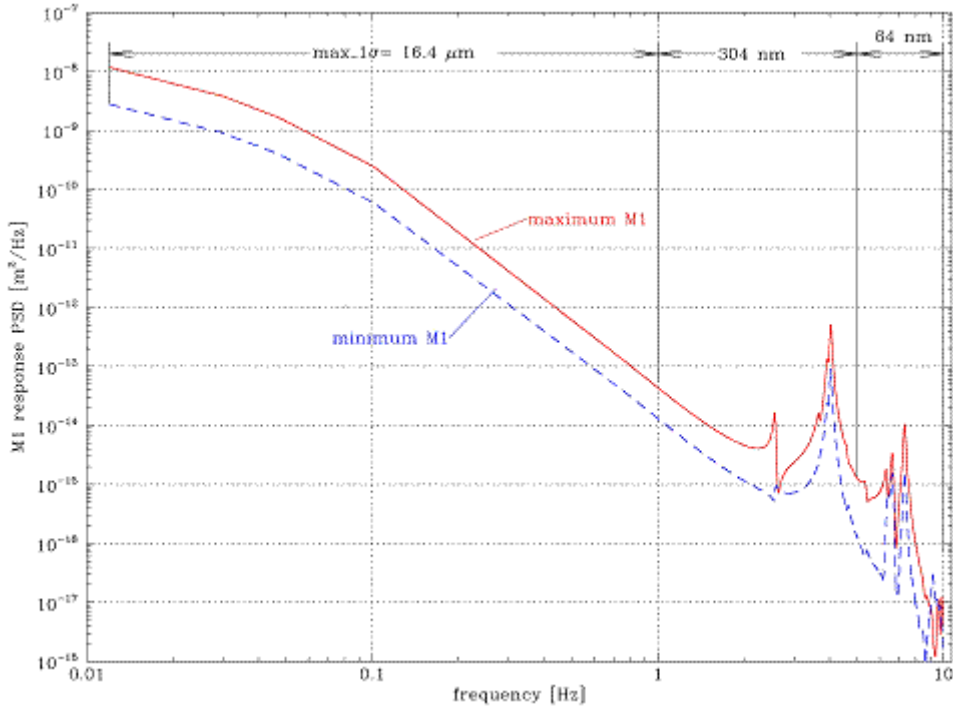|	1σ displacement in [µm]		
Frequency range [Hz]:	0.012 to 1	1 to 5	5 to 10
Absolute segment piston M1	13.8	0.239	0.037
Differential piston between segments M1	0.922	0.016	0.003
Absolute segment piston M2	37.3	1.463	0.659
Differential piston between segments M2	5.7	0.210	0.110

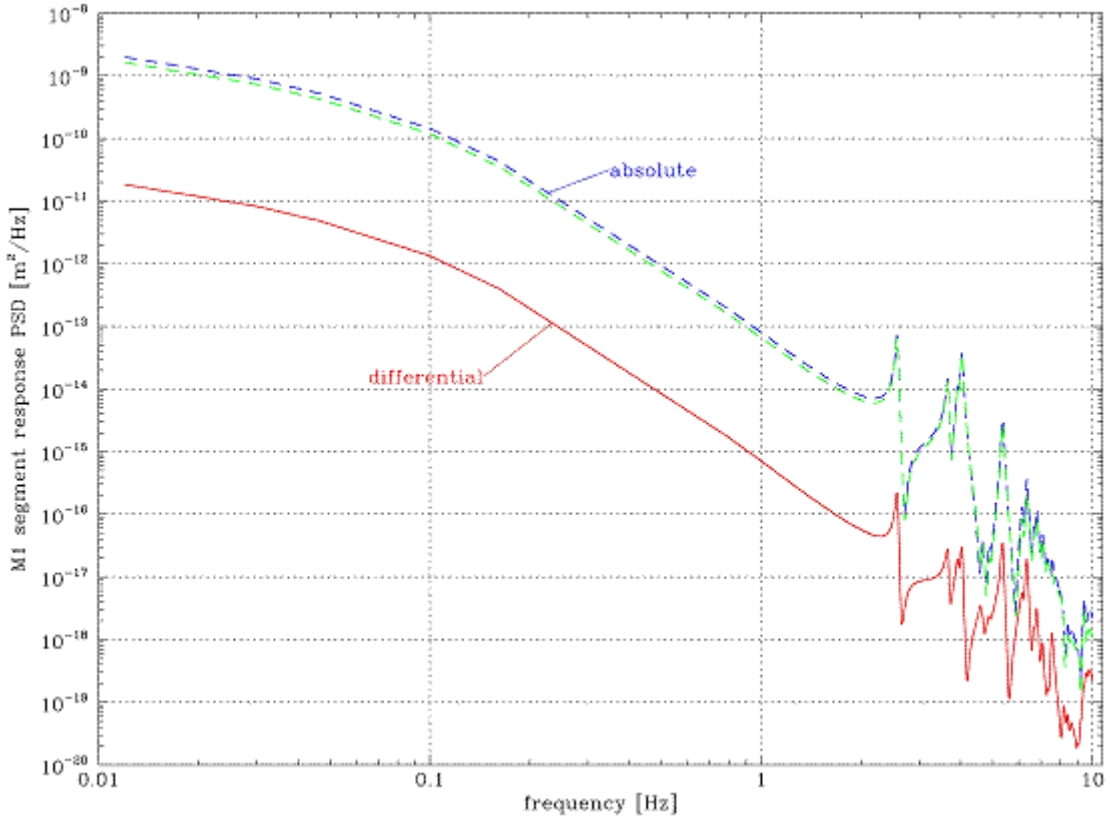*Table 9-20: 1σ maximum displacements of M1 and M2 segments (part of the mirror area loaded).*

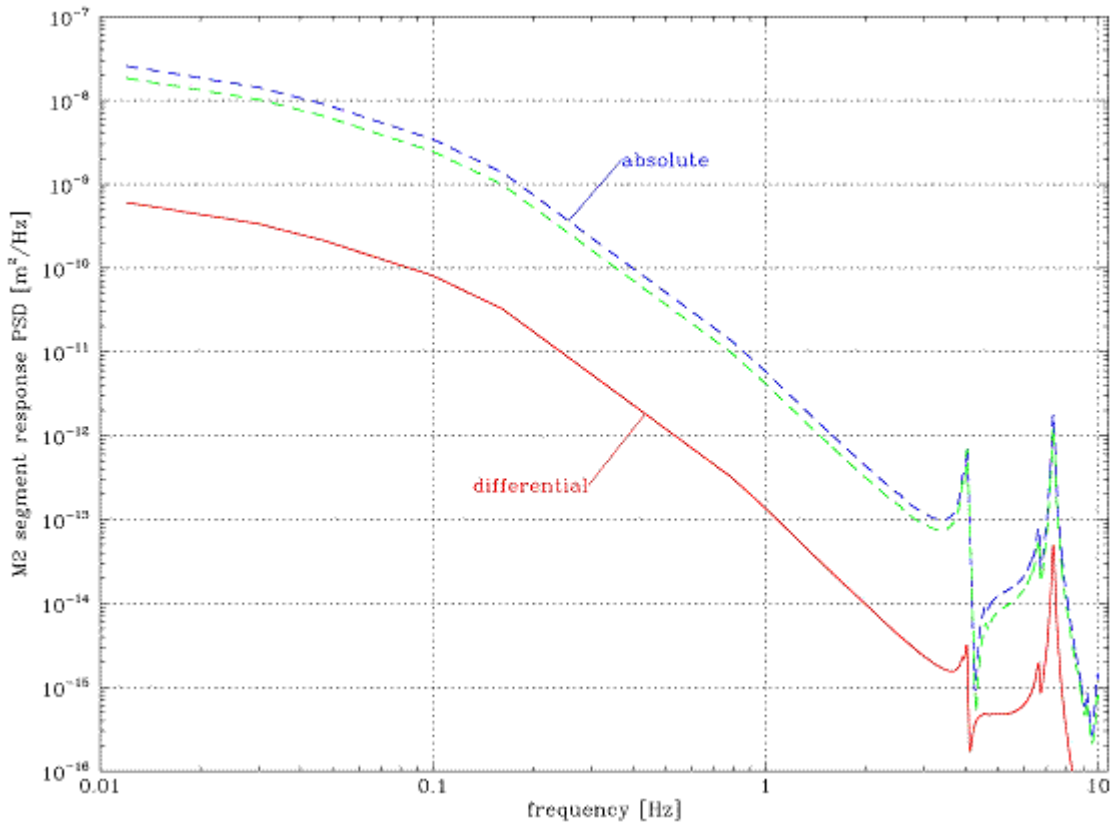Figure 9-77: 1σ response PSD of segments piston displacement of M1.

Figure 9-78: 1σ response PSD of segments piston displacement of M2.

Telescope structure and kinematics

An independent hand-calculation of the 1σ response PSDs of a single spring-mass system simulating the stiffness of a single M1 segment cell structure compares very well with the appropriate FE Analysis result.

In section 7.5.5 control loop simulations of individual mirror segments under dynamic wind loading are carried out to evaluate the closed loop phasing error assuming a single spring-mass system for the M1 cell structure (equivalent to the locked rotor frequency of 2.6 Hz). It is foreseen to simulate the phasing error by including the full dynamics of the telescope structure (e.g. M1 and M2 cell) in terms of the reduced state space model.

9.5.4.3   Effect of soil and foundation

In general the response of the soil influences the motion of the structure and the response of the structure influences the soil motion. The importance of this so-called soil-structure interaction depends on numerous parameters like soil material properties. structure mass and stiffness and foundation size. just to name some of them. The effect of the soil-structure interaction on the dynamic performance of OWL has been investigated depending on various soil properties and telescope foundation thicknesses. because the telescope site and its soil properties have not yet been chosen. For this purpose part of the soil and foundation structure has been modeled and attached to the 2002 OWL FE model. Focussing on changes in the modal properties of the telescope and changes in the influence of disturbances onto mirror positions. these dynamic effects are investigated applying the Finite Element Method in combination with a typical range of possible soil properties. Static strength considerations are out of the scope of these simulations. but must especially be considered for dimensioning the telescope foundation.

Soil shows in general a very non-linear and inhomogeneous behaviour. Assuming linear properties is a simplification. which is only valid for very small amplitudes of displacements and forces. The interaction between soil and telescope means firstly a finite stiffness for the foundation. but moreover energy transport by mechanical waves from the telescope to the ground and vice versa. Applying the FE method only a finite domain of soil can be included requiring appropriate transmitting boundary conditions at the artificial bounds. which means a matching of the local impedance properties at the boundaries. which do not exist in reality. To match this impedance. each boundary node is connected to a discrete damper with damping constants $d_{ni}=\rho c_P A_i$ and in the tangential plane with $d_{ti}=\rho c_S A_i$ (where A_i is the equivalent boundary area represented by node I. ρ is the density and c_P and c_S are the wave velocities for compression and shear waves. respectively).

Modelling the soil in sufficient resolution requires on one hand to use at least 6 FE-nodes per wavelength. On the other hand the transient boundary should be applied at least one wavelength distant from the source of radiation. in this case the telescope. This results in a modelled soil-cylinder of 150m height and 450m diameter. which corresponds to about three times the telescope dimensions (see Figure 9-79). Since most of the important modes are symmetric along the symmetry plane perpendicular to the altitude axis. only half of the structure has been modelled.

At present only the general effects are investigated assuming homogeneous soil properties covering the field from soft and light tuff stone (Young's modulus E=500 MPa) up to very stiff basalt or granite (E=80000 MPa). In addition to that. a quasi-rigid soil is modelled (E=1000000 MPa). which aims at representing the reference conditions used in the telescope global FE model (see section 9.1).

Since the telescope distributes its load onto a large area of ground. the effective stiffness of the soil is considerably higher than the one of the telescope. Under static wind load conditions and for soft tuff stone the deflection of M1 and M2 is increased by 3.3% and 1.8%. respectively. Therefore. these deflections are dominated by the flexibility of the telescope. (For massive basalt or granite rock the soil stiffness can be fully neglected.)

Adding the soil and foundation to the telescope model introduces –in addition to the telescope modes– pure ground modes (without any elastic deformations of the telescope) and mixed modes with deformations of both the telescope and the ground. The ground dominated eigenfrequencies depend on the structural soil properties. the size of the modelled soil volume and the boundary conditions. (Lower stiffness. higher density and larger volume of modelled soil

tend to decrease the eigenfrequencies.) For a sufficiently large modelled volume. the ground modes start already below the telescope eigenfrequencies.
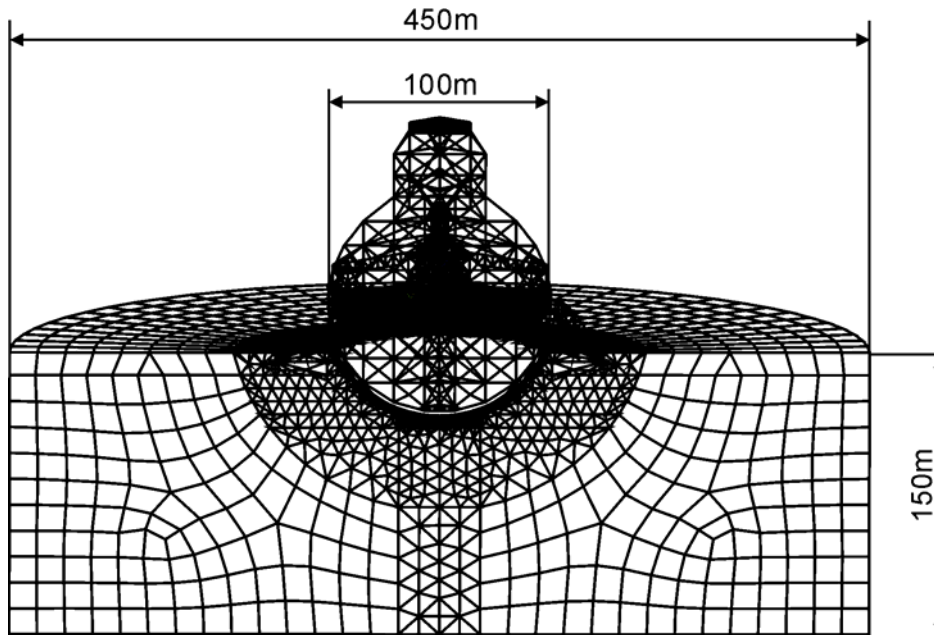
Figure 9-79: FE-model and major dimensions of the OWL with foundation and soil.

In order to better assess the influence of the soil under typical load conditions. the transfer functions due to wind load distribution have been calculated for different models. As can be seen in the transfer functions in Figure 9-80 the difference in terms of the horizontal displacement of the primary mirror between the extreme models is not significant. The models represent quasi-rigid soil and fixed boundaries (dash-dotted line) and very soft soil (tuff stone) and non-reflecting boundary conditions (solid line). Both graphs are very similar and the maximum difference between the transfer functions is in the order of 1/10 of the peak amplitude. i.e. the transfer function is only slightly influenced by the soil. For stiffer soil properties. these effects are even smaller and diminish fully for massive rock like basalt or granite.

Based on the investigation of the soil-structure interaction of OWL it can be concluded that only a small dynamic effect of the ground can be expected within the range of the material parameters for the soil under research. It is expected that this conclusion is also valid for the actual baseline design of the 2004 OWL model. because its mass and modal properties are in the same order of magnitude as the previous model used for this study.

The influence of the foundation thickness variation in the range of the analysed values of 1.5. 3 and 6m is very small. The main reason is the relatively light telescope structure and the large area the telescope is supported on. which results in a mean ground pressure of 12 kN/m^2 only. Thus in relation to the telescope specific stiffness the foundation specific stiffness is high and the total deformations are dominated by the telescope flexibility. As the telescope mass is only 0.02%-0.04% of the soil volume modelled. telescope vibrations will involve ground vibrations of only very small amplitude. Though. this implies also nearly no radiation of energy out of the telescope structure into the foundation. which would cause an additional damping effect. The theoretical effect of the soil stiffness on the natural frequency of the system as illustrated in [35] complies well with the predictions of the FEA. e.g. a soil Young's modulus of 500 MPa corresponds to a frequency ratio[67] of 0.96 and a soil Young's modulus of 2000 MPa corresponds to a frequency ratio of 0.99.

More details of the study about the dynamic effects of ground and foundation can be found in RD36.

---

[67] Frequency ratio is the ratio between the natural frequency of the soil-structure system and the "fixed-base" system (rigid soil).
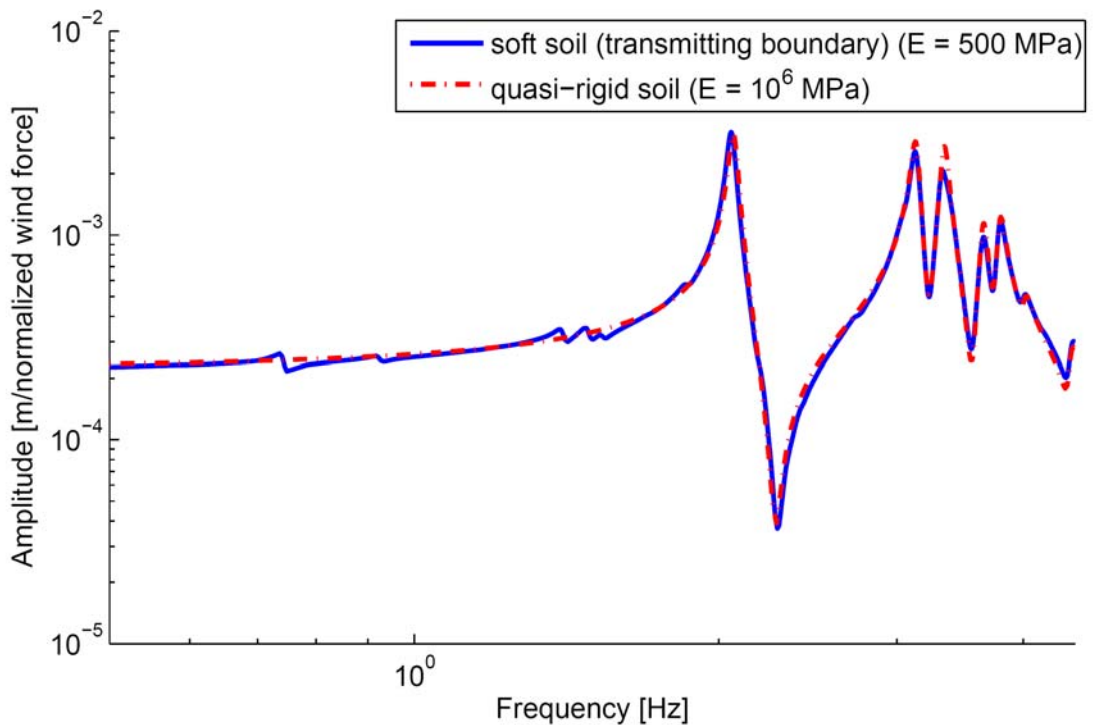
Figure 9-80: Transfer function from wind load to y-deflection of M1.

9.5.5   Safety Analysis

In order to assess the structural safety of OWL. several analysis studies have been carried out to evaluate the maximum stress and safety margins under various survival load conditions. As the permanent maximum stresses caused by gravity are relatively high. the individual survival load case results have to be superimposed to comply with realistic load combination requirements. This will be done in phase B of the project. Fortunately. the maximum stress regions of the gravity cases are in many cases different from those of the survival load cases (TBC). In these cases the maximum stress of the combined load cases will not increase.

9.5.5.1   Wind

The survival wind speed for the telescope is specified to be 30 m/s (TBC). To evaluate the maximum displacements and stresses. the results obtained with the static wind load analyses described in section 9.5.2.2 have been scaled with a factor of 9 (=$30^2/10^2$). The resulting maximum stress. displacement and safety margin values are summarised in Table 9-21.

Altitude angle	Max. von Mises stress	Max. displacement
	[MPa]	[mm]
Zenith	45	9
30	44	12
60	29	11

Table 9-21: Maximum stresses. safety margins and displacements or survival wind load cases.

The maximum stress of 45 MPa and the maximum displacements of 12 mm caused by pure survival wind load are not critical.

9.5.5.2   Earthquake

Depending on the site selected for the observatory. seismic aspects might be an important design driver for the telescope structure. In order to assess the expected level of displacements and stresses. three quasi-static load cases have been applied to each of the three 2002 OWL models (zenith. 60º and horizon orientation):

- 1g load in vertical z-direction

- 1g in vertical z- and horizontal x-direction

- 1g in vertical z- and horizontal y-direction

This load scenario represents approximately an earthquake with a maximum horizontal ground acceleration of 0.2 g which corresponds to a site with moderate seismic activities. For comparison. MLE on Paranal is 0.34 g and on La Palma 0.04 g.

The stress results of these analyses indicate that several structural beams of the 2002 model exceed the allowable stress limit by about 20 % and would have to be modified by using higher quality steel (St52) and/or by changing their cross-sections. The stress and safety factor verification for the 2002 model due to a 0.2 g level earthquake can be realised with moderate effort. However. under Paranal-like seismic conditions much more effort in terms of design modifications and design measures would be required. Some of the possible measures are listed here:

- Reinforcement of the beam structure around the altitude cradles.

- Considering the higher damping capacity of the bogies due to sliding friction.

- Implementation of local and/or global passive damping devices.

Significant design improvements in the region around the altitude cradles could be already achieved in the latest design version 2005. This results in a considerable increase of the cross elevation frequency and reduces the stresses and dynamic impact due to earthquake loads.

In phase B it is foreseen to use the Response Spectrum Analysis method to verify the structure under seismic loading. This method has been used for the VLT and is the standard technique. After conducting a geotechnical investigation and a hazard analysis of the observatory site. site specific parameters will be defined. Based on these parameters. two different seismic scenarios will be specified. the Operating Basis Earthquake (OBE) and the Maximum Likely Earthquake (MLE). The OBE is defined as an earthquake of moderate size with high probability of occurrence and the MLE is defined as an earthquake of large magnitude but with low probability of occurrence. More details about the Response Spectrum method and the determination of the spectrum for Paranal are provided in [36].

9.5.5.3   Buckling

The collapse of large structures due to buckling is an important safety aspect. Therefore. the OWL framework structure has to be designed such to withstand loadings that could cause buckling. Buckling failure might occur at loads smaller than that would be predicted from stress and strain calculations alone. Therefore. an extensive buckling analysis study based on the 2002 models has been performed (see RD30).

By using the linear buckling analysis the theoretical buckling strength of an ideal linear-elastic structure can be evaluated. The eigenvalues calculated by the linear buckling analysis represent buckling load factors. As imperfections and non-linearities prevent most of the real structure from achieving their theoretical elastic buckling strength. the linear buckling approach often yields insufficiently conservative results. Therefore. the nonlinear buckling analysis approach is more accurate and recommended for the verification evaluation. This technique employs a nonlinear static analysis with gradually increasing loads to find the critical load level.

Linear eigenvalue buckling and. wherever needed. non-linear buckling analyses have been carried out based on the earthquake loading scenario and the three 2002 models explained in section 9.5.5.2. The objective is to determine the critical load values at which the structure becomes unstable. The stability verification has been carried with all the framework beams of

the 2002 FE models by following the procedures defined in the standard norm DIN 18800. part 2.

1. Linear buckling and static analyses to calculate the lowest buckling mode shapes and the shapes for the static bending line.

2. Non-linear buckling analyses based on the pre-deformed buckling mode shapes. The maximum imperfections of these mode shapes were scaled according to the norm DIN 18800.

3. Evaluate global buckling stability and critical load factors for all beams.

The minimum critical load factor is calculated to be 1.7 and occurs for the horizontal altitude configuration when the unit gravity acts in vertical z- and horizontal y-direction simultaneously. As a result of the buckling analysis study it can be concluded that some moderate design modifications are needed for the 2002 design to meet the buckling failure requirements. It is expected that the increased stiffness inherent in the 2005 design will also be beneficial for the sensitivity to buckling failure.

9.5.5.4 Fatigue

In order to assess the risk of the structural failure of the telescope due to fatigue loading. an analysis study has been carried out (see RD32). Wind gust is considered to be the most critical load which could lead to fatigue problems of telescopes. as it is a dynamic load with a large number of amplitude cycles. Based on the 2002 FE model of OWL. simplified wind load distributions have been applied to the zenith configuration. The load distribution follows a wind speed profile over height with maximum 13 m/s at 100 m height above ground. Two load cases with wind directions in x- and y-direction respectively have been considered in separate analyses. The wind forces have been applied for each load case in two ways:

• Classification of the structure in framework groups according to DIN 1055 with consideration of the shadow effect.

• Uniform applied wind forces on all beams considering the wind speed profile. but without the shadow effect (worst case).

As the dead weight is a permanent load and contributes to the stress distribution significantly. it has been superimposed to the wind load distributions. By comparing the stresses due to pure dead weight with those of the combined load cases. the constant mean and variable amplitude portions can be evaluated. This is important for the assessment of the fatigue risk. Fortunately. the maximum stresses caused by wind are located in areas with low permanent stress levels. The maximum stress amplitude caused by the wind load applied results in 17 MPa for all load cases investigated. The mean stress at this position is only 8 MPa.

According to the Eurocode 3. part 1-1. a fatigue verification of a structure is only needed. if the maximum variable stress amplitude is above 19 MPa. This requirement is already fulfilled with the present wind load assumptions which are considered to be conservative. e.g. wind gust of 13 m/s corresponds to a static wind speed of about 40 m/s. the number of cycles under these conditions are far below the critical load cycle values and the locations of high stresses due to wind change vary often due to different telescope configurations and wind directions.

Nevertheless. Smith diagrams have been calculated to illustrate the mean and amplitude stress for each node in the structure with respect to the materials' endurance limit. permissible stress. alternating and pulsating strength.

Figure 9-81 displays a typical Smith diagram representing a uniform wind load case in x-direction with the component stress versus the mean stress. The red and blue dots are the lower and upper stress values. As can be seen. the majority of the stresses lie very close to the diagonal dashed line which represents the constant mean stress and are far away from the materials' limit strength curves (solid curves). The amplitudes are small. but due to the gravity load some static stress points are relatively high as already pointed out. They exceed the limit strength curve of the St37 material (red). but are still well inside the limit strength curve of the St52 material (dark purple).
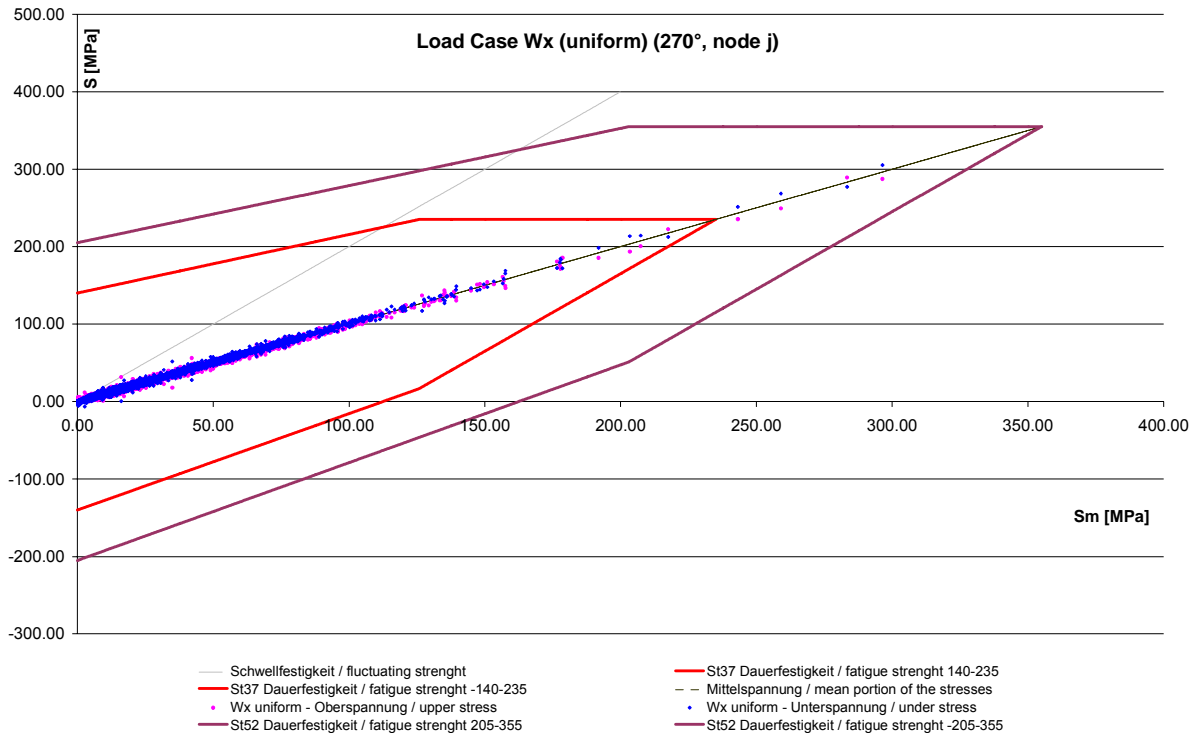
Figure 9-81: SMITH diagram

It has been demonstrated. that the 2002 model is insensitive to fatigue loading like wind and the risk of structural failure due to fatigue is very small. As the 2004 and 2005 OWL designs are much stiffer than the 2002 design. it is expected that fatigue remains a negligible issue.

9.5.5.5   Pretension of ropes

Since the purpose of the structural ropes is to provide sufficient tension stiffness in all altitude configurations (see 9.4.4.2). they have to be preloaded accordingly. This pretension process will change the existing stress distribution due to gravity. Therefore. an optimisation study has been performed with the 2002 FE model of OWL (see RD32). The objective was to evaluate an optimal pretension of all ropes by

- maintaining a certain minimum pretension of all cables for the two extreme altitude configurations under gravity.

- minimising the stresses and

- respecting the allowable strength limits of the framework structure and the cables.

Many optimisation analyses and iterations have been carried out to find a valid and preliminary optimal solution. because two different analytical models had to be optimised and ANSYS allows only a single-objective optimisation. The best solution of the optimisations results in a 5 % increase of the maximum stress caused by gravity without pretension. By changing the relevant parts in the structure into higher strength material (St52) the stress and safety factor requirements can be fulfilled. In phase B a multi-objective optimisation program will be used to find a better optimum for the pretension distribution.

Careful and extensive analyses will be required to simulate the pretension process. because the structural stresses react quite sensitive to variations of the cable pretension. As the 2005 model is considerably stiffer than the 2002 model. a significant stress level reduction is expected which is also beneficial for the pretension process.

Telescope structure and kinematics

9.6   Structure design Options

9.6.1   Base line High configuration (2005 design)

The Figure 9-82 shows the baseline configuration which has the altitude axis at 38.49 meters from the ground level. This height allows the primary mirror to remain above the ground level for a rotation of 50° from zenith. From 50° to 60° the primary mirror sinks partially bellow the ground level. However the small concerned portion of the primary mirror and the observation range close to the horizon. make this configuration acceptable in relation to the thermal turbulence disturbance. The various drawbacks. listed in the table below. which are generated by the increase in height. are justified by the fact that the thermal turbulence is minimized. Thermal turbulences are critical for a 100 m primary mirror where quasi "micro climates" can be generated. These aspects will be studied in more details during the next project phases.

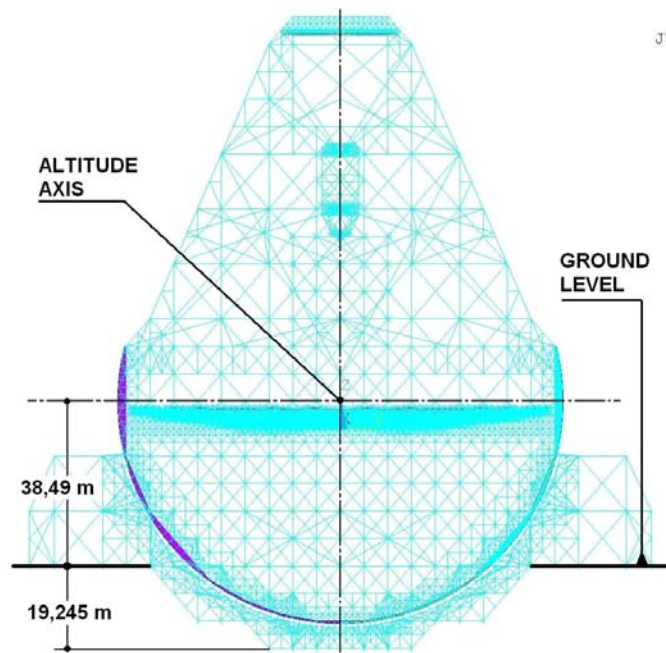| Advantages	Disadvantages
Less thermal turbulence.	More structural steel is required.
Less excavation depth for the foundation.	Lower dynamic and static performance.
	More complex operation and maintenance.
	Larger enclosure.

Table 9-22: High configuration

Figure 9-82: Base line. High configuration

9.6.2   Glass Ceramic low configuration

Figure 9-83 shows low configuration which has the altitude axis at 25.66 meters from the ground level. This height allows the primary mirror to remain above the ground level only for a rotation of 30° from zenith. From 30° to 60° the primary mirror sinks partially bellow the ground level. This may cause thermal turbulences on the primary mirror. The various advantages of this configuration (see table below). do not compensate for the time being the fact that dangerous

Telescope structure and kinematics

thermal turbulence on the primary mirror. may degrade the image quality. even after AO. Realization of opening in the foundation. to vent the primary mirror. are complex. expensive and counter productive in term of stiffness.

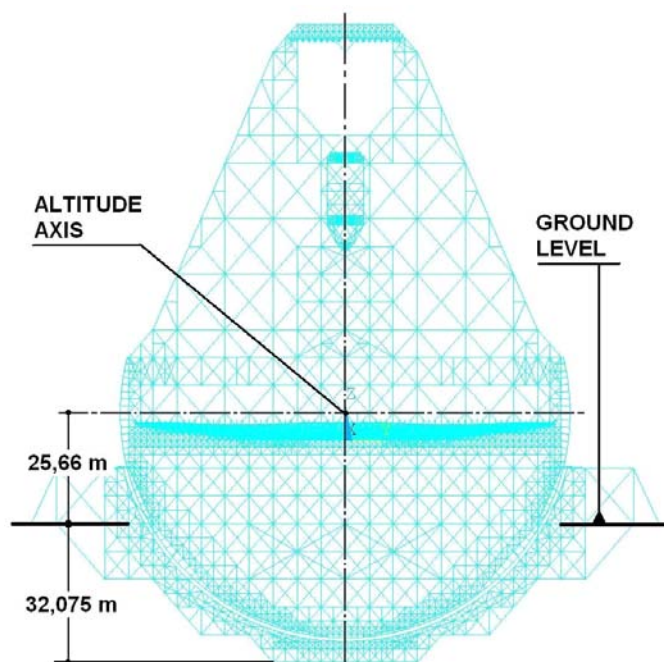| Advantages	Disadvantages
Less structural steel is required	High thermal turbulence
Higher dynamic and static performance	More excavation depth for the foundation
Easier operation and maintenance	
Smaller enclosure	

Table 9-23: Low configuration.

Figure 9-83: Low configuration

9.6.3 SiC high and low configurations

Options 2 (2005 SiC High) and 3 (2005 SiC Low) take into account SiC substrate and the implementation of Composite Materials of the upper part of the altitude structure.

Main Advantages of using SiC substrate and composite material are:

- Reduction of Rotating mass.

- Increase of static and dynamic performance.

- No air conditioning need for the primary and secondary mirrors.

- Higher safety factor for the primary and secondary mirrors.

- Decrease of cost on several other telescope subsystems

    o Mechanical Structure.

    o Drive and bearings.

    o Tracks and foundation.

Telescope structure and kinematics

o   Maintenance and Operational costs.

Main disadvantages of using SiC substrate and composite material are:

- SiC substrate technology is not fully validated as per today.

- Composite material can limit eventual retrofitting of the telescope.

A dedicated study to Composite material structural elements applied to ELT including OWL is planned in the ELT Design Study (see appendix A-1.4). Further details about the study can be found in the study Statement of Work RD512.
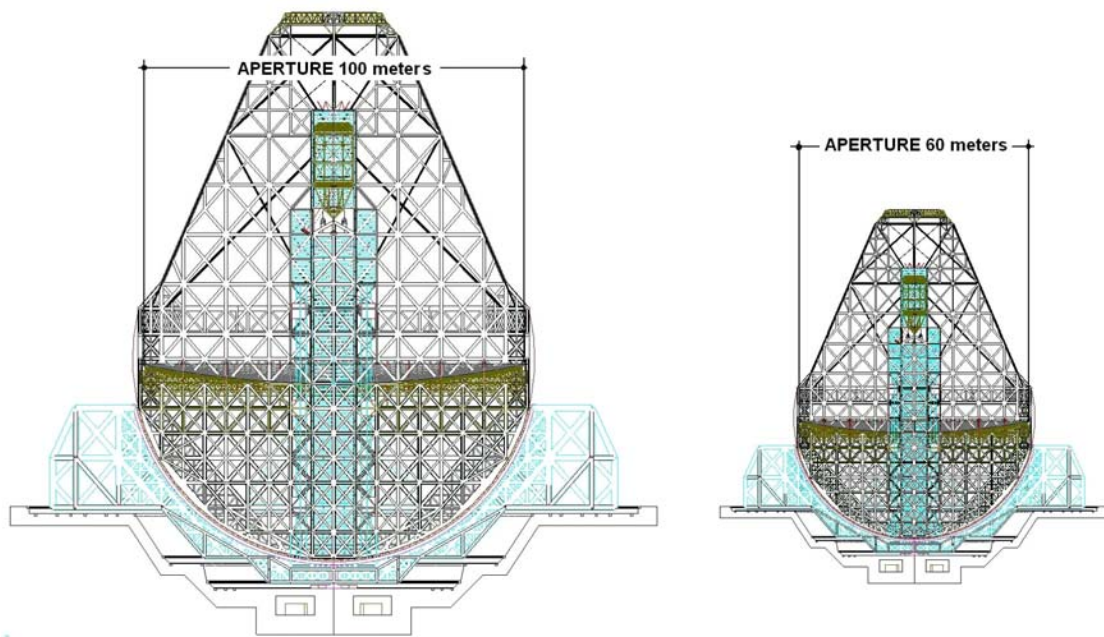
9.6.4   Glass Ceramic 60 m configuration

Figure 9-84: OWL scaled down 60 meters

Option 4 is a scaled down to 60m of the 2005 100m optomechanical design (see Figure 9-84). This design has been developed in order to get a first order values related to performance and costs. More accurate evaluation will require a design based on a dedicated optical design tailored to the 60 m aperture and taking into account the maximum size of the active mirrors which should be 8.3 m.

The obvious main advantages of this design are:

- Reduction of Rotating mass.

- Increase of static and dynamic performance.

- Higher safety factor for the primary and secondary mirrors.

- Decrease of cost on several other telescope subsystems

   o   Mechanical Structure.

   o   Drive and bearings.

   o   Tracks and foundation.

   o   Maintenance and Operational costs.

Main disadvantages of having an aperture of 60 m are science related. Therefore they are not discussed in this section.

#	Design Option.	Total Rotating Mass [tons]	Altitude Structure Mass [tons]	Dynamic Performance		
				Parallelogram mode (X axis direction) [Hz]	Locked Rotor Mode [Hz]	Torsion Mode [Hz]
1	100 m 2005 design Zerodur. Steel. Kevlar ropes. High configuration.	13347	7174	2.35	2.68	3.39
2	100 m SiC. Kevlar ropes. Composite M2 tower. High configuration.	12136	5963	2.6	3	3.5
3	100 m SiC. Kevlar ropes. Composite M2 tower. Low configuration	10095	5963	2.6	3	3.3
4	60 m Zerodur. Steel Kevlar ropes High configuration	6457	2753	4.3	4.7	6

Table 9-24. Design options. overall properties.

The Options 2. 3. and 4 have indicative values and need further refinement and optimization (performance should increase)

— ⌘ ⌘ —